Design of Optical Transceiver Systems for CMOS Image Sensor-based and Photodiode-based Visible Light Communication

by

Bo XU

A Thesis Submitted to

The Hong Kong University of Science and Technology
in Partial Fulfillment of the Requirements for
the Degree of Doctor of Philosophy
in the Department of Electronic and Computer Engineering

August 2022, Hong Kong

Authorization

I hereby declare that I am the sole author of the thesis.

I authorize the Hong Kong University of Science and Technology to lend this thesis to other institutions or individuals for the purpose of scholarly research.

I further authorize the Hong Kong University of Science and Technology to reproduce the thesis by photocopying or by other means, in total or in part, at the request of other institutions or individuals for the purpose of scholarly research.

Signature redacted
Bo XU

August 2022

Design of Optical Transceiver Systems for CMOS Image Sensor-based and Photodiode-based Visible Light Communication

by

Bo XU

This is to certify that I have examined the above PhD thesis and have found that it is complete and satisfactory in all respects, and that any and all revisions required by the thesis examination committee have been made.

Signature redacted

Prof. C. Patrick YUE, ECE Department (Thesis Supervisor)

Signature redacted

Prof. Andrew Wing On POON (Head of ECE Department)

Thesis Examination Committee:

1. Prof. C. Patrick YUE (Supervisor) Department of Electronic and Computer Engineering

2. Prof. Wing-hung KI Department of Electronic and Computer Engineering

3. Prof. Yansong YANG Department of Electronic and Computer Engineering

4. Prof. Hongyu YU Department of Mechanical and Aerospace Engineering

5. Prof. Hao YU (External Examiner) School of Microelectronics,

Southern University of Science and Technology

Department of Electronic and Computer Engineering
The Hong Kong University of Science and Technology
August 2022

To my parents

Acknowledgment

First, I would like to express my sincere gratitude to my Ph.D. supervisor Prof. C. Patrick YUE. It was his insights into the world, his passion for life and work, his constant curiosity, and his thoughts on novel things that have had a profound impact on me and my study. His patience, encouragements, and precious guidance lead me to the right track of my research. It has been a wonderful experience to study in Prof. YUE's group. I have learned more than how to conduct research, and I will keep all I learned and carry this valuable experience with me for the future endeavors.

I would like to express my gratitude to Prof. Wing Hung KI, Prof. Yansong YANG, Prof. Hongyu YU, and Prof. Hao YU for their kindness of serving as my thesis examination committee members during this special period and giving suggestions to my research.

Gratefulness also goes to the colleagues in Optical Wireless Lab, including Dr. Xianbo LI, Dr. Weimin SHI, Dr. Li WANG, Dr. Babar HUSSAIN, Mr. Jian KANG, Ms. Yiru WANG, Mr. Fredrick HONG, Mr. Rehan AZMAT, Mr. Fuzhan CHEN, Ms. Zilu LIU, Ms. Xinyi LIU, Mr. Chongyun ZHANG and others for the valuable discussions. Special thanks to Dr. Li WANG, Dr. Babar HUSSAIN, and Dr. Xianbo LI for their guidance and suggestions when I encountered difficulties in my research.

I would like to thank my friends Tianxin MIN, Zilu LIU, Xinyi LIU, Yiru WANG, Su YUAN and Yanchen FAN for all the accompany and generous help during the past years. I will cherish the friendship and good times we spent together.

Finally, I would like to express my expression to my parents for their encouragement and unconditional support. Their unlimited love and unwavering support have given me the courage to overcome any difficulties in my life.

Table of Contents

Title Page		i
Authorization	Page	ii
Signature Page	3	iii
Acknowledgm	nents	v
List of Figures	5	X
List of Tables		xiv
Abstract		XV
CHAPTER 1	Introduction to Visible Light Communication	1
1.1 R	tesearch Background of VLC Technology	1
1.2 N	Notivation of Research	5
1.3 T	hesis Contributions	7
1.3.1 C	Contributions of CIS-based VLC System	7
1.3.2 C	Contributions of PD-based VLC System	8
1.4 O	Organize of Thesis	9
1.5 R	Leferences	10
CHAPTER 2	CMOS Image Sensor-based VLC Transceiver System	13
2.1 Ir	ntroduction of CIS-based VLC Transceiver System	13
2.2 D	Discrete VLC Transmitter	14
2.2.1	VLC Light Sources	14
2.2.2	2 VLC Modulator	15
2.2.3	Coding and Modulation Schemes	17
2.3 C	CMOS Image Sensor-based VLC Receiver	19
2.3.1	CMOS Image Sensors	19
2.3.2	2 Rolling Shutter Effects	20
2.3.3	Software Supported Receiver and Decoding Scheme	21
2.4 A	applications of CIS-based VLC System	22
2.4.1	·	
2.4.2		

	2.4.3 Vehicle Communication	24
2.5	References	
СНАРТІ	ER 3 Visible Light Communicati	ion Enabled Smart Home Control System with 3D
Indoor L	ocalization	
3.1	Introduction	
3.2	Related Works of Smart Home	e Control System29
3.3	Design of High-Power VLC L	ightbulb31
	3.3.1 Design of Power Manager	ment Block32
	3.3.2 Design of BLE Control C	Sircuit35
3.4	Theoretical Analysis of Propo	osed Smart Home Control System 36
	3.4.1 Architecture Design of Sr	mart Home Control with Cloud Server36
	3.4.2 Smart Home Control	l with Direction Angle Data Supported 3D
	Positioning	37
3.5	Smart Home Control System I	Prototype and Performance Evaluation39
	3.5.2 Performance Evaluation of	of CIS-based VLC Enabled Smart Home Control
	System.	43
	3.5.3 Verification of Direct	ctional Angle Data-Assisted 3D Indoor VLF
	Algorithm	44
3.6	References	46
CHAPTI	ER 4 Photodiode-based VLC Tra	ansceiver System50
4.1	Introduction of PD-based VLO	C Transceiver System50
4.2	Integrated VLC Transmitter	51
	4.2.1 Architecture of Integrated	1 VLC Transmitter 52
	4.2.2 Different Types of Light S	Sources53
	4.2.3 Modulation Scheme	
4.3	Integrated VLC Receiver	56
	4.3.1 Architecture of Typical P.	D-based VLC Receiver56
	4.3.2 Different Types of PDs	57
4.4	Equalization Schemes	57
	4.4.1 Passive and Active Equal-	izers

	4.4.2	Digital Based Equalization	58
	4.4.3	Hybrid Equalization	58
4.5	Ap	plications of PD-based VLC System	59
	4.5.1	High-speed Point-to-Point VLC	59
	4.5.2	Smart Display	60
	4.5.3	Underwater Communication	60
4.6	Re	ferences	61
СНАРТІ	ER 5	Design of PAM-4 VLC Transmitter with Feed Forward Equalization	64
5.1	Int	roduction	64
5.2	An	alysis of Modulation Bandwidth Extension Schemes	64
	5.2.1	Device Limitation	65
	5.2.2	Principle of PAM-4 Scheme	66
	5.2.3	Principle and Implementation of FFE	67
	5.2.4	Passive Equalizer	71
5.3	Arc	chitecture of Proposed PAM-4 VLC Transmitter with FFE	72
	5.3.1	Schematic of VLC Transmitter System	72
	5.3.2	Current-Steering DAC-based LED Driver	73
	5.3.3	Digital Baseband	74
5.4	Sin	nulation Results and Discussion	77
	5.4.1	Verification of Digital Baseband	77
	5.4.2	Verification of 6-bits DAC-based LED Driver	78
	5.4.3	Verification of Equalization Schemes	78
	5.4.4	Results Discussion	81
5.5	Re	ferences	81
CHAPTI	ER 6	Design of PAM-8 VLC Transceiver System Employing Neural Networ	k-based
FFE and	Post-E	qualization	83
6.1	Mo	odeling of Proposed PD-based VLC System	83
	6.1.1	μ-LED Model	83
	6.1.2	PD Model	85
	6.1.3	LOS Channel Model and Underwater Channel Model	85

		6.1.4	Bandwidth Limitation and Nonlinearity	88
	6.2	Lin	nk Budget Analysis	90
	6.3	An	alysis of Equalization Methods	93
		6.3.1	Passive Equalizer	94
		6.3.2	FFE	94
		6.3.3	DNN and RBF-NN	95
	6.4	Arc	chitecture of PD-based VLC Transceiver Circuits	98
		6.4.1	Transmitter in PD-based VLC System	99
		6.4.2	Receiver in PD-based VLC System	100
	6.5	Sin	nulation Results and Discussion	101
		6.5.1	Pre-equalization Performance Evaluation	102
		6.5.2	Post-equalization Performance Evaluation	105
		6.5.3	Training Performance Evaluation	107
	6.5.	4 Co	mparison with Other VLC Systems with Neural Network	109
	6.6	Re	ferences	110
CH	APTI	ER 7 (Conclusion, Future Work, and Publications	113
	7.1	Co	nclusion	113
	7.2	Fut	ture Work	115
	7.3	Pul	blications	117

List of Figures

Fig. 1.1. Electromagnetic spectrum with corresponding wavelength and frequency 2
Fig. 1.2. Illustration of principle of VLC technology
Fig. 1.3. Network topology of VLC system [1.3]: (a) Peer-to-peer topology; (b) Star topology;
(c) Broadcast topology
Fig. 1.4. Various applications of VLC technique in the indoor scenario [1.9]4
Fig. 2.1. System block diagram of CIS-based VLC transceiver
Fig. 2.2. VLC modulator block diagram in CIS-based VLC transmitter
Fig. 2.3. Encoding mechanisms of two types of RLL coding scheme
Fig. 2.4. Schematic of CMOS image sensor and the conversion in pixel
Fig. 2.5. Mechanism of rolling shutter effect adopted in CIS-based VLC system.
21
Fig. 2.6. Image processing and corresponding VLC ID code conversion in software supported
VLC receiver. 22
Fig. 3.1. Application scenarios of the proposed CIS-based VLC enabled smart home control
system
Fig. 3.2. Schematic of high-power LED lightbulb with VLC functionality
Fig. 3.3. Detailed design of power management circuits. (a) AD-DC converter circuit. (b) DC-
DC converter circuit
Fig. 3.4. Simulated waveforms of designed VLC-based LED lightbulb
Fig. 3.5. Process of VLC data transmission in BLE module
Fig. 3.6. Architecture of CIS-based VLC enabled smart home control system
Fig. 3.7. Imaging geometry of proposed direction angle data-supported 3D positioning system
[3.28]
Fig. 3.8. Details of PCB for the designed VLC LED lightbulb. (a) Schematic of LED and power
management board. (b) Schematic of BLE control board. (c) Layout of LED and power
management board. (d) Layout of BLE control board
Fig. 3.9. Prototype of VLC LED lightbulb
Fig. 3.10. Experiment setup for measuring the VLC link distance

Fig. 3.11. Impact of diffuser diameter and illuminance of lightbulbs on the VLC link distance.
(a) Diffuser diameter versus VLC link distance. (b) Illuminance versus VLC link distance 43
Fig. 3.12. Demonstration of the proposed CIS-based VLC enabled smart home control
system44
Fig. 3.13. Measured 3D world coordinates of camera with imagines captured at four
positions
Fig. 4.1. Architecture of traditional PD-based VLC transceiver system
Fig. 4.2. Typical architecture of integrated VLC transmitter
Fig. 4.3. Modulated waveforms of (a) OOK modulation scheme, and (b) PAM-4 scheme 55
Fig. 4.4. (a) Spectrum diagram of OFDM containing different subcarriers with frequency over-
lapping; (b) Constellation diagram of 16-QAM
Fig. 4.5. Typical architecture of PD-based VLC receiver
Fig. 5.1. (a) Typical equivalent circuit model of LED; (b) Simulated modulation bandwidth of
this LED model
Fig. 5.2. Principle of PAM-4 scheme corresponding eye diagram of PAM-4 signal
Fig. 5.3. (a) Principle of the waveform combination in FFE; (b) Improvement on the NRZ eye
diagram by adopting FFE
Fig. 5.4. Analysis of calculating the tap weights in FFE
Fig. 5.5. Implementation methods of applying a 3-tap FFE to transceiver circuits. (a) Analog
implementation method. (b) Digital implementation method
Fig. 5.6. Schematic of the adopted passive equalizer
Fig. 5.7. Architecture of proposed PD-based VLC transmitter system
Fig. 5.8. Schematic of current-steering DAC-based driver with CML structure74
Fig. 5.9. (a) Block diagram of 16 x 6 LUT in the digital baseband; (b) Schematic of 6-trasistor
SRAM cell; (c) Structure of 16:1 MUX and connection with LUT
Fig. 5.10. Mapping rule of LUT for selecting DAC input data according to FFE data76
Fig. 5.11. Simulated DAC input data with FFE data serving as selecting signal77
Fig. 5.12. Simulated waveforms of 6-bits DAC-based LED driver. (a) DAC input data. (b) DAC
output driving currents
Fig. 5.13. Simulated modulation bandwidth of transmitter

Fig. 5.14. Transient eye diagram simulation results of proposed PAM-4 VLC transmitter under
1.2 Gbps PAM-4 data transmission: (a) without equalization; (b) with both FFE and passive
equalizers80
Fig. 6.1. Compact equivalent circuit model of μ-LED
Fig. 6.2. Simulated and measured bandwidth curves of μ -LED.
Fig. 6.3. Equivalent circuit model of PD.
Fig. 6.4. Simulated path loss versus distance in free space channel and water channel 88
Fig. 6.5. Effects of limited bandwidth of LED at transmitted signal
Fig. 6.6. (a) Normalized spectrum response distribution of LED; (b) Responsivity curve of PD.
91
Fig. 6.7. BER performance of OOK, PAM-4, and PAM-8 modulation schemes versus SNR.92
Fig. 6.8. Simulated 20 W transmitted power through free space and water channel: (a) Received
optical power by PD versus communication distance; (b) Received photocurrent of PD versus
communication distance
Fig. 6.9. Analysis of receiver SNR versus distance in both free space and water channels 93
Fig. 6.10. Structure of NN-based FFE
Fig. 6.11. Structure of DNN.
Fig. 6.12. Structure of RBF-NN.
Fig. 6.13. Architecture of proposed PD-based VLC system
Fig. 6.14. Schematic of CML LED driver.
Fig. 6.15. Schematic of TIA circuit.
Fig. 6.16.(a) Calculated correlation coefficient for DAC input and output data versus DAC
resolution; (b) Calculated error rate for ADC input and sampled data versus ADC
resolution
Fig. 6.173 dB bandwidth extension of transmitter through using passive equalizer 104
Fig. 6.18. Eye diagrams of PAM-8 signal transmission with passive equalizers at LED output:
(a) 2.7 Gbps data rate without FFE; (b) 2.7 Gbps data rate with FFE; (c) 3.6 Gbps data rate
without FFE; (d) 3.6 Gbps data rate with FFE
Fig. 6.193 dB bandwidth and gain of receiver AFE including PD

Fig. 6.20.Simulated results of BER vs. data rate: (a) using RBF-NN or DNN as equalizer with
3 m free space channel; (b) through 3 m free space or 1.2 m water channel with RBF-NN106
Fig. 6.21. Simulated eye diagrams of PAM-8 signal with RBF-NN as post-equalizer: (a)
Communication data rate of 2.7 Gbps with 3 m free space channel; (b) Communication data
rate of 3.6 Gbps with 3 m free space channel; (c) Communication data rate of 3.3 Gbps with
1.2 m water channel; (d) Communication data rate of 4.2 Gbps with 1.2 m water channel 107
Fig. 6.22. Training convergence curves of RBF-NN: (a) for 2.7 Gbps data transmission; (b) for
3.6 Gbps data transmission
Fig. 6.23. Simulated results of training time vs. data rate with RBFNN or DNN as
equalizer

List of Tables

<u>Table 2.1 Operating Modes of Different PHYs for OWC System</u>	17
Table 3.1 Comparison of Related Works on Smart Home Control System	<u></u> 30
<u>Table 3.2 Component Values of Designed AC-powered VLC Lightbulb</u>	34
<u>Table 3.3 Measured Working State of Lightbulb</u>	42
<u>Table 3.4</u> <u>Measured Direction Angle, Coordinates and Positioning Error of Camera</u>	46
<u>Table 4.1 Comparison of Different Types of Light Sources</u>	54
<u>Table 5.1</u> Component Values of Equivalent LED Model	66
<u>Table 5.2 Analysis of Eye Diagram</u>	80
<u>Table 5.3 Performance Summary of Proposed PAM-4 VLC Transmitter</u>	81
<u>Table 6.1 Simulation Parameters for the VLC Link Model</u>	87
<u>Table 6.2 VLC Link Budget Calculation</u>	93
<u>Table 6.3 Comparison of RBF-NN and DNN</u>	98
<u>Table 6.4 Comparison of Neural Network Enabled VLC Systems</u>	110

Design of Optical Transceiver Systems for CMOS Image Sensor-based and Photodiode-based Visible Light Communication

by Bo XU

Department of Electronic and Computer Engineering

The Hong Kong University of Science and Technology

Abstract

Visible light communication (VLC) is the possible solution to radio-frequency spectrum congestion problem due to its sufficient electromagnetic bandwidth. This thesis focuses on the PCB level design of transmitter in CMOS image sensor (CIS)-based VLC system with smart home control application and schematic level design of PD-based VLC system with traditional feed-forward equalization (FFE) as well as neural network (NN)-based equalization to solve limitations.

In the first part, an AC-powered driverless VLC lightbulb is designed to provide practical implementation of CIS-based VLC system. It is adopted as beacon to transmit unique ID code in proposed VLC enabled smart home control system, which aims to solve low control accuracy and security issues in RF-based systems. A smartphone with control app serving as receiver works with cloud server to manage smart devices. A directional angle assisted indoor VLP algorithm for calculating user's 3D location is adopted to further improve security and control accuracy.

In the second part, to improve the communication data rate and scale down VLC transmitter size, an integrated PAM-4 VLC transmitter with both digital and analog equalizations is

proposed. A passive equalizer and digital FFE are adopted to extend the narrow bandwidth limited by LED. The highest transmission data rate of the proposed VLC transmitter is 1.2 Gbps.

In the third part, to overcome channel loss and further increase data rate, a PAM-8 VLC transceiver system which combines passive equalizer, NN-based FFE as pre-equalization and RBF-NN as post-equalization is presented. This VLC transceiver system is implemented in a co-simulation platform of MATLAB and Cadence with free-space and underwater channel models. This proposed VLC system can achieve the data rate of 3.6 Gbps with bit error rate of 3.8 x 10-3 with 3 m free space channel. The training time of RBF-NN is decreased for 86.7 % comparing with DNN.

CHAPTER 1 Introduction to Visible Light

Communication

1.1 Research Background of VLC Technology

In recent years, the number of smart devices which support the Internet of Things (IoT) has increased dramatically and it has been predicted that the number of global active IoT connections will reach 21.5 billion in 2025 [1.1]. With this rapid increase, radiofrequency (RF)based communication systems are facing a severe congestion problem due to the limited resource of spectrum bandwidth. As shown in Fig. 1.1, the spectrum bandwidth of the RF signal ranges from 20 kHz to 300 GHz which covers from the upper limit of audio frequency to the lower limit of infrared frequency, and the contained microwave covers 300 MHz to 300 GHz. To support billions of devices with 300 GHz frequency bandwidth, the radio spectrum for communication will be crowded. Therefore, exploring other spectrum resources and utilizing electromagnetic waves beyond 300 GHz for communication has attracted research focuses. Visible light owns a wide unlicensed spectrum starting from 430 THz to 790 THz as presented in Fig. 1.1, which is more than 1000 times wider compared with the radio spectrum. This sufficient bandwidth resource provides a possible solution to the radio spectrum congestion problem. Moreover, the lighting infrastructures utilizing LEDs as a light source have become the mainstream for illumination in the living environments due to its energy efficiency and high-intensity properties. The popularity of using LEDs to illuminate has brought the consideration of combining illumination with communication. The technology of utilizing visible light as a signal carrier to transmit communication data is called visible light communication (VLC) [1.2], which is normally realized by the high-speed switching of a light source. When the switching frequency of a light source is higher than the refresh rate of human eyes, people will not experience the flicker of the light source. Since LED can support highfrequency switching and can be modulated with its driving current, it has become the suitable light source for delivering the transmitted data in VLC technology.

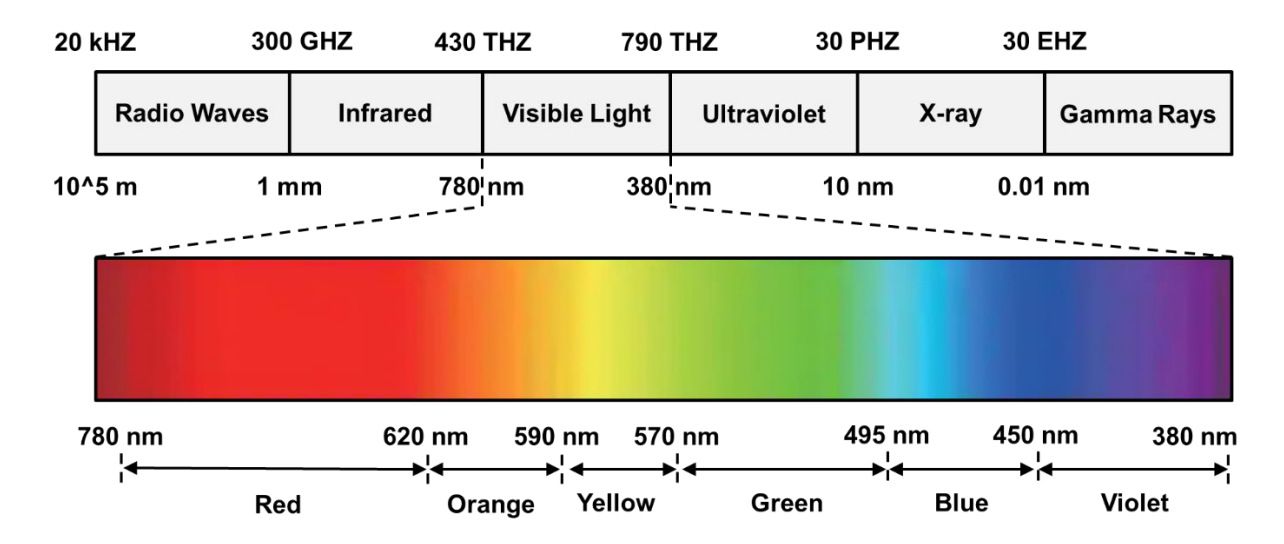


Fig. 1.1. Electromagnetic spectrum with corresponding wavelength and frequency.

A simple illustration of VLC technology is presented in Fig. 1.2. The visible light is utilized as a medium to transmit data through modulating the light source. The modulation of the light source corresponds with the electrical signal with the mapping rule that the off-state represents data "0" and on-state represents "1". A photodiode (PD) or CMOS image sensors (CISs) with corresponding receivers will recover the data from the optical signal while humans only notice the light. These two types of receivers have their own advantages and can be adapted to different applications. For the PD-based VLC transceiver system, it is suitable for high-speed communication scenarios with a dedicated receiver, and it can be utilized to transmit signals with a data rate as high as Gbps. For the CIS-based VLC transceiver system, the more appropriate occasion is combining with existing mobile devices such as smartphones and robots to conveniently constitute a VLC system, and its data rate is normally low due to the image-based decoding process.

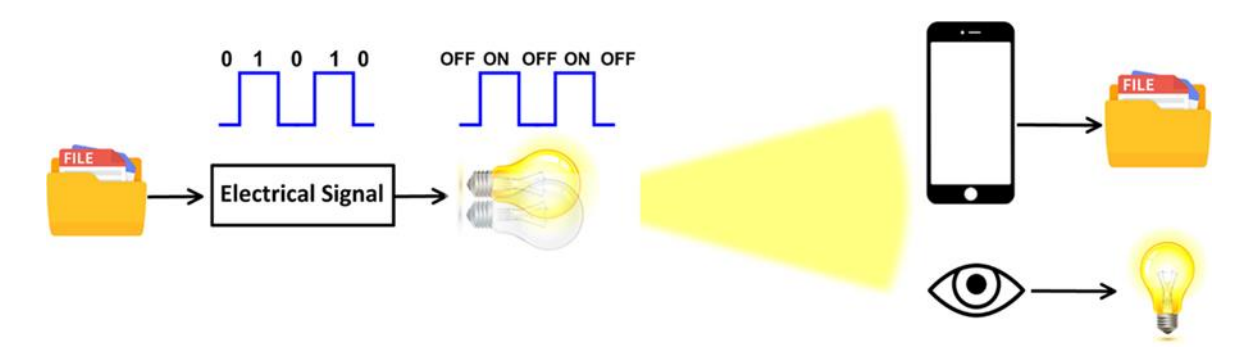


Fig. 1.2. Illustration of principle of VLC technology.

The IEEE standard association has published guidance for designing the VLC system which is IEEE 802.15.7 [1.3]. This standard classifies the devices involved in optical wireless communication (OWC) into three classes: infrastructure, mobile, and vehicle. According to this standard, the highest-level design standard of the VLC system, which is the network topology, can be divided into three categories according to the connection methods among devices. As shown in Fig. 1.3, these three network topologies are peer-to-peer topology, star topology, and broadcast topology. The peer-to-peer topology is the simplest and most basic structure among these three networks, and it allows two devices to communicate with each other in a two-way communication method. This network topology is suitable for point-to-point high-speed VLC systems. The star topology is presented in Fig. 1.3. (b) and it can support multiple devices with two-way communication. One device serves as the coordinator while other devices are the clients. This network topology is suitable for wireless access points but suffers from the problem of channel interference. The broadcast topology is a one-way communication method, in which one device broadcasts information to other devices without the uplink. This topology is suitable for low-speed VLC systems such as an advertising system, indoor positioning system, and an indoor navigation system.

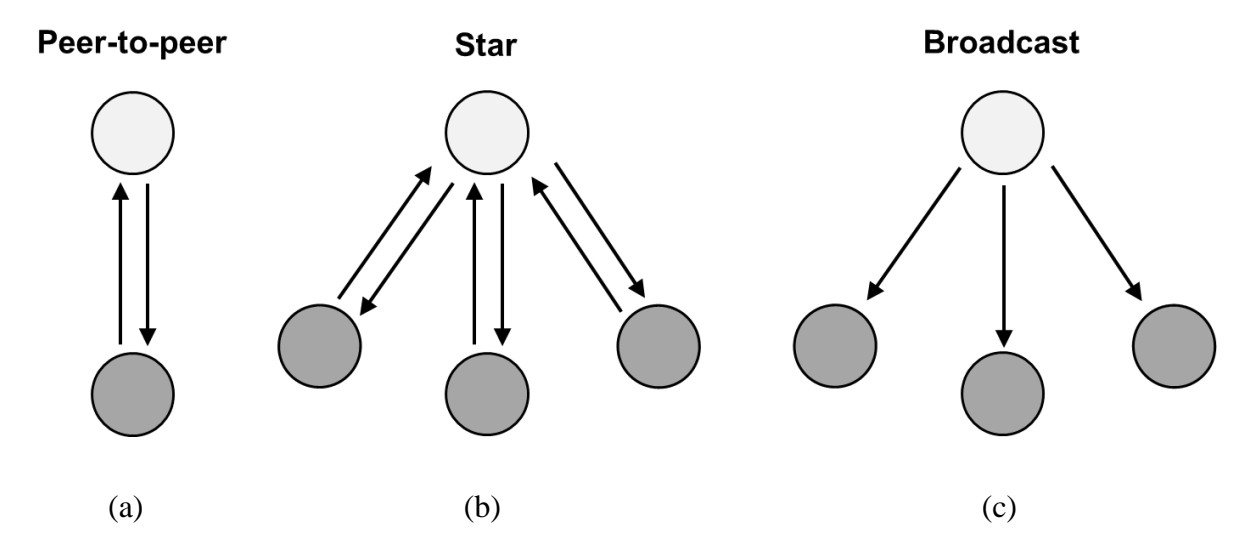


Fig. 1.3. Network topology of VLC system [1.3]: (a) Peer-to-peer topology; (b) Star topology; (c) Broadcast topology.

VLC technology features enormous spectrum bandwidth, compliant with existing infrastructures, has no electromagnetic interference (EMI), and has high communication security due to the characteristics of visible light. Since the conventional RF-based communication systems are congested and suffer from EMI as well as safety issues. These characteristics of visible light promise the VLC transceiver systems as a supplementary solution for the RF-based communication systems, especially for the occasions where RF-based systems suffer from challenges. The applications of VLC systems are various such as information broadcasting [1.4], indoor positioning [1.5], smart wearable display [1.6], underwater communication [1.7], and vehicle communication [1.8]. As presented in Fig. 1.4, there are various applications provided by the VLC technique in the indoor environment. The VLC light source can provide illumination with data transmission and serve as a data access point to the devices within the cover range of the light source and support these devices to access the internet. The downlinks are supported by VLC to guarantee high-speed data transmission for television, mobile devices, and desktops. The uplink can adopt the RF-based communication method for simplifying the handshake and data transfer to finally realize a two-way communication system. The VLC light source can be managed by the light control module to flexibly adjust the luminance and color temperature.



Fig. 1.4. Various applications of VLC technique in the indoor scenario [1.9].

1.2 Motivation of Research

The VLC system can be divided into two categories according to the light signal detector in the receiver, which are the CIS-based VLC system and the PD-based VLC system. The first type of VLC system is suitable for mobile devices equipped with CIS, and it is widely adopted in the indoor positioning system. The second type of VLC system is designed for higher speed communication with dedicated receiver equipped with PD, and it can be utilized to realize point-to-point communication in various occasions.

The CIS-based VLC system is suitable for indoor VLP applications and can be applied to IoT systems. However, the present CIS-based VLC system has several disadvantages such as a large external LED modulator, and a lack of convenient implementation methods of changing the data [1.10]. A dedicated LED modulator with a more compact size can contribute to reduce the power consumption of VLC lights and the cost of manufacture. Moreover, with a compact scale, the LED modulator can be integrated into the VLC lights so that no extra space is wasted for installing the modulator. For the method of revising transmitted data, the traditional method of changing the data is complicated, which requires the rewrite process through an external programmer. If the process of rewriting data can be executed remotely with real-time control, managing transmitted data will be convenient. Besides, for the IoT application based on RFbased communication systems, the safety issue [1.11] and accurate control remain as challenging problems due to the complex encryption algorithm and information disclosure caused by RF signals. However, CIS-based VLC has implementation challenges which prevent its widespread usage in real-world applications. VLC hardware currently reported in the literature is mainly based on experimental prototypes and do not meet the requirements for practical deployment including compact size, low power consumption, compatibility with existing lighting infrastructure in homes, e.g., light sockets, remote connectivity, and support of a smartphone as the signal receiving and controlling device. Therefore, there exists a need for development of compact LED modulator hardware that can be easily integrated in the existing form factors of residential lighting at low cost and low power consumption, and comes with a standard socket that can allow for direct plug-n-play installation. In addition, the LED

modulator hardware should come with remote connectivity based on existing wireless technologies for establishing a wireless uplink via smartphone.

In this thesis, a dedicated designed VLC modulator for CIS-based VLC system is proposed to provide a compact LED modulator that be installed into the VLC light source. A remote-control method through Bluetooth is also proposed for revising the transmitted data, which also simplifies the management of multiple VLC light sources. A CIS-based VLC system is designed and implemented for the IoT application with Bluetooth remote control of light source, and this system contributes to the smart home control system in the aspect of improving information security through the VLC technique. Moreover, the research on CIS-based VLC system supported smart home control system also aims to increase the low control accuracy problem in RF-based control systems through the VLP technique.

However, the design of CIS-based VLC system owns several disadvantages. Firstly, the VLC lightbulb serves as a signal beacon and transit VLC ID code, it introduces the requirement of implementing a VLC transmitter for real VLC data transmission. Secondly, the design of low speed VLC system is based on discrete components which causes noise, large parasitic components, and increases the system scale and power consumption. Thirdly, the designed low speed VLC system lacks high-order modulation schemes, pre- and post-equalizations for overcoming the device and channel limitations as well as increasing the communication data rate. Since the PD-based VLC system is designed for high-speed VLC to transmit real VLC data instead of ID code and is normally adapted to point-to-point communication, integrated design is an important solution for the PD-based VLC system to overcome the mentioned drawbacks of CIS-based VLC system. A highly integrated VLC system can reduce the parasitic components so that the modulation bandwidth of the whole system can be extended, and the noise effect can also be mitigated. For the previous research on integrated VLC system design, most merely focus on circuit design and neglect the study of equalization methods which causes a rather low communication data rate for the integrated VLC system. In the integrated PD-based VLC system, the major limitation on modulation bandwidth is caused by the intrinsic parasitic capacitance of the LED device. Through applying the pre- and post-equalization schemes to the transmitter and receiver, this bandwidth limitation can be alleviated, and the overall transmission data rate can be increased. Moreover, with high-order modulation, the efficiency of channel modulation bandwidth can be improved thus contributing to the communication data rate. Compared with the discrete PD-based VLC system, the research on high-order modulation schemes is also neglected. In [1.12], a fully integrated VLC transmitter is designed and implemented in 0.35 um process with 266 kbps data rate. [1.13] proposed a micro-LED display driver with VLC transmitter implemented in 0.5 um process to achieve a data rate of 1.25 Mbps. [1.14] presented a VLC receiver with an ambient light rejection function with a data rate of 24 Mbps at a 1.6 m distance. In [1.15], a fully integrated receiver in 0.13 um technology for visible laser communication is presented with a maximum data rate of 500 Mbps. However, it can be noticed that all of these works only focus on the design of either the transmitter or the receiver without systematically evaluating the integrated transceiver system. Besides, these integrated design works perform with a rather low data rate compared with the discrete PD-based VLC transceiver systems [1.16]-[1.17] due to the lack of suitable equalization schemes as well as high-order modulation schemes.

The research on PD-based VLC system design in this thesis not only focuses on the integrated circuit design which includes analog front-ends of VLC transceiver but also explores the hybrid equalization schemes such as passive equalizer, digital-based FFE and neural network-enabled digital equalization. High-order modulation schemes are also studied for making up for the overlook in previous integrated VLC system designs. Moreover, to systematically analyze the limitations in the communication channel, modelling of LED and PD devices is also included. To completely analyze the performance of PD-based VLC system, comparison of using different channel models is important. Modeling of both free space channel and water channel are conducted with a mathematical discussion of the channel loss.

1.3 Thesis Contributions

1.3.1 Contributions of CIS-based VLC System

The thesis contributions to CIS-based VLC system and its application areas are summarized below:

- 1. A smart home control system via the combined usage of VLC and RF communication is proposed. The method provides precise and secure management of multiple smart devices through VLC by dividing the control region into distinct zones based on the position of the user. In addition, we describe and experimentally validate the system implementation architecture that illustrates how to integrate three key elements i.e., VLC lightbulb, smartphone application, and cloud-based server to build a scalable SHS.
- 2. The design of a driver-less AC-powered VLC lightbulb with wireless control via Bluetooth is presented to support plug-n-play capability into standard electrical sockets at home. Through experimental verification, we demonstrate that the proposed lightbulb meets the practical requirements of deployment in a real-life environment by supporting illumination, communication, and high-accuracy positioning, simultaneously.
- 3. A directional angle-assisted 3D indoor VLP algorithm is proposed to calculate the world coordinates of the user. This algorithm can be adopted in smart home control systems for orientation-based and location-based control applications, such as directional control, specific point management and navigation for robots to increase accuracy, security and diversity.

1.3.2 Contributions of PD-based VLC System

The thesis contributions to the integrated transceiver design of PD-based VLC system are summarized below:

- A PAM-4 VLC transmitter is proposed for the high-speed PD-based VLC system. This
 VLC transmitter utilizes an integrated structure to decrease system size and parasitic
 components. It combines FFE implemented in the digital baseband with analog-based
 passive equalizer to extend the limited bandwidth.
- A high-speed PAM-8 VLC transceiver system is proposed and simulated through the cooperation of MATLAB and Cadence. The analog front-end of transmitter and receiver, LED model, LOS channel model, and PD model are both designed in Cadence, while the

- digital baseband, binary-weighted DAC in transmitter and flash ADC in receiver are implemented in MATLAB.
- 3. Neural network (NN)-based equalization schemes are proposed and adopted as the pre- and post-equalization schemes in this PAM-8 VLC system. In the transmitter, FFE is implemented through a traditional NN, which is applied in the baseband for modulation bandwidth extension with the benefits of higher accuracy of the tap weights. In the receiver, a radial basis function neural network (RBF-NN) is proposed and adopted as the post-equalization scheme in the baseband, which is utilized to compensate for channel loss and solve the problems of modulation bandwidth limitation. With the RBF serving as an activation function, this post-equalization can achieve much better performance compared with traditional deep neural network (DNN) based equalization. With the cooperation of NN-based FFE and analog-based passive equalizers severing as pre-equalization and the RBF-NN designed as post-equalization, the achievable highest data rate with 3 m free space channel is 3.6 Gbps.
- 4. Different communication channels have been taken into consideration and compared for the designed PAM-8 VLC system. The proposed NN supported PD-based VLC transceiver system is also applied to realize underwater VLC. A water channel model is designed and analyzed for simulating the performance of underwater VLC with same transceiver. This underwater VLC system is compared with experimental results and verified the feasibility of proposed hybrid equalization scheme in water channel.

1.4 Organize of Thesis

The rest of this thesis are organized as follows. In chapter 2, a brief introduction for the CIS-based VLC system is presented. The optical devices, detailed structures of transmitter and receiver, as well as the typical coding, modulation and decoding schemes are discussed. Then the common applications of CIS-based VLC system are presented. In chapter 3, a specific CIS-based VLC system is designed and fabricated. It is applied to support a smart home control system providing high precision indoor localization for users. Both the experimental and measured results are presented to verify the feasibility of this system. Chapter 4 systematically

introduces the PD-based VLC system including its optical devices, typical architectures of transmitter and receiver, analysis of transmission channel, different equalization schemes, and common applications. In chapter 5, the design of a high-speed PAM-4 VLC transmitter with feed-forward equalization is described. This transmitter will be adopted into the PD-based VLC system, and it utilizes a high-order modulation scheme as well as passive equalizer and FFE to extend limited modulation bandwidth. The simulation results prove the feasibility of this proposed VLC transmitter. In chapter 6, a PAM-8 VLC transceiver system with hybrid equalization schemes is proposed. Modelling and link budget analysis of free space and water channels are presented. Passive equalizer, FFE and neural are adopted as the pre-equalization while network-based equalizer is used as the post-equalization. The simulation results validate the proposed hybrid equalization scheme in both free space channel and water channel. Finally, chapter 7 concludes this thesis and presents future works.

1.5 References

- [1.1] C. Perera, A. Zaslavsky, P. Christen and D. Georgakopoulos, "Context Aware Computing for The Internet of Things: A Survey," in *IEEE Communications Surveys & Tutorials*, vol. 16, no. 1, pp. 414-454, First Quarter 2014.
- [1.2] T. Komine and M. Nakagawa, "Fundamental analysis for visible-light communication system using LED lights," in *IEEE Transactions on Consumer Electronics*, vol. 50, no. 1, pp. 100-107, Feb. 2004.
- [1.3] IEEE Standard for Local and Metropolitan Area Networks—Part 15.7: Short-Range Wireless Optical Communication Using Visible Light, *IEEE Std* 802.15.7-2011, Sep. 2011.
- [1.4] H. Ma, L. Lampe and S. Hranilovic, "Coordinated Broadcasting for Multiuser Indoor Visible Light Communication Systems," in *IEEE Transactions on Communications*, vol. 63, no. 9, pp. 3313-3324, Sept. 2015.
- [1.5] Y. Zhuang, et al., "A Survey of Positioning Systems Using Visible LED Lights," in *IEEE Communications Surveys & Tutorials*, vol. 20, no. 3, pp. 1963-1988, third quarter 2018.

- [1.6] X. Li, B. Hussain, J. Kang, H. S. Kwok and C. P. Yue, "Smart µLED Display-VLC System With a PD-Based/Camera-Based Receiver for NFC Applications," in *IEEE Photonics Journal*, vol. 11, no. 1, pp. 1-8, Feb. 2019.
- [1.7] H. M. Oubei, et al., "Performance Evaluation of Underwater Wireless Optical Communications Links in the Presence of Different Air Bubble Populations," in *IEEE Photonics Journal*, vol. 9, no. 2, pp. 1-9, Apr. 2017.
- [1.8] I. Takai, T. Harada, M. Andoh, K. Yasutomi, K. Kagawa and S. Kawahito, "Optical Vehicle-to-Vehicle Communication System Using LED Transmitter and Camera Receiver," in *IEEE Photonics Journal*, vol. 6, no. 5, pp. 1-14, Oct. 2014.
- [1.9] Dilukshan Karunatilaka, et al., "LED based indoor visible light communications: state of the art," in *IEEE Communications Surveys & Tutorials*, vol. 17, no. 3, pp. 1649–1678, Mar. 2015.
- [1.10] S. Shao, et al., "An Indoor Hybrid WiFi-VLC Internet Access System," in 2014 IEEE 11th International Conference on Mobile Ad Hoc and Sensor Systems, 2014, pp. 569-574.
- [1.11] K. Zhao and L. Ge, "A Survey on the Internet of Things Security," in 2013 Ninth International Conference on Computational Intelligence and Security, 2013, pp. 663-667.
- [1.12] F. Che, L. Wu, B. Hussain, X. Li and C. P. Yue, "A Fully Integrated IEEE 802.15.7 Visible Light Communication Transmitter With On-Chip 8-W 85% Efficiency Boost LED Driver," in *Journal of Lightwave Technology*, vol. 34, no. 10, pp. 2419-2430, May, 2016.
- [1.13] L. Wu, et al., "An AMLED microdisplay driver SoC with built-in 1.25-Mb/s VLC transmitter," in 2015 Symposium on VLSI Circuits (VLSI Circuits), 2015, pp. C328-C329.
- [1.14] X. Li, B. Hussain, L. Wang, J. Jiang and C. P. Yue, "Design of a 2.2-mW 24-Mb/s CMOS VLC receiver SoC with ambient light rejection and post-equalization for Li-Fi applications," in *Journal of Lightwave Technology*, vol. 36, no. 12, pp. 2366-2375, 15 June15, 2018.
- [1.15] J. Kosman, et al., "29.7 A 500Mb/s -46.1dBm CMOS SPAD receiver for laser diode visible-light communications," in 2019 IEEE International Solid-State Circuits Conference-(ISSCC), 2019, pp. 468-470.
- [1.16] Y. Wang, L. Tao, X. Huang, J. Shi and N. Chi, "8-Gb/s RGBY LED-based WDM VLC system employing high-order CAP modulation and hybrid post equalizer," in *IEEE Photonics Journal*, vol. 7, no. 6, pp. 1-7, Dec. 2015

[1.17] T. Z. Gutema, H. Haas and W. O. Popoola, "WDM Based 10.8 Gbps Visible Light Communication with Probabilistic Shaping," in *Journal of Lightwave Technology*, 2022 (Early Access).

CHAPTER 2 CMOS Image Sensor-based VLC Transceiver System

2.1 Introduction of CIS-based VLC Transceiver System

CMOS image sensor (CIS) is widely adopted in various smart mobile devices as the camera, and CIS can be utilized to covert the visible light to pixel images. Therefore, using the CIS to receive visible light signal is possible and a VLC system based on CIS is proposed [2.1]. The traditional CIS-based VLC transceiver system is utilized to transmit the visible light signal from LED light source to smart mobile devices and it consists of transmitter utilizing illuminating lights and receiver based on camera sensors. As shown in Fig. 2.1, the typical transmitter in CIS-based VLC system is comprised of ID controller unit, OOK modulator and LED driver. The modulated signal will be sent to the LED light in the manner of controlling the on and off states of the light, therefore, the ID data can be transmitted as a light signal. For the receiver of CIS-based VLC system, this light signal will be detected by the image sensors of mobile devices and captured as images with patterns. Then the process of these captured images will be performed in software to get the transmitted data.

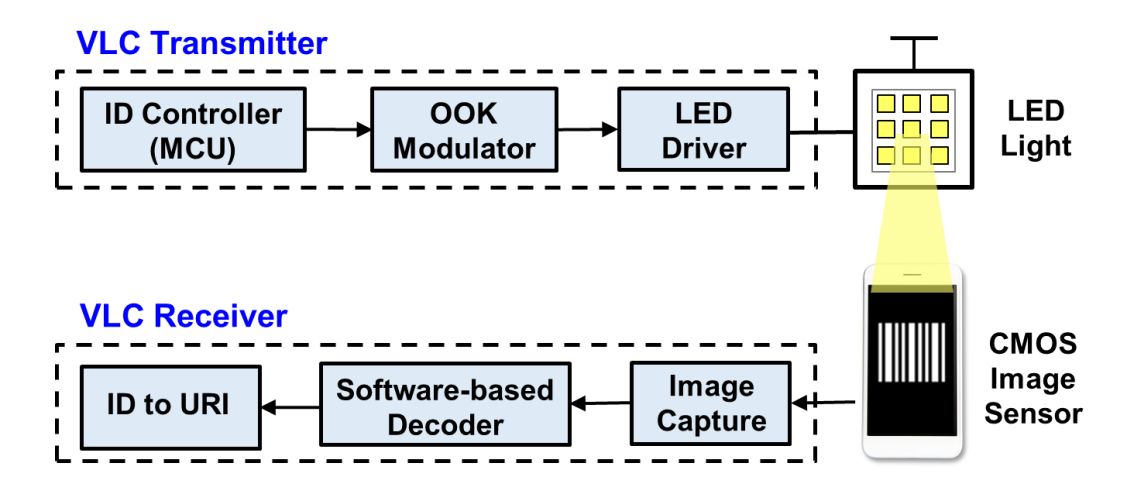


Fig. 2.1. System block diagram of CIS-based VLC transceiver.

CIS-based VLC transceiver system owns several advantages in practical applications [2.2]. Firstly, this system structure is simple and convenient to realize. For the VLC transmitter, it can

be realized by changing the existing illumination infrastructures to signal sources through adding a dedicated modulator between the power source and the LED light; for the VLC receiver, it simply utilizes the ubiquitous smart mobile devices to process the transmitted signals. Secondly, this system is scalable since it can be utilized for the cooperative work with existing RF-based networks such as Wi-Fi, Bluetooth, and Zig-Bee. Moreover, it can support multiple mobile devices to work synchronically. Lastly, this system is flexible and can be combined with many other applications such as indoor positioning systems, robot navigation and smart home systems. However, the CIS-based VLC transceiver system also suffers from disadvantages, especially a low communication data rate. The data rate of the CIS-based VLC system is limited by the characteristic of CIS that it can only recognize low-frequency signals, as well as the narrow channel bandwidth caused by the white LED light source.

Taking the system structure and the advantages mentioned before into consideration, the CIS-based VLC transceiver system can be applied to the existing infrastructures. The transmitter can be transformed from the illumination structures, and this will convert the normal lights to smart light source. The receiver is smart mobile devices such as smartphones, smart tablets, and robots. Therefore, the main application scenarios of CIS-based VLC transceiver system are smart lighting, indoor visible light positioning (VLP) and vehicle communication.

2.2 Discrete VLC Transmitter

In CIS-based VLC transceiver system, the transmitter is usually constructed by discrete components for the purpose of cost effective and easy to implement. The typical structure of discrete VLC transmitter is presented in Fig. 2.1, and it can be divided into two main blocks named as VLC light source and VLC modulator separately.

2.2.1 VLC Light Sources

For the VLC light source, since CIS-based VLC system is normally combined with existing illumination infrastructures, the common light sources are commercial white LED luminaires which can be classified into two categories.

- 1. The blue LED with phosphor coating [2.3]. This type of white LED generates blue light from the LED chip and covers this chip with a yellow phosphor coating. After transverses through the coating, the blue light combining with the yellow phosphor filter is converted to white light. For a VLC system, this type of light source is cost-effective but has a quite narrow communication bandwidth due to the filtering of phosphor coating.
- 2. The red-green-blue (RGB) combination LEDs [2.4]. This type of white LED directly mixes red, green, and blue lights with appropriate wavelengths together to produce white light. This RGB LED without the attenuation of phosphor coating owns a wider communication bandwidth comparing with the first type. However, it increases the cost of manufacturing the LED lights since it consists of three different LED chips in one package.

Light source is one main factor that limits the data rate of CIS-based VLC system. These commercial white LEDs own large turn-on and turn-off time which can be 20 ns to 100 ns due to the large intrinsic junction capacitance of LED up to 5 nF and parasitic capacitance of traces as well as support circuits [2.5]. The large capacitance increases the RC time constant τ of LED which means that it requires longer time to reach the steady state and causes the latency. This long latency of switching time leads to the limitation of flicking frequency to less than 10 MHz in the worst case. Therefore, using OOK modulation to transmit data directly can be limited to a maximum data rate of 10 Mbps. Moreover, the phosphor coating also increases the switching time of LED due to the excitation process of phosphors for emitting lights. As for the modulation bandwidth of LED, it is also limited by this large intrinsic junction capacitor since the modulation bandwidth is inversely proportional to the value of capacitor. And the typical modulation bandwidth of commercial LED is 5-20 MHz.

2.2.2 VLC Modulator

There are two types of CIS-based VLC transceiver system, the first one is directly transmitting data sequence containing communication information to the receiver; the second one is sending an ID code instead of data signal and the corresponding data is stored in cloud server. Since the communication data rate of CIS-based transceiver system is normally as low as several kbps to several Mbps, the second type of system is more widely adopted. The ID code transmission will

transform the light source to a beacon so that to fully utilize the limited data rate for realizing complex functions. The block diagram of CIS-based VLC modulator is presented in Fig. 2.2 and it consists of power management circuits, ID controller with communication module, OOK modulation circuit and LED driver circuit.

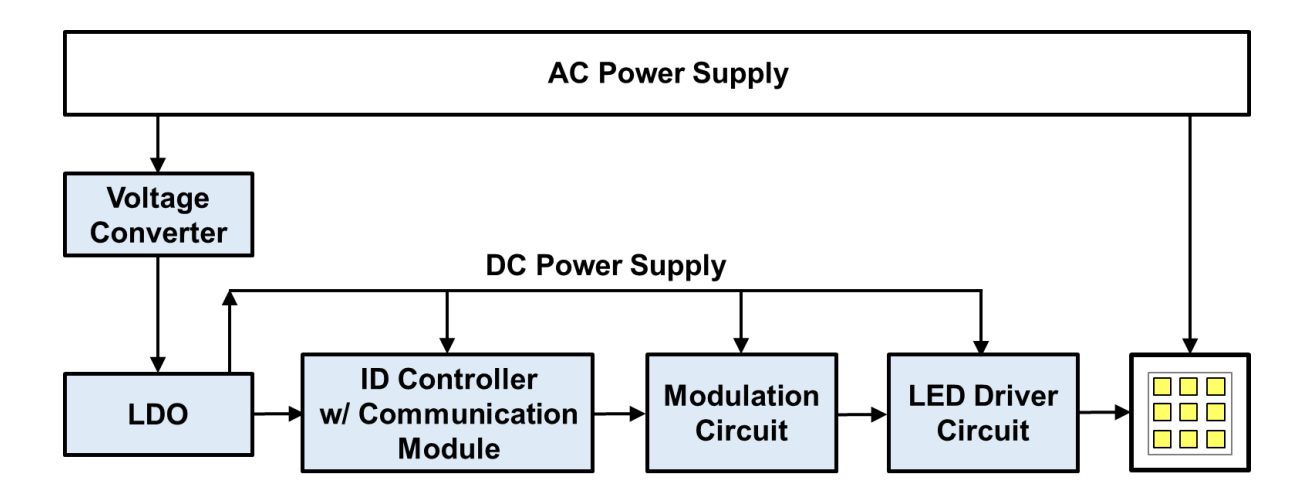


Fig. 2.2. VLC modulator block diagram in CIS-based VLC transmitter.

Since most of the lighting infrastructures are supplied by an AC power source while the ID controller, modulator, and LED driver re a DC power supply, the power management circuit is necessary in the VLC modulator. In the power management circuits, an AC-DC converter circuit will first convert the AC input voltage to a DC output and send it to the following LDO unit. The LDOs will adjust the DC output from the converter to different DC supply voltages according to the voltage requirements of subsequent modules. The ID controller is a microprogrammed control unit (MCU) where the data of the ID code can be written in and stored. This ID code will be sent out through the I/O port to the following OOK modulator. Moreover, to simply change the stored ID code in the modulator and improve the scalability of the CIS-based VLC transmitter, a communication module is added to the ID controller unit. With this communication module, the ID code can be changed remotely through Bluetooth or Wi-Fi. In the modulation circuit, this ID code data will be converted to a corresponding voltage signal with OOK modulation to control the working state of the LED driver. To save the whole area of the VLC modulator, a high threshold MOSFET is normally designed as the LED driver to manage the on and off states of the light source by connecting the voltage signal from the

OOK modulator to the gate of this MOSFET. Therefore, the VLC modulator will modulate the visible light with stored ID code and realize the function of light signal generation.

2.2.3 Coding and Modulation Schemes

IEEE 802.15.7 standard [2.6] has defined the physical layer (PHY) and medium access control (MAC) sublayer utilized for short-range optical wireless communication (OWC) system, which includes VLC system. According to this standard, the coding and modulation scheme for CIS-based VLC system with different data rate ranges are presented in table 2.1. For the PHY-I, since this layer is designed for short frames, it can support Reed-Solomon (RS), convolutional coding (CC) and run-length limiting (RLL) coding schemes. The communication data rate of this layer is lowest so that its modulation mode is simple scheme like on-off keying (OOK) and variable pulse position modulation (VPPM). For the PHY-II, its data rate is medium so that it only support RS and RLL coding schemes with same modulation methods as PHY-I. For the PHY-III, its data rate is highest, so it utilizes RS coding for long frame and CSK modulation to increase data rate.

Table 2.1 Operating Modes of Different PHYs for OWC System

PHY Type	Coding Scheme	Modulation	Data Rate
PHY-I	RS, CC, RLL	OOK, VPPM	11.67 – 266.6 kbps
PHY-II	RS, RLL	OOK, VPPM	1.25 – 96 Mbps
PHY-III	RS	CSK	12 – 96 Mbps

The discrete VLC transmitter suffers from the flicker problem and unbalanced DC level when the working state of the light source is directly determined by transmitted data. This problem can be solved by the RLL coding scheme since it can adjust the DC level in the manner of changing the ratio of turn-on and turn-off time to a constant value. Therefore, RLL coding scheme is widely adopted in CIS-based VLC transmitters to balance DC level, mitigate light source flicker and recover clock. There are two types of RLL coding schemes: the Manchester

coding and the 4B6B coding [2.7]. The mechanisms of these two coding schemes are presented in Fig. 2.3. It can be noticed that the Manchester coding scheme translates the original bit "0" to two bits "01" and the bit "1" to "10" so that to keep the ratio of "0" to "1" as a constant value of 50%. For the 4B6B coding, it follows the coding schedule from 4 bits to 6 bits while guaranteeing the constant duty ratio of 50%. Although these two coding schemes ensure the 50% duty ratio, they reduce the communication data rate by the factor of 1/2 and 2/3 separately.

The typical modulation schemes in CIS-based VLC systems are OOK and VPPM since the data rate is relatively low. OOK is one of the simplest modulation schemes and it works with Manchester coding scheme. It directly converts the encoded bit "0" to the low voltage level while converting the bit "1" to the high voltage level. For the VPPM, it cooperates with the 4B6B coding scheme and utilizes the position of pulse to represent encoded data. If the pulse locates at the left side of one symbol period, it represents logic "0". Correspondingly, the right-side position represents logic "1". The pulse width can be changed according to the requirement of light luminance. With a higher duty ratio in each symbol period, the luminance of the VLC light source will also increase.

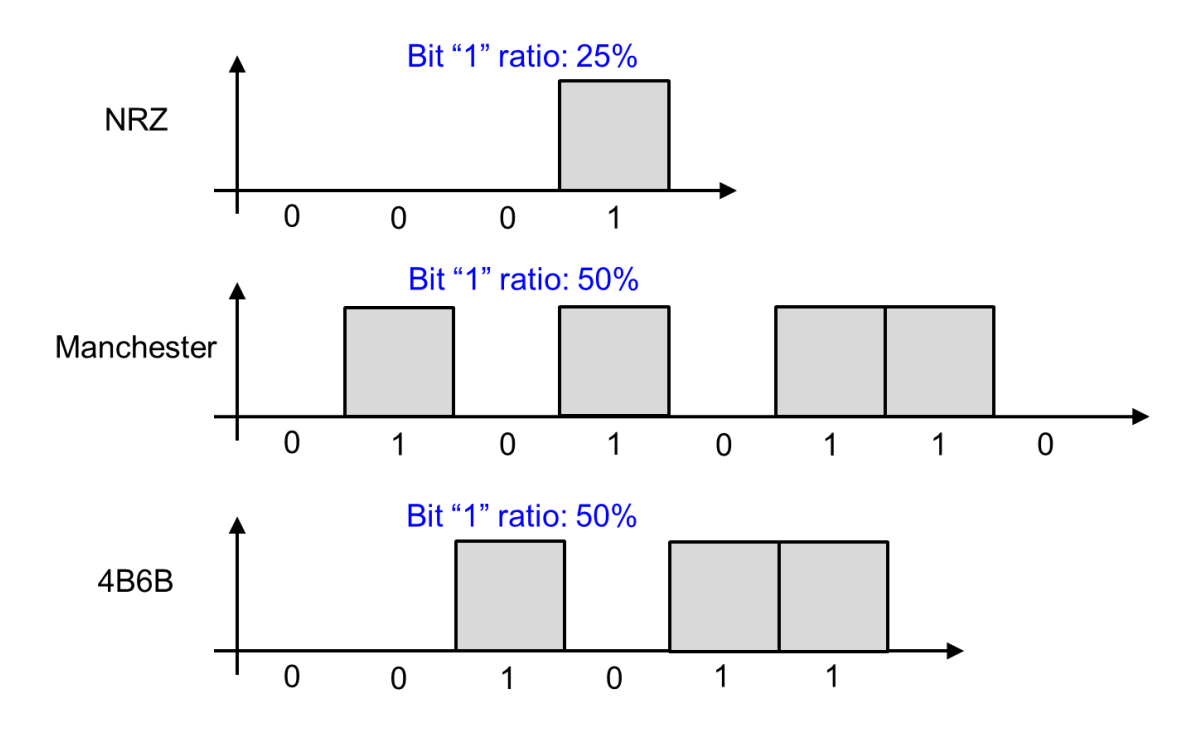


Fig. 2.3. Encoding mechanisms of two types of RLL coding scheme.

2.3 CMOS Image Sensor-based VLC Receiver

CIS-based VLC receiver normally consists of a camera as a light detector and a software-supported receiver built into the smart mobile device. The camera will convert the light signal to pixel patterns and the process of the captured patterns will be performed in software programs. After image processing, a binary data sequence can be acquired, and it will be decoded to get the originally transmitted data. If this data is an ID code, it will be sent to the back-end cloud server for more information.

2.3.1 CMOS Image Sensors

CMOS image sensor is the device where light is transformed into the digital signal output. The schematic of CIS and the conversion process in the pixel are presented in Fig. 2.4. The left side shows the architecture of CIS, and it consists of an image sensor pixel array, a row select logic circuit, a column select logic circuit, an analog amplifier, and an analog to digital converter (ADC) circuit [2.8]. All circuit blocks and the sensor array are integrated together in a single chip. The right side presents the signal conversion process in each pixel unit. Firstly, the visible light signal from the light source is detected by the photosensitive diode in the sensor array where the photoelectric effect happens, and the electrons are generated from photons and stored in the junction capacitor. Secondly, the row and column select logic circuits choose the corresponding pixel with the time sequence control signal, then the CMOS in this pixel conduct and the stored voltage is read out as photoelectric current to the analog amplifier. Thirdly, the generated current signal is amplified to a voltage signal and the SNR is also increased. Lastly, the amplified voltage signal is converted to digital output signal through ADC.

Background light can lead to noise and interfere the signal transmission in VLC system. For the CIS-based VLC system, it owns the advantage that it can automatically filter out the background light noise. Since the ambient background light is several orders of magnitude less than the visible light signal itself, when the camera sensitivity is set to be as low as only the direct visible light signal can be detected by the image sensor through changing the ISO of camera, the weaker background light noise cannot generate photoelectric current in the image

senor pixels due to the sensitivity limitation. Therefore, the background noise is filtered by the CIS automatically. As for the reflected lights, they can also be filtered out automatically by the CIS to get rid of the multi-path interference. Due to the propagation loss of channel and absorption of reflector, the strength of reflected light signals is also several orders of magnitude less than the original visible light signal. Similar as the background light, the reflected lights can be filter out by decreasing the sensitivity of camera.

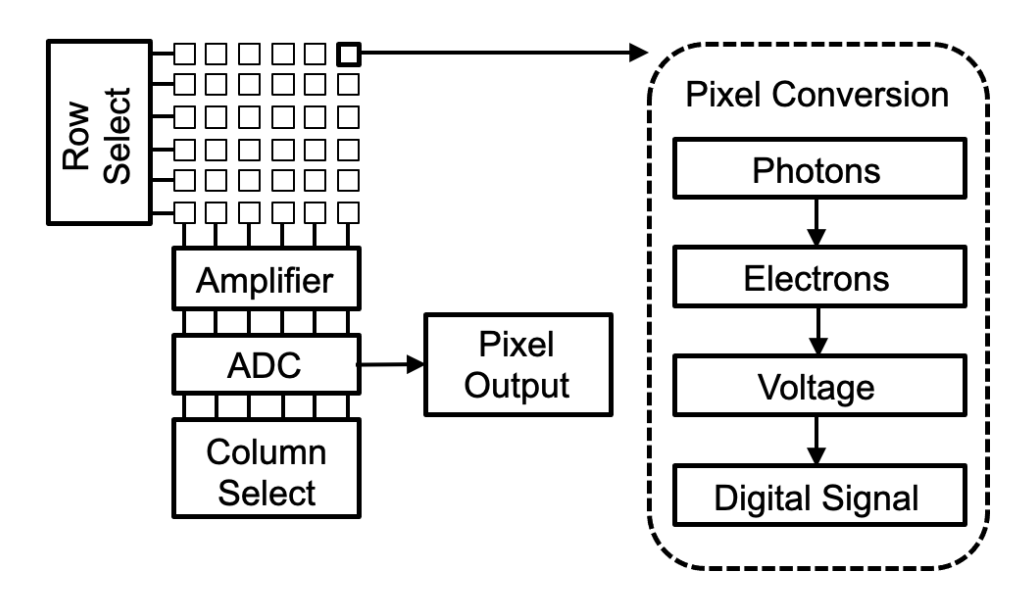


Fig. 2.4. Schematic of CMOS image sensor and the conversion in pixel.

2.3.2 Rolling Shutter Effects

Rolling shutter effect [2.9] is the image capture method of the CMOS sensor camera and it is the core mechanism for realizing the function of the CIS-based VLC system. As mentioned in the last section, a CMOS camera can convert light signal to digital output signal which is proportional to the intensity of visible light. In CMOS camera, the pixel array is activated and exposed row-by-row, then the corresponding pixel outputs of the activated rows are sampled and stored in sequence. After the scanning process of all rows of pixels is finished, the scanned lines are combined to form a complete image frame and it is called as "rolling shutter effect".

In CIS-based VLC system, the rolling shutter effect can be utilized to detect the transmitted visible light signal [2.10]. If the switching frequency of light source is similar or lower to the scanning speed of rolling shutter but higher than the frame rate of CIS, there are bright and dark

strips appearing at one image frame. As illustrated in Fig. 2.5, when light source turns on, the first row of pixel array is exposed to the high light intensity and the bright strip is recorded as the first line in captured pattern. Since the scanning frequency is higher than switching frequency, when light source turns off, the next row of pixels is activated and exposed to low intensity so that dark strip is presented in the pattern. After all the rows are activated, the bright and dark strips construct final pattern containing the transmitted signal, which is sent to the software supported receiver for subsequent image processing. However, due to the limitation of CIS scanning speed of pixels and frame rate of CIS which is up to 30 fps, the switching frequency of light source cannot be too high which also limits the data rate of CIS-based VLC system.

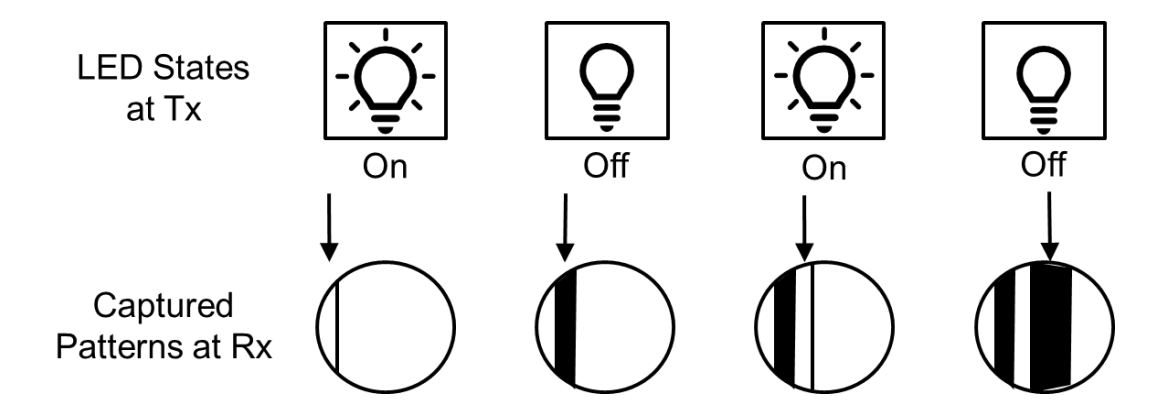


Fig. 2.5. Mechanism of rolling shutter effect adopted in CIS-based VLC system.

2.3.3 Software Supported Receiver and Decoding Scheme

The image processing procedures of the captured pattern are performed in the software-supported receiver for convenience. As presented in Fig. 2.6, the entire process contains four steps to decode the transmitted light signals. The first step is determining the region of interest (ROI). After the image containing bright and dark strips is captured through a CIS in smart mobile device, it is cropped to the ROI containing the rolling shutter patterns. The second step is detecting the threshold for decoding. With the obtained ROI, the pixel values of its contained rolling shutter pattern are read out and the maximum and minimum values can be determined. Then the thresholds are calculated as the middle point of maximum and minimum values as the red line shown in Fig. 2.6. The third step is applying these obtained threshold values to convert the digital pixel output values into a binary stream. The pixel values larger than the threshold

are converted to bits "1" s and those smaller than the threshold are converted to bits "0" s. Finally, the different binary streams are combined together to form a complete data frame consisting of a preamble, payload (ID code), and error check sequence [2.11]. The binary streams are decoded according to the relevant coding scheme adopted at the transmitter. This payload (ID code) is sent to the back-end cloud server, where the light ID code is matched to the information stored in the database. With the light ID code, the server responds to the receiver with the corresponding information.

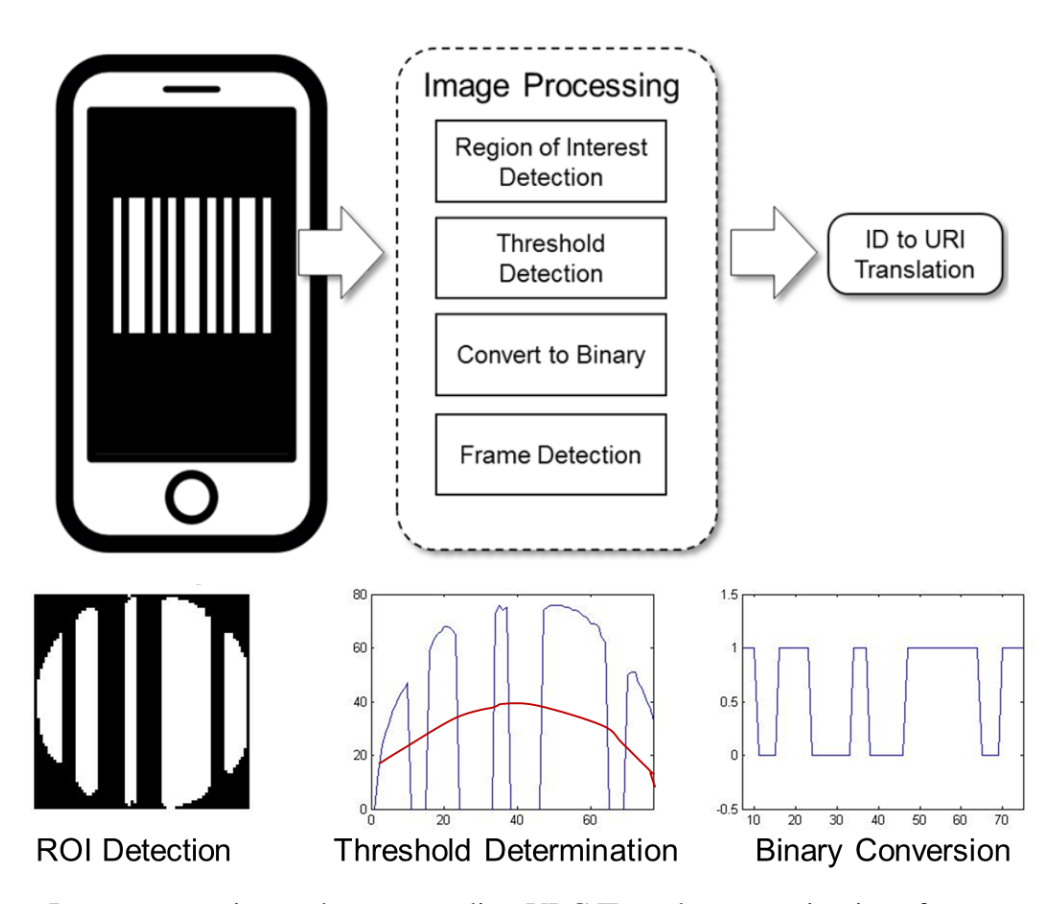


Fig. 2.6. Image processing and corresponding VLC ID code conversion in software supported VLC receiver.

2.4 Applications of CIS-based VLC System

The CIS-based VLC system is convenient to install and cost-effective due to utilizing existing infrastructures. Moreover, it owns high scalability and is a supplementary component to the RF-based communication systems. CIS-based VLC system can be adopted for occasions where the LED lights and smart mobile devices are equipped to extend the application scenarios.

2.4.1 Smart Lighting

Indoor illuminating infrastructures such as LED lights, LED tubes, and advertising lightboxes can be equipped with VLC technology to provide smart lighting applications [2.12]. In domestic circumstance, the commonest luminaire is LED light which can be transformed to a beacon. Therefore, the users can access specific information related to the data transmitted by LED light, such as the working states of other devices and location data. Moreover, cooperating with the wireless sensor network (WSN) for automatically managing the intelligent appliances according to the living environment contributes to build a user-friendly smart home. In public indoor occasions with a high density of population such as schools, offices, and hospitals, LED tubes are common for illumination. The VLC technique can be applied for broadcasting information without radio spectrum congestion and electro-magnetic interference (EMI). The advertising lightboxes installed in shopping malls where the indoor environment is complex can be integrated with the VLC technique to navigate the customers for or help the merchants to advertise their products.

2.4.2 Indoor Visible Light Positioning

Indoor visible light positioning (VLP) [2.13] is one of the main applications for the CIS-based VLC system. The indoor positioning service is provided to the people or mobile devices such as robots for locating, tracking, and navigation in the indoor environments. Traditional positioning systems are implemented with the support of RF technology and the most common one is the global positioning system (GPS). However, these positioning systems suffer from low accuracy when adopted to the indoor environment. Compared with the RF-based positioning systems, the VLP system owns the advantages that it can provide indoor positioning with accuracy as high as centimeter-level with higher communication security. Besides, the VLP system is free from electromagnetic interference (EMI) and compliant with existing infrastructures. CIS-based VLC system is suitable for implementing indoor VLP function since it directly utilizes the smartphones and the mobile devices equipped with cameras as receiver, which are consistent with the positioning targets in VLP system.

The typical indoor positioning system supported by the CIS-based VLC normally consists of a light source, a VLC receiver, and a back-end cloud server. The light source performs as a signal beacon, and it will continually broadcast unique ID code in the manner of modulated visible light. This modulated light signal can be detected by the camera of VLC receiver. Then the image processing and decoding procedures are performed in the smartphone to decode the transmitted VLC ID code. With this received ID code, the process for estimating the received signal strength or angle data can be finished with the support of a cloud server. These data are prepared for the indoor localization algorithm. The most common localization algorithm in the VLP system is the triangulation technique, which requires calculating the distance between the VLC transmitter and receiver or the angle of field of view (FOV) at the receiver. To determine the value of distance or angle, several algorithms can be applied such as angle of arrival (AOA), received signal strength (RSS), and time of arrival (TOA) [2.14], and the calculation process can utilize cloud server resources for speeding up. Moreover, a VLP system can be adapted to navigate the robots [2.15]. The robot will utilize the mounted camera to collect the fingerprint distribution of VLC light sources. With the cooperation of simultaneous localization and mapping (SLAM) technique and light detection and ranging (LiDAR) technique, a VLP system with multi-sensor fusion technology will be able to provide high accuracy indoor navigation to mobile devices under various situations.

2.4.3 Vehicle Communication

CIS-based VLC system can be employed to the communication in traffic system for the purpose of improving traffic safety and constructing a smart transportation. The vehicle communication system can be divided into two categories according to the communication objects.

- Vehicle to vehicle (V2V) communication [2.16]. This type of vehicle communication
 utilizes the car lights as light source to transmit visible light signals between the vehicles.
 To receive the light signal, the vehicle supporting V2V communication should be equipped
 with cameras. The transmitted signals can be short information including various cautions
 or seeking help signals to avoid traffic accidents.
- 2. Vehicle to infrastructure (V2I) communication [2.17]. In V2I system, the fixed infrastructures such as streetlights and traffic lights can be utilized to transmit signals to the

vehicles. Meanwhile, the vehicles can also become transmitter and send information to the infrastructures along the lanes. The transmitted information in V2I system normally includes traffic guiding signals, traffic status and warnings. It contributes to intelligent transportation as well as avoid accidents.

2.5 References

- [2.1] C. Danakis, et al., "Using a CMOS camera sensor for visible light communication," in 2012 IEEE Globecom Workshops, pp. 1244-1248, 2012.
- [2.2] T. Yamazato, et al., "Image-sensor-based visible light communication for automotive applications," in *IEEE Communications Magazine*, vol. 52, no. 7, pp. 88-97, July 2014.
- [2.3] H. L. Minh, et al., "80 Mbit/s visible light communications using pre-equalized white LED," in 34th European Conference on Optical Communication (ECOC), pp. 1–2, 2008.
- [2.4] S. Chen and C. Chow, "Color-Shift Keying and Code-Division Multiple-Access Transmission for RGB-LED Visible Light Communications Using Mobile Phone Camera," in *IEEE Photonics Journal*, vol. 6, no. 6, pp. 1-6, Dec. 2014.
- [2.5] T. P. Lee, "Effect of junction capacitance on the rise time of led's and on the turn-on delay of injection lasers." in *The Bell System Technical Journal*, vol. 54, no. 1, pp. 53-68, 1975.
- [2.6] "IEEE Standard for Local and metropolitan area networks--Part 15.7: Short-Range Optical Wireless Communications," in *IEEE Std 802.15.7-2018 (Revision of IEEE Std 802.15.7-2011)*, pp.1-407, 23 April 2019.
- [2.7] K. A. S. Immink, "Runlength-limited sequences," in *Proceedings of the IEEE*, vol. 78, no. 11, pp. 1745-1759, Nov. 1990.
- [2.8] A. El Gamal and H. Eltoukhy, "CMOS image sensors," in *IEEE Circuits and Devices Magazine*, vol. 21, no. 3, pp. 6-20, May-June 2005.
- [2.9] C. -K. Liang, et al., "Analysis and Compensation of Rolling Shutter Effect," in *IEEE Transactions on Image Processing*, vol. 17, no. 8, pp. 1323-1330, Aug. 2008.
- [2.10] P. Ji, H. Tsai, C. Wang and F. Liu, "Vehicular Visible Light Communications with LED Taillight and Rolling Shutter Camera," in 2014 IEEE 79th Vehicular Technology Conference (VTC Spring), 2014, pp. 1-6.

- [2.11] B. Hussain, et al., "Li-Fi based secure programmable QR code (LiQR)," in *Proc. JSAP-OSA Joint Symposia*, Fukuoka Japan, Sep. 2017, p. 6p_A409_6.
- [2.12] Kevin Warmerdam, et al., "Visible light communications for sensing and lighting control," *IEEE Sensors Journal*, vol. 16, no. 17, pp. 6718–6726, Sep. 2016.
- [2.13] Y.-S. Kuo, P. Pannuto, K.-J. Hsiao, and P. Dutta, "Luxapose: Indoor positioning with mobile phones and visible light," in *Proc. 20th Annu. Int. Conf. MobiCom*, pp. 447–458, 2014. [2.14] P. H. Pathak, et al., "Visible Light Communication, Networking, and Sensing: A Survey, Potential and Challenges," in *IEEE Communications Surveys & Tutorials*, vol. 17, no. 4, pp. 2047-2077, Fourthquarter 2015.
- [2.15] Kejie Qiu, Fangyi Zhang, Ming Liu, "Let the light guide us: VLC-based localization," in *IEEE Robotics & Automation Magazine*, vol. 23, no. 4,pp. 174–183, Dec. 2016.
- [2.16] T. Yamazato, et al., "Image-sensor-based visible light communication for automotive applications," in *IEEE Commun. Mag.*, vol. 52, no. 7, pp. 88–97, Jul. 2014.
- [2.17] S.-H. Yu, et al., "Smart automotive lighting for vehicle safety," in *IEEE Commun. Mag.*, vol. 51, no. 12, pp. 50–59, Dec. 2013.

CHAPTER 3 Visible Light Communication Enabled Smart Home Control System with 3D Indoor Localization

3.1 Introduction

With the fast development of intelligent electronics, smart devices have dramatically increased in both variety and quantity and have been applied in locations such as homes, shopping malls, hospitals, and factories. This tremendous increase has spawned the IoT network technology [3.1], which serves to exchange information among different smart devices and support them working in a system. IoT technology has dramatically contributed to the development of smart living concepts, such as smart industry, smart transportation, smart city, and especially, smart home system (SHS) [3.2]. To improve ease of living, increasingly domestic appliances have been designed and equipped with intelligent functions in SHSs, like timing, remote management, voice control, and adaptive adjustment with sensors [3.3] [3.4]. With such comprehensive intelligent features integrated into one system, users can adjust their living environments for the most comfort and safety.

However, the explosive growth in SHSs has brought several challenges, two of which are the efficient and convenient control of multiple smart devices and the guarantee of information security. To meet the first challenge, commercial SHSs adopt a hub as the center of the system and utilize networking technologies such as Wi-Fi, Bluetooth, near-field communication (NFC) and ZigBee for communication among the smart devices and the controlling device [3.5] [3.6]. Although these RF-based control methods simplify the control process by combining multiple smart devices into one system, they suffer from poor location accuracy in small areas with a high density of devices. For example, users may find it difficult to distinguish the same type of device installed in neighboring rooms through a smartphone due to the low positioning accuracy [3.7], which is caused by EMI, signal reflection, environmental absorption, noise, etc. This leads to inconvenience for the user, which defeats the objective of a SHS. The second challenge, possible information disclosure, arises because RF signals can easily penetrate walls, causing security concerns. Such leaks in information threaten the safety of SHSs, which consists of non-

repudiation, authorization, availability, privacy, confidentiality, authenticity and integrity [3.8]. The countermeasures for solving security issues such as attribute access control systems, anonymization and cryptographic technics are also discussed. However, these techniques are complex for implementation, increasing the cost of system and decreasing convenience to users.

CIS-based VLC technique [3.9] enabled smart home control system is a potential solution to the mentioned problems. Due to the unique characteristics of visible light in terms of line-of-sight (LOS) capability, compatibility with existing lighting infrastructure, and absence of EMI, VLC technique is considered as a potential indoor communication method with high security and low cost. The high-security characteristic of VLC can contribute to solve the mentioned safety problem in RF-based SHSs. In addition, a CIS-based VLC system can be applied to indoor localization with centimeter-level accuracy as mentioned in chapter 2 [3.10], which means indoor VLP could potentially solve the user location problem in SHSs and provide the much-needed convenience of location-based control.

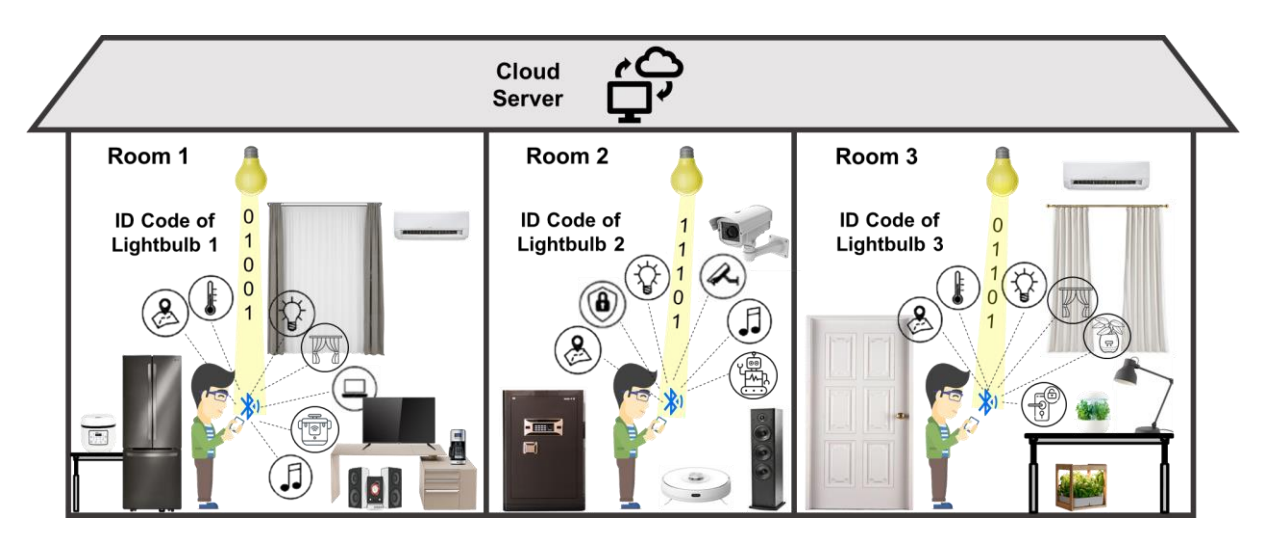


Fig. 3.1. Application scenarios of the proposed CIS-based VLC enabled smart home control system.

This chapter presents a practical VLC-based smart home control system using a VLC-integrated LED light bulb [3.11] along with a 3D indoor localization algorithm based on VLP to address the issues of secure, efficient and convenient management of smart home devices. In the application scenario presented in Fig. 3.1, the lightbulb transmits light signals containing a

unique ID, which can be decoded by the smartphone. Then, the user can control the smart devices through Bluetooth with assistance from the cloud server and without signal interference from neighboring rooms. The VLP algorithm utilizes the directional angles of the smartphone and position of the lightbulb to calculate the user's position and orientation.

3.2 Related Works of Smart Home Control System

The smart home control system is an extremely important sub-system of SHS since it organizes intelligent appliances into a network and manages their working states. It aims to provide users with a convenient, power-efficient, and secure method to adjust their living environments. With this significant role, researchers are focusing on smart home control systems, with research emphases from system architecture to significance, various control methods, and system applications. To provide consumers with better services, seven design principles for smart home control systems are concluded for programming the software of the control system [3.12]. Power line communication (PLC) assisted smart home control system [3.13] [3.14] utilizes the power line to transmit control messages among smart devices, and supply power considering the environment parameters collected from wireless sensor network (WSN) to save energy. This system offers high accuracy control but suffers from low scalability as it relies on a fixed power line. IoT-based smart home control system [3.15] [3.16] includes WSN to provide information, as well as a control system based on a gateway, cloud server, and smartphone app. This scalable control system offers remote management functions but owns poor control accuracy with the unsolved security problem. Another type of smart home control system is supported by information fusion [3.17] which consists of information fusion-based controller, power line, Bluetooth wireless networking, and computational units. It collects external factors and utilizes a fuzzy neural network (FNN)-based information fusion algorithm to determine the states of smart devices automatically. This system combines wireless and wireline networking for scalability and accuracy but lacks consideration of security. A smart home control system based on ZigBee [3.18] [3.19] utilizes ZigBee with the IEEE 802.15.4 standard for communication and provides automatic energy management for energy saving. However, this system also faces accuracy and security problems. After introducing the definition of smart home security system, the related tools, and cryptographic technologies for guaranteeing the security of SHSs are proposed in [3.20]. For IoT-based SHS, the authentication technology [3.21] contributes to improving its system security but decreases convenience to users.

To date, only a few works have proposed the use of VLC in the context of SHSs. The idea of using purely VLC based bidirectional communication for smart home connectivity is proposed in [3.22]. In [3.23], authors present an encryption mechanism to prevent intrusion of adjacent adversaries in smart home settings. However, the related practical deployment scenarios and challenges are not discussed. The security of VLC-based smart home system implementation is discussed in [3.24], where an automated user authorization scheme based on proximity to visible light is presented for smart home settings. In addition to the lack of positioning accuracy, the presented design is based on a small prototype with a PD used as receiver, making it impractical for integration with a consumer smartphone and real-world deployment.

Table 3.1 Comparison of Related Works on Smart Home Control System

Refe	erence	[3.13]	[3.15]	[3.17]	[3.19]	[3.21]	[3.24]	This Work
Main Te	echnology	PLC + WSN	IoT + Big Data	Information Fusion	ZigBee	ІоТ	VLC	VLC + VLP
	inication thod	PLC + ZigBee	Wi-Fi	Bluetooth + PLC	ZigBee	Wi-Fi	VLC	VLC + BLE + Wi-Fi/LTE
Core I	Devices	ZigBee Coordinator, Power Line, PLC TRx	Microcontroller, Sensors, Cloud Server, Smartphone	IF-based Controller, Power Line, Computational Unit	RF-based Devices, Sensors	Gateway, Cloud Server, Smartphone	Evaluation board, Smart home Gateway, Smartphone	VLC Lightbulb, Cloud Server, Smartphone
System S	Scalability	Low	High	Middle	High	High	Low	High
User Co	nvenience	Middle	High	High	Middle	Low	Low	High
Control Accuracy		High	Low	Middle	Low	Low	Middle	High
Consid ered	Security Issue	No	No	No	No	Yes	Yes	Yes
	Indoor Positioning	No	No	No	No	No	No	Yes

The related works on smart home control systems are summarized and compared with this work in Table 3.1. It can be noticed that the works based on RF networks lack high accuracy control and system security, while wireline-based systems are poor at scalability. The proposed system solves these issues and provides high-precision indoor localization for users.

3.3 Design of High-Power VLC Lightbulb

In the proposed CIS-based VLC-enabled smart home control system, the core hardware infrastructure is made up of the VLC LED lightbulb which serves as beacon and generates the light signal. Considering that the typical ceiling height of housing is around 3 m and suitable illumination intensity needs to be more than 300 lx, the VLC link distance should cover this range and the total output power of lightbulb must provide sufficient illumination for lighting. Furthermore, most VLC-enabled light sources require an external modulator, which is inconvenient for installation for standard ceiling light socket.

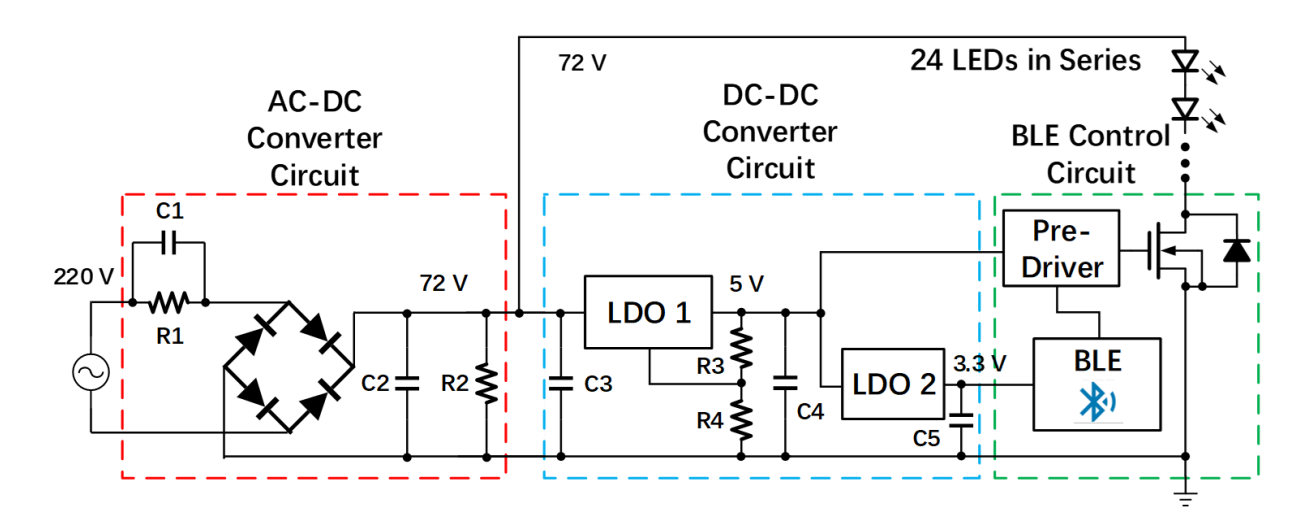


Fig. 3.2. Schematic of high-power LED lightbulb with VLC functionality.

To meet the above requirements, the proposed solution is shown in Fig. 3.2. The driver-less VLC lightbulb consists of four parts: an AC-DC converter circuit, a DC-DC converter circuit, a Bluetooth low energy (BLE) control circuit [3.25], and 24 LEDs connected in series. The power management block converts the AC input voltage to a suitable DC output and supply power to the control block as well as the LED series. The BLE control block is the critical

circuit in CIS-based VLC transmitter, the database is contained by this block and it performs as the encoder as well as the modulator to determine the transmitted light signal. The LED series is supplied by the output voltage from the power management block and its driving current is managed by the BLE control block.

3.3.1 Design of Power Management Block

The power management block consists of an AC-DC converter circuit and a DC-DC converter circuit. As shown in Fig. 3.3 (a), the AC-DC converter circuit is comprised of two resistor-capacitor (RC) pairs and a bridge rectifier. The first RC pair is connected in series with the bridge rectifier, and the impedance of C1 can be employed as voltage divider decreasing the input voltage while R1 is the bleeder resistor. The capacitance of C1 can be determined with:

$$X_c = 1/(2\pi f C) , \qquad (3.1)$$

where X_c is the capacitive reactance of capacitor C1, C is its capacitance value and f is the frequency of AC voltage. The required value of X_c for dividing the input voltage can be determined as follows:

$$I_{i,R} \approx V_{total}/X_c, \tag{3.2}$$

where V_{total} is the decreased value of input 220 V AC voltage by using the voltage divider which is equal to 148 V and I_{LED} is the driving current of LEDs provided by the datasheet of LED which is 130 mA. The total number of LEDs can be calculated by:

$$P_{LED} = N_{LED} \times V_{LED} \times I_{i_R} , \qquad (3.3)$$

where P_{LED} is the target electric power of this lightbulb equal to 10 W, V_{LED} is the 3 V supply voltage of each LED. Therefore, the total number of required LEDs is 24. The bridge rectifier converts the decreased AC input voltage to a 72 V DC output and the following RC filter connected in parallel with rectifier smooths the ripple of this 72 V output voltage which is utilized to supply both LED series and subsequent control block. Therefore, the calculated value of C1 is around 2.7 uF for decreasing the 220 V AV input voltage to 72 V.

As presented in Fig. 3.3 (b), the DC-DC converter circuit consists of two low dropout regulators (LDOs) and supporting passive components. In DC-DC converter circuit, the first LDO decreases 72 V DC input voltage to 5 V and supplies the pre-driver with R3 and R4 serving as

output voltage controller. The second LDO converts 5 V to 3.3 V DC voltage and guarantees BLE module to work at proper voltage. To analyze the working states of these two LDOs, the efficiency and loss are calculated with equations below:

$$\eta = \frac{V_{out}I_{out}}{V_{in}(I_{out} + I_q)} \times 100\% \approx \frac{V_{out}}{V_{in}} \times 100\%$$
 (3.4)

$$P_{loss} = (V_{in} - V_{out}) \times I_{out}$$
(3.5)

where V_{out} is the output voltage of LDO, I_{out} is the output current, V_{in} is the input voltage of LDO and I_q is the quiescent current which is uA level and much smaller than the output current so that it can be neglected. For the LDO1, the output voltage is 5 V, the output current is 28 mA, the input voltage is 72 V and the quiescent current is 83 uA, thus the efficiency of LDO1 is 6.9%. For the LDO2, the output voltage is 3.3 V, the output current to the BLE module is 15 mA, the input voltage is 5 V and the quiescent current is 1 uA, so that the efficiency of LDO2 is 66%. As for the power loss, LDO1 owns a loss of around 1.9 W and the power loss of LDO2 is 0.03 W. The capacitors C3, C4 and C5 help to smooth the input and output DC voltage of LDOs. The first LDO decreases 72 V DC input voltage to 5 V and supplies the pre-driver. The second LDO converts 5 V to 3.3 V DC voltage and guarantees the BLE module to work at the proper voltage.

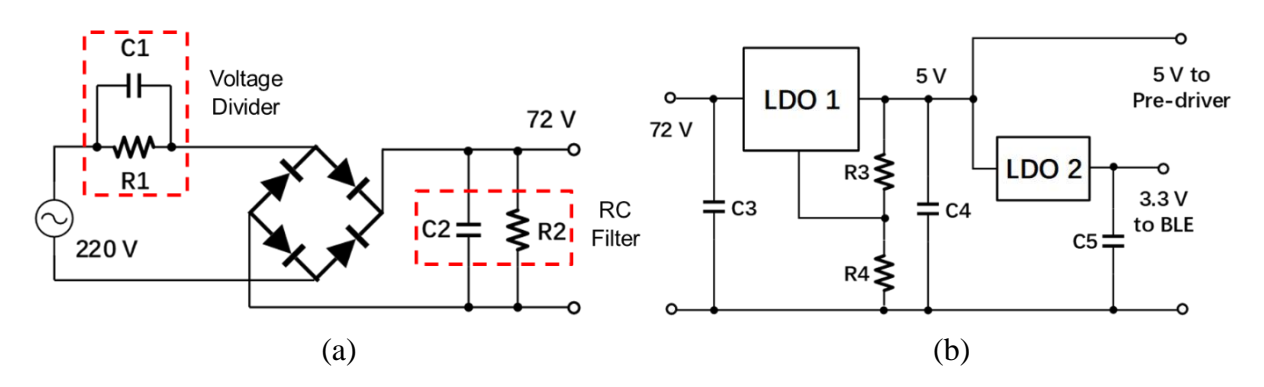


Fig. 3.3. Detailed design of power management circuits. (a) AD-DC converter circuit. (b) DC-DC converter circuit.

The components values and part numbers of designed AC-powered VLC lightbulb are summarized in table 3.2. The R1 and R2 are determined by empirical value of 470 k Ω and they are the bleeder resistors which help to neutralize the remaining charges in the capacitors during power-off state while they can be treated as open circuit during power-on state, which

guarantees less power waste. C3, C4 and C5 are determined by the datasheet of two LDOs with the suggested values for filtering input and output ripples.

Table 3.2 Component Values of Designed AC-powered VLC Lightbulb

Components	R1	R2	R3	R4	
Values	470 kΩ	470 kΩ	20 Ω	270 Ω	
Components	C1	C2	C3	C4	C5
Values	2.7 uF	47 uF	10 uF	10 uF	4.7 uF
Components	Bridge Rectifier	LDO1	LDO2	LEDs	
Part Numbers	MB10F	TL783CKTTR	XC6206P332MR	CREE- JE2835	
Components	BLE Module	Pre-Driver	Power MOSFET		
Part Numbers	CC2541_M24	1EDN7550B	IPD320N20N3G		

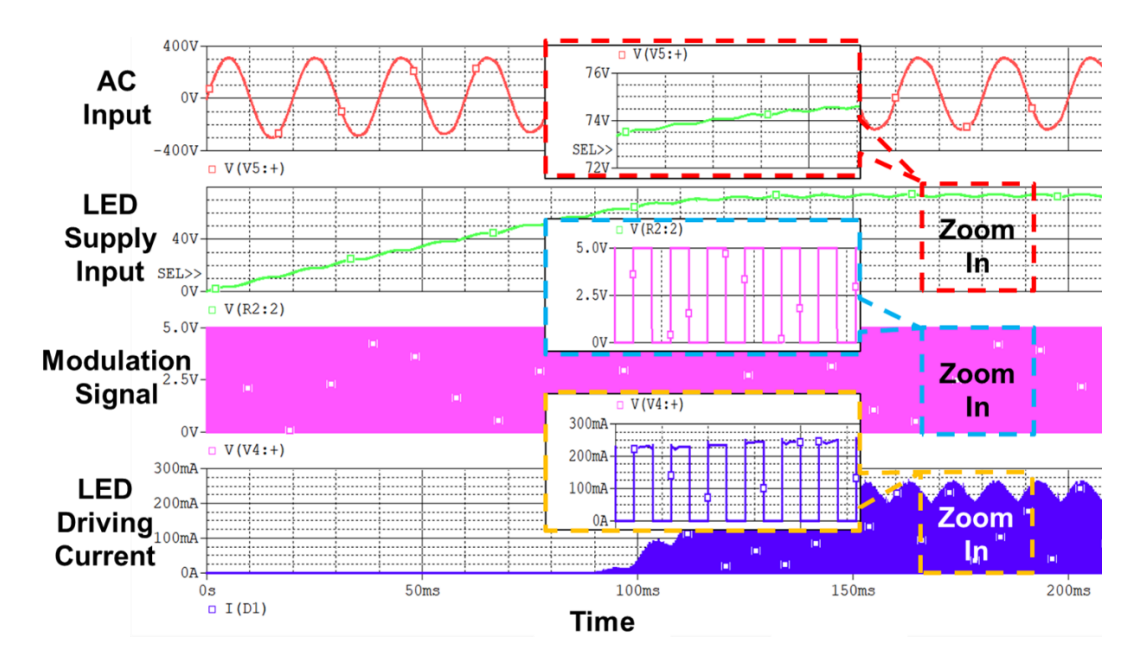


Fig. 3.4. Simulated waveforms of designed VLC-based LED lightbulb.

Fig. 3.4 shows the simulated results of the designed high-power VLC lightbulb. The AC input voltage, LED supply input voltage, modulation signal, which is then stored as VLC signal in the BLE module, and LED driving current, are analyzed and presented below in sequence. The

right-hand side of Fig. 3.4 shows the zoomed-in waveforms of these four analyzed voltage and current signals. The simulated supply voltage for the LEDs is around 74 V, while the average value of the driving current is 130 mA, which is consistent with the designed values of total operating voltage and driving current. It can also be noticed that the waveform of the driving current changes in line with the modulation signal.

3.3.2 Design of BLE Control Circuit

The BLE control circuit realizes the function of the normal extra modulator, but with a more compact scale that can be integrated into the shell of the lightbulb. This block contains a predriver, a BLE module, and a high-threshold power MOSFET. The BLE module loads the VLC ID code and sends out the pulse-width modulation (PWM) waveforms through a serial peripheral interface (SPI). To meet the requirement of output power driving capability, a CMOS inverter-based driver is inserted between the I/O of BLE module and the power MOSFET. The power MOSFET acts as a switch controlling the on/off states of LEDs under a switching speed of 8-16 kHz, and it is chosen to sustain a drain-to-source voltage of up to 72 V during the LED off state.

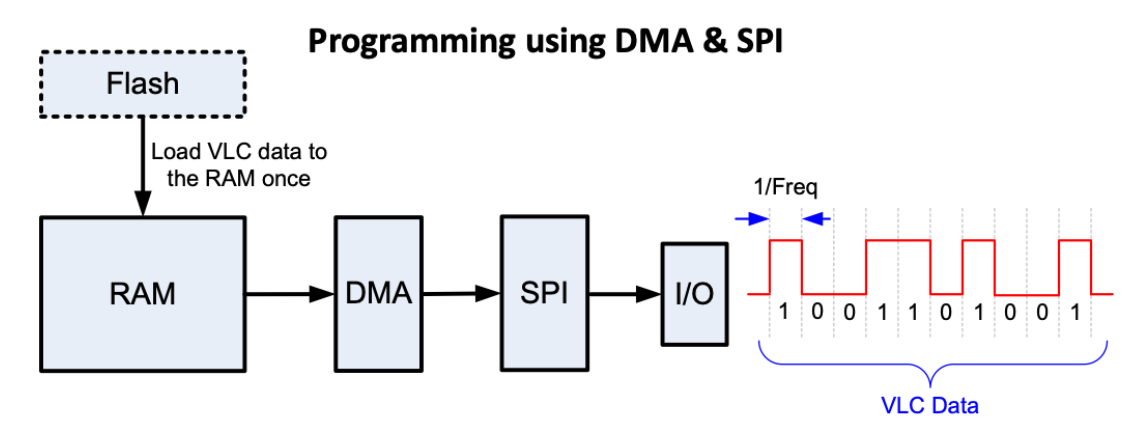


Fig. 3.5. Process of VLC data transmission in BLE module.

The process of VLC signal transmission in the BLE control block is presented in Fig. 3.5 [3.26]. In the flash, the transmitted VLC ID code is written in and stored. When the BLE control block is powered on, this stored VLC ID code is loaded to the random access memory (RAM) area at once. To access the direct memory access (DMA) controller, the start address of this RAM is

the source address of the DMA controller. Since this following DMA controller works under the repeated mode, the loaded ID code is continuously sent to the SPI. This SPI module is configured with the same frequency as the transmitted VLC ID code. After triggered, this SPI module sends the VLC ID code out to the I/O sustainedly, which is directly connected to the pre-driver module in the BLE control block. This VLC ID code transmission method using the DMA controller and the SPI module to program signal owns the advantage of no interrupts. Compared with the traditional VLC ID code transmission method implemented through CPU and timer, this method gets rid of reading data under the control of interrupt signals from timer since this method transmits VLC ID code in continuous mode. Therefore, this VLC signal programming method using DAM and SPI can guarantee the VLC ID code is transmitted without interrupts.

3.4 Theoretical Analysis of Proposed Smart Home Control System

3.4.1 Architecture Design of Smart Home Control with Cloud Server

The CIS-based VLC enabled smart home control system consists of the hardware infrastructure made up by driver-less AC-powered VLC lightbulbs with standard E27 socket supporting direct plug-n-play capability, a back-end cloud server storing the world coordinates of the lightbulbs and information of the smart devices in a look-up table (LUT), and a smartphone software application that implements the VLC decoding algorithm, Bluetooth-based control for the smart devices, and interface with the information stored in cloud server. These three components network and manage various smart devices in the SHS.

The proposed architecture and signal flow are presented in Fig. 3.6. After the lightbulb sends out the VLC signal containing a unique ID code, the user receives this signal through the smartphone app which captures the image of the lightbulb as a rolling shutter pattern because of the CIS-based camera operation. Then the smartphone software decides the threshold of contrast ratio for each captured pattern and decodes it into "0" or "1" according to an adaptive threshold algorithm [3.27]. With this decoded ID code, the smartphone transmits it to the cloud server through a Wi-Fi or LTE link. In the cloud server, the location data of each lightbulb is

stored corresponding to its ID code. Additionally, the Bluetooth MAC addresses of the smart devices installed in the same room as the lightbulb are recorded in terms of the ID code of the lightbulb. Therefore, each lightbulb has a pre-recorded file in the cloud server with its location data in a global map and the MAC address information of the smart devices co-located in the same room. After matching the ID code received from the smartphone, the cloud sever can then provide the corresponding location data with the MAC addresses of the co-located smart devices. Since all smart devices are continuously broadcasting, the smartphone will detect many devices in different rooms in a home as the Bluetooth signal can penetrate through walls. With the returned MAC address, the smartphone can now identify which smart devices are installed in the same room as the VLC lightbulb and send out connection request only to these devices. Through the Bluetooth connection, the user can then manage and control these smart devices.

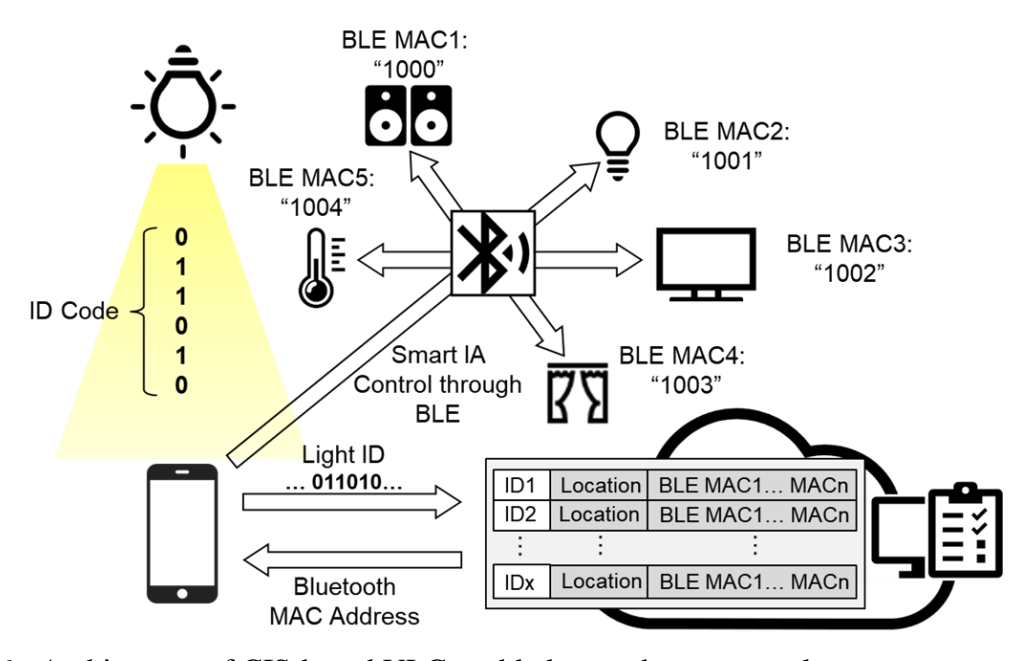


Fig. 3.6. Architecture of CIS-based VLC enabled smart home control system.

3.4.2 Smart Home Control with Direction Angle Data Supported 3D Positioning

Security is a major concern in several application scenarios, particularly in residential environments. The traditional RF-based communication technologies such as Wi-Fi, Bluetooth and ZigBee face a security challenge since the signal can penetrate through walls allowing someone outside the house premises to control the devices inside. If the smart devices are managed with position-based authorization i.e., the user can only control the device by being at

a specific area inside the house defined via precise 3D position coordinates, security of the system can be significantly improved. In addition, high precision positioning can further help to simplify control using orientation angle of smartphone for distinguishing multiple identical smart devices in close proximity. For instance, the user can directly point the phone to the target device to establish a connection based on the current location and orientation.

Inspired by the two propositions above, a smart home control system based on an orientation-supported 3D positioning algorithm [3.28] is proposed to further increase the precision of indoor positioning. The proposed 3D positioning algorithm relies on the principle of projective geometry, where the smartphone camera takes a picture of the LED light bulb in the ceiling and the corresponding projection of the light on the image is used to determine the relative position of the smartphone w.r.t the LED light [3.29], as presented in Fig. 3.7. The positioning algorithm follows the principle of the pinhole camera model, which is given as follows:

$$s \begin{bmatrix} u \\ v \\ 1 \end{bmatrix} = K \begin{bmatrix} X_C \\ Y_C \\ Z_C \end{bmatrix}, \tag{3.6}$$

where X_C , Y_C , and Z_C represent 3D coordinates of the LED light w.r.t the camera coordinate frame. The camera transforms these 3D points into 2D pixel coordinates u and v, with s being the scaling factor, on the image plane using the transformation matrix K. The matrix K, called the camera intrinsic matrix can be expanded to rewrite (3.6) as follows:

$$s \begin{bmatrix} u \\ v \\ 1 \end{bmatrix} = \begin{bmatrix} f_x & \gamma & u_0 & 0 \\ 0 & f_y & v_0 & 0 \\ 0 & 0 & 1 & 0 \end{bmatrix} \begin{bmatrix} X_C \\ Y_C \\ Z_C \end{bmatrix}, \tag{3.7}$$

where f_x and f_y , are the focal length of the x-axis and y-axis respectively, (u_0, v_0) are the center coordinates of the image plane, and γ is the skew coefficient between the x-axis and y-axis. Since the information of the LED light's position is in the 3D world coordinates (X_W, Y_W, Z_W) , a transformation needs to be performed to convert from world frame to the camera frame. This transformation is performed by inserting a 3×3 rotation matrix $R_{3\times3}$ and a 3×1 translation matrix $T_{3\times1}$ in (4) as follows:

$$z_{c} \begin{bmatrix} u \\ v \\ 1 \end{bmatrix} = \begin{bmatrix} f_{x} & \gamma & u_{0} & 0 \\ 0 & f_{y} & v_{0} & 0 \\ 0 & 0 & 1 & 0 \end{bmatrix} \underbrace{\begin{bmatrix} r_{3\times3} & r_{3\times1} \\ r_{1} & r_{2} & r_{3} & \overleftarrow{x_{0}} \\ r_{4} & r_{5} & r_{6} & y_{0} \\ r_{7} & r_{8} & r_{9} & z_{0} \end{bmatrix}}_{1} \begin{bmatrix} X_{w} \\ Y_{w} \\ Z_{w} \\ 1 \end{bmatrix},$$
(3.8)

It is important to note that the translation matrix $T_{3\times 1}$ given in (3.8) represents the 3D coordinates of the camera w.r.t the LED light assuming the coordinates of the LED to be (0, 0, Z_w), where Z_w is the height of the LED light measured from the ground up. Therefore $T_{3\times 1}$ becomes the 3D position of the smartphone and is treated as the target unknown in (3.8). On other hand, $R_{3\times 3}$ can be calculated using the built-in inertial sensors of the smartphone, which provide the three smartphone orientation angles i.e., roll (φ_x) , pitch (φ_y) , and azimuth (φ_z) , as shown in Fig. 3.7. The expansion of $R_{3\times 3}$ based on orientation angles is given by:

$$\mathbf{R}_{3\times3} = \mathbf{R}_{z}\mathbf{R}_{x}\mathbf{R}_{y}$$

$$= \begin{bmatrix} \cos\varphi_{z} & \sin\varphi_{z} & 0\\ \sin\varphi_{z} & \cos\varphi_{z} & 0\\ 0 & 0 & 1 \end{bmatrix} \times \begin{bmatrix} 1 & 0 & 0\\ 0 & \cos\varphi_{x} & \sin\varphi_{x}\\ 0 & -\sin\varphi_{x} & \cos\varphi_{x} \end{bmatrix} \times \begin{bmatrix} \cos\varphi_{y} & 0 & \sin\varphi_{y}\\ 0 & 1 & 0\\ -\sin\varphi_{y} & 0 & \cos\varphi_{y} \end{bmatrix}, (3.9)$$

To calculate $T_{3\times 1}$ by using formula (3.6), of the light's projection on the image i.e., (u, v) and the 3D world coordinates of the LED light, i.e., X_W , Y_W , Z_W , along with the calculated rotation matrix $R_{3\times 3}$ are put in the equation. The scaling factor s, can be calculated by:

$$Z_c = -\frac{a}{r},\tag{3.10}$$

where a is the length of the semi-major axis of the ellipse at the image plane and r is the diameter of the LED lightbulb.

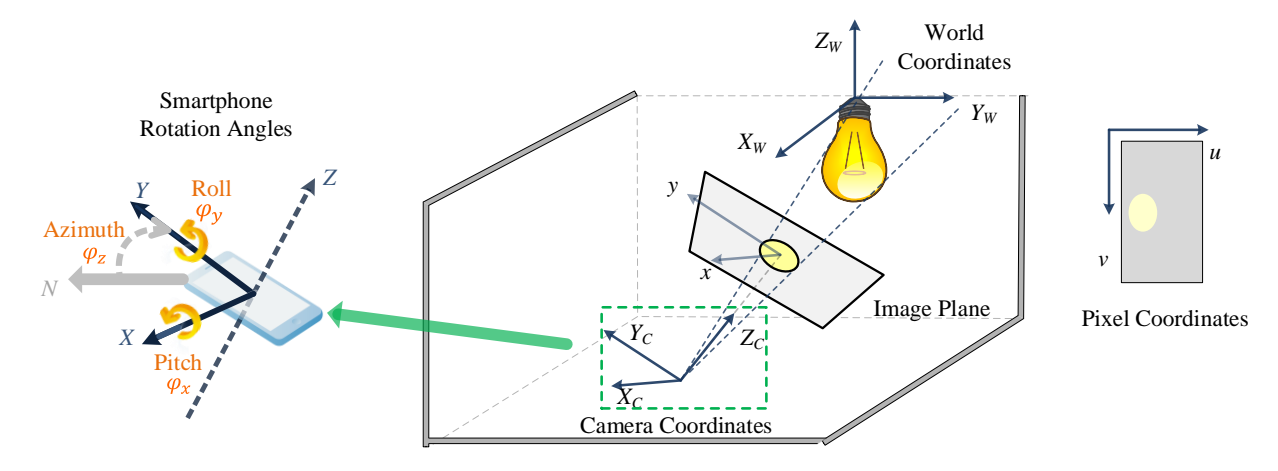


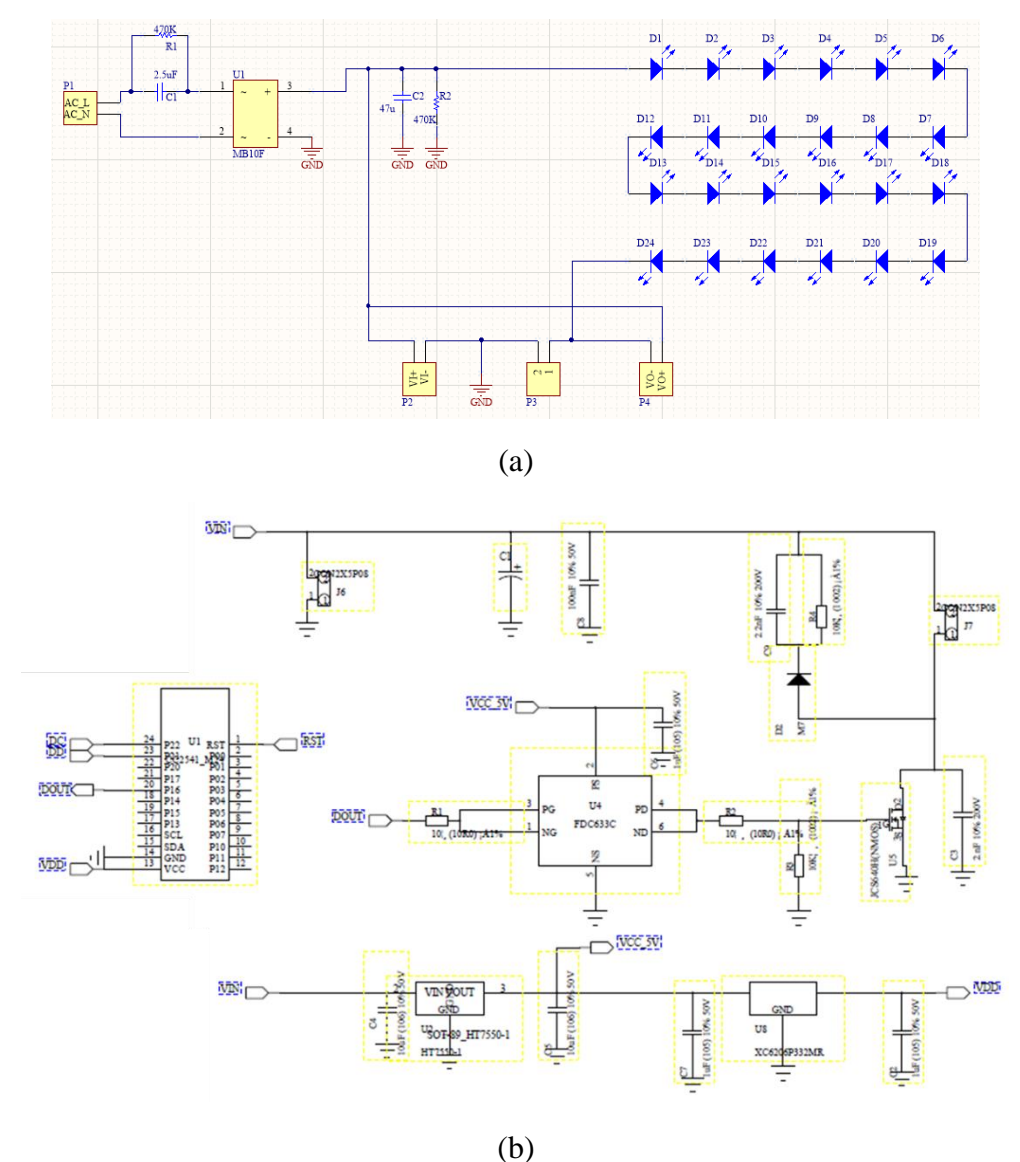
Fig. 3.7. Imaging geometry of proposed direction angle data-supported 3D positioning system [3.28].

3.5 Smart Home Control System Prototype and Performance

Evaluation

3.5.1 Prototype of VLC Lightbulb

The detailed schematic and layout design of PCB for the proposed AC-powered VLC lightbulb are presented in Fig. 3.8. In Fig. 3.8 (a) and (c), the schematic and layout design of power management board are presented, which consists of the AC-DC converter circuit and 24 LEDs connected in series. The diameter of this PCB board is 9 cm for fitting the size of lightbulb enclosure. The schematic and layout design of BLE control board are shown in Fig. 3.8 (b) and (c), which is comprised of DC-DC converter circuit and BLE control circuit. The size of this PCB board is 3 cm×5 cm and this compact design targets to get rid of external modulator for the practical applications. Moreover, the heat sinks are applied to the LDO1 and power MOSFET for heat emission.



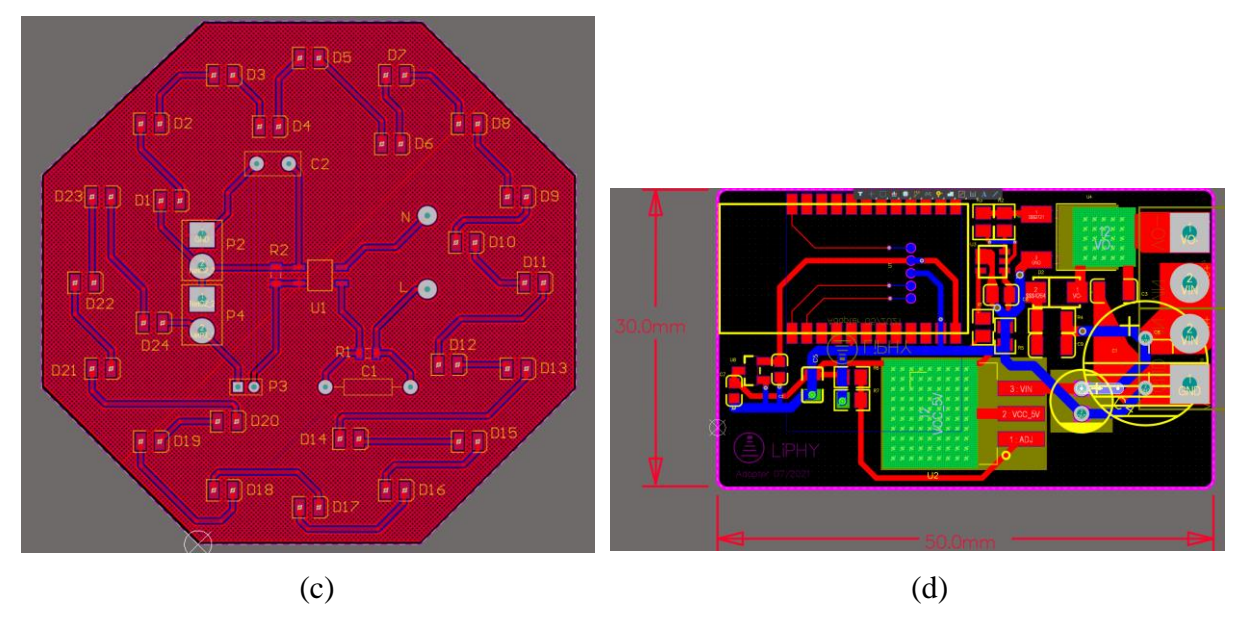


Fig. 3.8. Details of PCB for the designed VLC LED lightbulb. (a) Schematic of LED and power management board. (b) Schematic of BLE control board. (c) Layout of LED and power management board. (d) Layout of BLE control board.

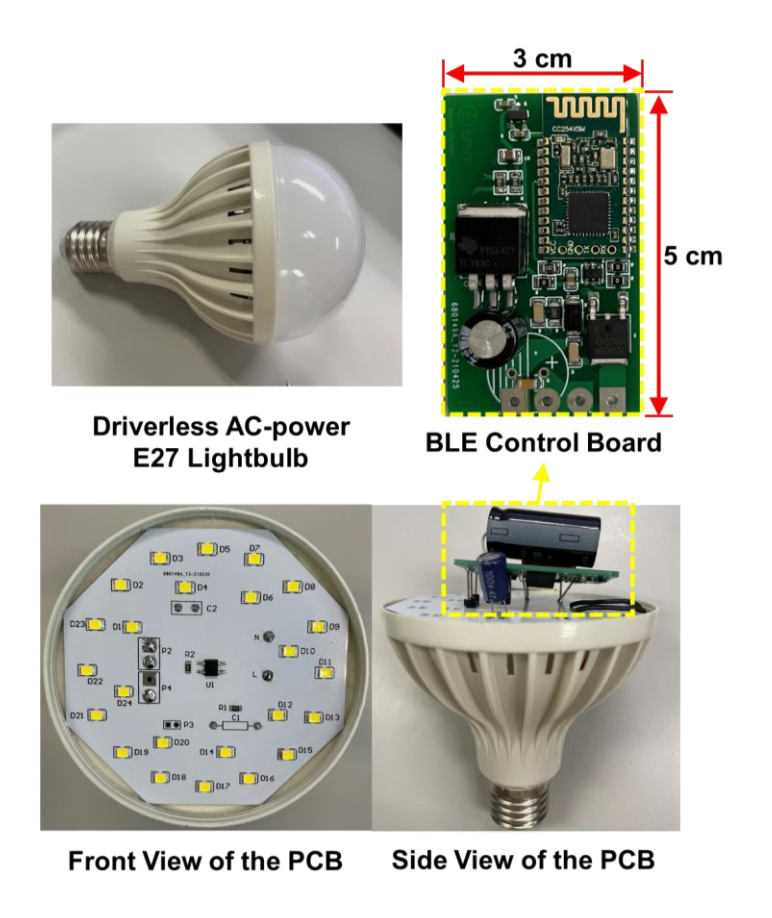


Fig. 3.9. Prototype of VLC LED lightbulb.

The proposed high-power VLC lightbulb is fabricated and retrofitted in a commercial 9-cm diameter AC lightbulb enclosure with a standard E27 socket, as shown in Fig. 3.9. The AC-DC converter circuit and LED string are combined on one PCB board corresponding to the layout of power management board, while the BLE control board is affixed on its back side. Both PCBs are enclosed in the lightbulb shell.

Table 3.3 Measured Working State of Lightbulb

Operating Voltage of LEDs	Driving Current of LEDs	Total Electric Power	VLC Link Distance	Illuminance @ 1.5 m
74.2 V	139 mA	10.3 W	3.4 m	362.45 lx

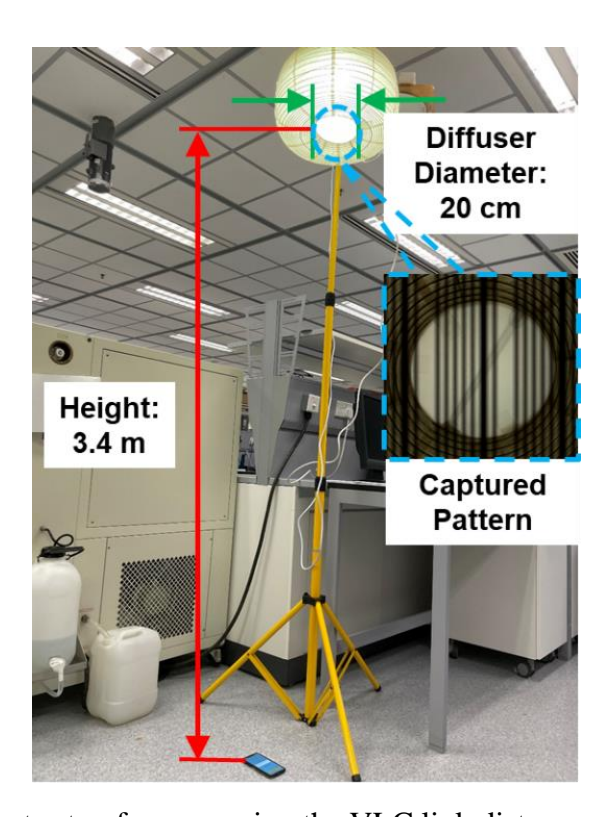


Fig. 3.10. Experiment setup for measuring the VLC link distance.

The measured results of this designed VLC lightbulb are summarized in Table 3.3. The LED string supply voltage is 74.2 V, and the driving current of the LEDs is 139 mA, which are highly consistent with the simulation results. The typical ceiling height in residential buildings is around 3 m while it requires more than 300 lx for illumination. To meet these consumer

application related requirements, we studied the relationships between the diffuser diameter and VLC link distance as well as the illuminance and distance. The setup for measuring VLC link distance is shown in Fig. 3.10, and the corresponding measured results are presented in Fig. 3.11. It can be noticed that the VLC link distance is proportional to the diffuser diameter. Thus, a 20-cm lamp housing is applied outside of lightbulb to reach a VLC link distance up to 3.4 m. The measured illuminance at 1.5 m from the lightbulb is 362.5 lx, which also meets the requirement for residential lighting.

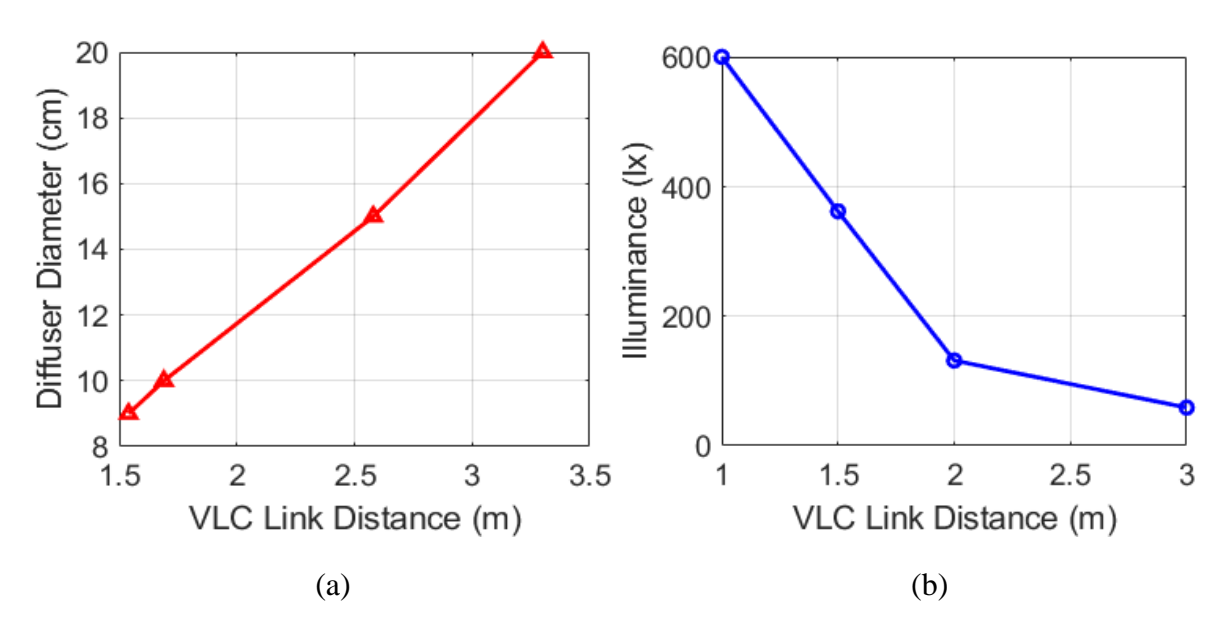


Fig. 3.11. Impact of diffuser diameter and illuminance of lightbulbs on the VLC link distance.

(a) Diffuser diameter versus VLC link distance. (b) Illuminance versus VLC link distance.

3.5.2 Performance Evaluation of CIS-based VLC Enabled Smart Home Control System

The demonstration of the CIS-based VLC enabled smart home control system consists of three lightbulbs and the user smartphone app are presented in Fig. 3.12. The three VLC lightbulbs are programmed with different ID codes, which are stored in the memory unit of the BLE module. Then, we record the corresponding location data and Bluetooth MAC addresses of the smart devices in the cloud server with the ID code of the lightbulb. The cloud server-based architecture provides several advantages. Firstly, it guarantees the safety of data storage; secondly, it simplifies the management of SHS with remote control function; lastly, the

modification of smart home network can be conveniently processed at cloud server through changing the stored information in the LUT.

It can be seen in Fig. 3.12 that the location of the lightbulb with ID code 1 is the kitchen and there are smart devices in the kitchen that can be controlled. ID code 2 identifies the dining room, where three controllable devices are located. Lastly, the ID code 3 indicates the bedroom where three devices that can be managed. When the user moves from kitchen where lightbulb 1 is installed to dining room where lightbulb 2 exists, the location and device information provided on the smartphone screen changes from kitchen to dining room correspondingly. At the same time, the Bluetooth connection between the smartphone and smarts devices are updated automatically when a different VLC ID code is received.



Fig. 3.12. Demonstration of the proposed CIS-based VLC enabled smart home control system.

3.5.3 Verification of Directional Angle Data-Assisted 3D Indoor VLP Algorithm

The verification of this proposed smart home control system which is based on a direction angle-supported 3D visible light positioning algorithm is conducted as an experiment. The experiment setup is the same as that shown in Fig. 3.10, and the horizontal area is $1.5 \text{ m} \times 1.5 \text{ m}$. The lightbulb is mounted at a height of 1.9 m with a diffuser diameter of 20 cm. The camera

resolution of smartphone used in experiment is 1920×1080 and the exposure time is 1/3000 s with ISO 100. The smartphone is placed in the delineated area, which is divided into a $20 \text{ cm} \times 50$ cm grid. The origin position in this experimental area is the projected point of the lightbulb at the horizontal plane. For the direction angle, the pitch angle φ_x and roll angle φ_y are limited from -40° to 40° , and the azimuth angle φ_z varies from -60° to 60° .

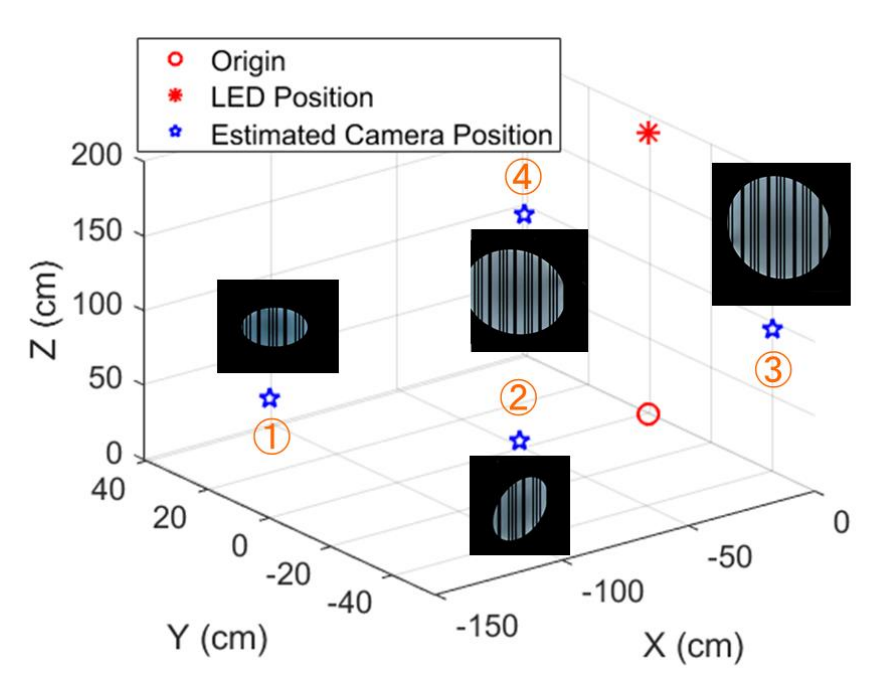


Fig. 3.13. Measured 3D world coordinates of camera with imagines captured at four positions.

The smartphone was placed at four different positions with different direction angles, and the captured images at these four positions with corresponding rolling shutter patterns are shown in Fig. 3.13. It is obvious that when the phone rotates and moves, the captured image will change from a circle to ellipse and vary in area, which will be quantized and applied into equation (3.8) to calculate the 3D world coordinates of the camera. The measured directional angle data and calculated coordinates of camera are presented in Table 3.4. To evaluate the proposed direction angle data-supported 3D indoor positioning algorithm, the positioning error rate (PER) is calculated by using the function adopted in [3.30]:

$$PER(\%) = \frac{\sqrt{\Delta x_0^2 + \Delta y_0^2 + \Delta z_0^2}}{\sqrt{x_0^2 + y_0^2 + z_0^2}} \times 100\% , \qquad (3.11)$$

where (x_0, y_0, z_0) is the measured word coordinates of camera and $(\Delta x_0, \Delta y_0, \Delta z_0)$ is the calculated absolute value of the positioning error. From Table 3.4, it is obvious that the 3D world coordinates of the user can be obtained using the VLC lightbulb with a PER of approximately 7%. In terms of precision, this PER translates into a positioning error of less than 15 cm which is sufficient for accurate and precise control of most smart home devices in close proximity.

Table 3.4 Measured Direction Angle, Coordinates and Positioning Error of Camera

Location	Direction Angle Data	x ₀ (cm)	y ₀ (cm)	z ₀ (cm)	PER
Position 1	$\varphi_x = 40^{\circ}, \ \varphi_y = 0^{\circ}, \ \varphi_z = 0^{\circ}$	-151	0	81	6.72%
Position 2	$\varphi_x = -23^\circ, \ \varphi_y = -39^\circ, \ \varphi_z = 90^\circ$	-117	-54	88	6.87%
Position 3	$\varphi_x = -18^{\circ}, \ \varphi_y = -4^{\circ}, \ \varphi_z = 90^{\circ}$	-10	-49	109	6.23%
Position 4	$\varphi_x = 20^{\circ}, \ \varphi_y = 8^{\circ}, \ \varphi_z = 90^{\circ}$	0	41	84	7.41%

3.6 References

- [3.1] A. Al-Fuqaha, et al., "Internet of things: A survey on enabling technologies, protocols, and applications," *IEEE Commun. Surveys Tuts.*, vol. 17, no. 4, pp. 2347-2376, 4th Quart. 2015. [3.2] M. R. Alam, M. B. I. Reaz and M. A. M. Ali, "A review of smart homes—Past, present, and future," *IEEE Trans. Syst. Man Cybern. C Appl. Rev.*, vol. 42, no. 6, pp. 1190-1203, Nov. 2012.
- [3.3] M. Zamora-Izquierdo, J. Santa, and A. Gomez-Skarmeta, "An integral and networked home automation solution for indoor ambient intelligence," *IEEE Pervasive Comput.*, vol. 9, no. 4, pp. 66-77, Oct. 2010.
- [3.4] S. Ahmed and D. Kim, "Named data networking-based smart home," *ICT Expre.*, vol. 2, no. 3, pp. 130-134, Aug. 2016.

- [3.5] K. E. Jeon, J. She, P. Soonsawad and P. C. Ng, "BLE beacons for internet of things applications: survey, challenges, and opportunities," *IEEE Internet Things J.*, vol. 5, no. 2, pp. 811-828, Apr. 2018.
- [3.6] A. N. Alvi, et al., "BEST-MAC: Bitmap-assisted efficient and scalable TDMA-based WSN MAC protocol for smart cities," *IEEE Access*, vol. 4, pp. 312-322, Jan. 2016.
- [3.7] R. Brena, et al., "Evolution of indoor positioning technologies: A survey," *J. Sensors*, vol. 2017, Mar. 2017.
- [3.8] N. Komninos, E. Philippou and A. Pitsillides, "Survey in smart grid and smart home security: issues, challenges and countermeasures," *IEEE Commun. Surveys Tuts.*, vol. 16, no. 4, pp. 1933-1954, 4th Quart. 2014.
- [3.9] T. Komine and M. Nakagawa, "Fundamental analysis for visible-light communication system using LED lights," *IEEE Trans. Consum. Electron.*, vol. 50, no. 1, pp. 100–107, Feb. 2004.
- [3.10] L. Li, et al., "Epsilon: A visible light based positioning system," in *Proc. 11th USENIX Symp. Netw. Syst. Design Implement. (NSDI)*, Seattle, WA, USA, Apr. 2014, pp. 331-343.
- [3.11] B. Xu, B. Hussain, X. Liu, T. Min, H. Cheng, and C. P. Yue, "Smart-home control system using VLC-enabled high-power LED lightbulb," in *Proc. IEEE 10th Global Conf. Consum. Electron.* (GCCE), Kyoto, Japan, Oct. 2021, pp. 744-745.
- [3.12] S. Davidoff, et al., "Principles of smart home control," in *Proc. 8th Int'l Ubiquitous Computing (UbiComp)*, Berlin, Heidelberg, 2006, pp. 19-34.
- [3.13] M. Li and H. Lin, "Design and implementation of smart home control systems based on wireless sensor networks and power line communications," *IEEE Trans. Indu. Electron.*, vol. 62, no. 7, pp. 4430-4442, Jul. 2015.
- [3.14] J. Han, C. Choi, W. Park, I. Lee and S. Kim, "PLC-based photovoltaic system management for smart home energy management system," *IEEE Trans. Consum. Electron.*, vol. 60, no. 2, pp. 184-189, May 2014.
- [3.15] A. R. Al-Ali, I. A. Zualkernan, M. Rashid, R. Gupta and M. Alikarar, "A smart home energy management system using IoT and big data analytics approach," *IEEE Trans. Consum. Electron.*, vol. 63, no. 4, pp. 426-434, Nov. 2017.

- [3.16] X. Mao, K. Li, Z. Zhang and J. Liang, "Design and implementation of a new smart home control system based on internet of things," in *Proc. Int. Smart Cities Conf. (ISC2)*, Wuxi, China, Nov. 2017, pp. 1-5.
- [3.17] L. Zhang, H. Leung and K. Chan, "Information fusion based smart home control system and its application," *IEEE Trans. Consum. Electron.*, vol. 54, no. 3, pp. 1157-1165, Aug. 2008. [3.18] D. Han and J. Lim, "Smart home energy management system using IEEE 802.15.4 and zigbee," *IEEE Trans. Consum. Electron.*, vol. 56, no. 3, pp. 1403-1410, Aug. 2010.
- [3.19] D. Han and J. Lim, "Design and implementation of smart home energy management systems based on zigbee," *IEEE Trans. Consum. Electron.*, vol. 56, no. 3, pp. 1417-1425, Aug. 2010.
- [3.20] R. J. Robles, T. H. Kim, D. Cook and S. Das, "A review on security in smart home development," *Int. J. Adv. Sci. Technol.*, vol.15, pp.13-22, Feb. 2010.
- [3.21] F. K. Santoso and N. C. H. Vun, "Securing IoT for smart home system," in *Proc. IEEE Int. Symp. Consum. Electron. (ISCE)*, Madrid, Spain, Aug. 2015, pp. 1-2.
- [3.22] S. V. Tiwari, A. Sewaiwar and Y. Chung, "Smart home technologies using visible light communication," in *Proc. IEEE Int. Conf. Consumer Electron. (ICCE)*, Las Vegas, NV, USA, Mar. 2015, pp. 379-380.
- [3.23] Y. U. Lee, K. Kang and G. Choi, "Secure visible light encryption communication technique for smart home service," in *Proc. IEEE Annual Comput. and Commun. Workshop and Conf. (CCWC)*, Las Vegas, NV, USA, Mar. 2019, pp. 0827-0831.
- [3.24] M. Haus, A. Y. Ding and J. Ott, "LocalVLC: Augmenting smart IoT services with practical visible light communication," in *Proc. IEEE Int. Symp. "A World of Wireless, Mobile and Multimedia Networks"* (WoWMoM), Washington, DC, USA, Jun. 2019, pp. 1-9.
- [3.25] B. Hussain, et al., "Li-Fi based secure programmable QR code (LiQR)," in *Proc. JSAP-OSA Joint Symposia*, Fukuoka Japan, Sep. 2017, p. 6p_A409_6.
- [3.26] B. Hussain, C. Qiu and C. P. Yue, "A universal VLC modulator for retrofitting LED lighting and signage," in *Proc. IEEE 8th Global Conf. Consum. Electron. (GCCE)*, Osaka, Japan, Oct. 2019, pp. 1008-1009.

- [3.27] C. Qiu, B. Hussain and C. P. Yue, "Bluetooth based wireless control for iBeacon and VLC enabled lighting," in *Proc. IEEE 8th Global Conf. Consum. Electron. (GCCE)*, Osaka, Japan, Oct. 2019, pp. 614-615.
- [3.28] Y. Wang, B. Hussain and C. Patrick Yue, "Arbitrarily tilted receiver camera correction and partially blocked LED image compensation for indoor visible light positioning," *IEEE Sensors J.*, vol. 22, no. 6, pp. 4800-4807, Mar. 2022.
- [3.29] R. Zhang, W.-D. Zhong, Q. Kemao, and S. Zhang, "A single LED positioning system based on circle projection," *IEEE Photon. J.*, vol. 9, no. 4, pp. 1–9, Aug. 2017
- [3.30] J. W. Lee, S. J. Kim, and S. K. Han, "3D visible light indoor positioning by bokeh based optical intensity measurement in smartphone camera," *IEEE Access*, vol. 7, pp. 91399–91406, Jul. 2019.

CHAPTER 4 Photodiode-based VLC Transceiver System

4.1 Introduction of PD-based VLC Transceiver System

The VLC transceiver system that can support high-speed data transmission normally utilizes a photodiode (PD) as the light signal receiver [4.1]. PD is a light detector device that can convert visible light to a photo-electric current and the receiver in the PD-based VLC system is dedicated designed. The PD-based VLC system is usually constructed by discrete components with separate digital baseband for easy implementation and cost-effective purposes. Meanwhile, the similarity between PD-based VLC systems and traditional optical wireline systems has attracted research interest in designing integrated VLC transceiver system for practical highspeed applications, reducing power consumption, achieving a more compact size and real-life implementation. A typical PD-based VLC transceiver system is presented in Fig. 4.1, which consists of a VLC transmitter, LEDs as light source, a PD as light detector, and a VLC receiver. In the VLC transmitter, the data sequence from source is firstly encoded and then sent to the modulator, in which the data sequence is modulated with different schemes according to the design requirement. Then the modulated signal is transmitted to the LED driver to control the driving current of light source and generate the corresponding light signals. The communication channel in the VLC system can be the free space or water. In the VLC receiver, the light signal is converted into a photo-electric current by the PD. Then the following transimpedance amplifier (TIA) unit converts this current into voltage with signal amplification for further process. The clock and data recovery (CDR) module extracts the clock and retimes the data for the subsequent demodulation and decoding processes.

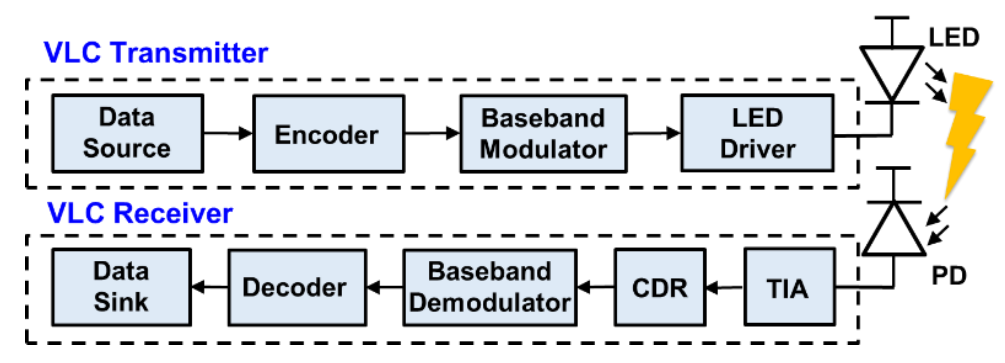


Fig. 4.1. Architecture of traditional PD-based VLC transceiver system.

Due to the characteristics of visible light, the PD-based VLC transceiver system owns several advantages comparing with traditional RF-based wireless communication systems. Firstly, the available spectrum bandwidth of visible light is much wider than that of radio waves. The electromagnetic spectrum of radio waves ranges from 20 kHZ to 300 GHz while the spectrum of visible light starts at 400 THz and ends at 800 THz, which is more than 1000 times wider comparing with the radio wave spectrum. Therefore, VLC system can provide a large spectrum capacity and solve the radio congestion problem in RF-based communication. Secondly, VLC system is more secure than RF-based systems for its LOS characteristic. The wavelength of visible light covers 380 nm to 780 nm which is shorter than radio waves, and the size of obstructions in buildings is much larger than the wavelength of visible light. Thus, the visible light travels in a straight line and is reflected when irradiating on the walls. With this LOS propagation characteristic, VLC technique can guarantee communication security and get rid of information disclosure since visible light cannot penetrate walls. Thirdly, the PD-based VLC system avoids EMI and radiation. Since the frequency of visible light is different from that of radio waves, using visible light to transmit signal causes no interference with the existing RFbased wireless systems. However, EMI exists widely in the RF systems and generates noise that can be harmful in the sensitive scenarios such as hospitals and airports. Besides, the nonionizing radiation caused by high energy radio waves is hazardous to health such as causing heating problem, which can be harmful for body tissues by exciting the electrons to higher energy state. Visible light, which owns much lower frequency, is out of this range and the intensity of normal luminance will not cause health problem. Lastly, PD-based VLC system is suitable for special communication channels like water [4.2]. The traditional RF-based systems suffer from difficulty in underwater communication since RF signals attenuate dramatically in the water. Visible light, especially the blue and green light, can transmit signals for much longer distance than the radio waves in the underwater circumstance due to its low attenuation. Besides, the visible light owns superior directivity and high collimation when propagating in water.

4.2 Integrated VLC Transmitter

The integrated design of VLC transmitter contributes to scale down the circuit size, decrease the consumed power and is suitable for high-speed data transmission. Except from dedicated

circuit design, choosing the suitable light source and modulation scheme are also critical for designing the appropriate VLC transmitter according to different application scenarios.

4.2.1 Architecture of Integrated VLC Transmitter

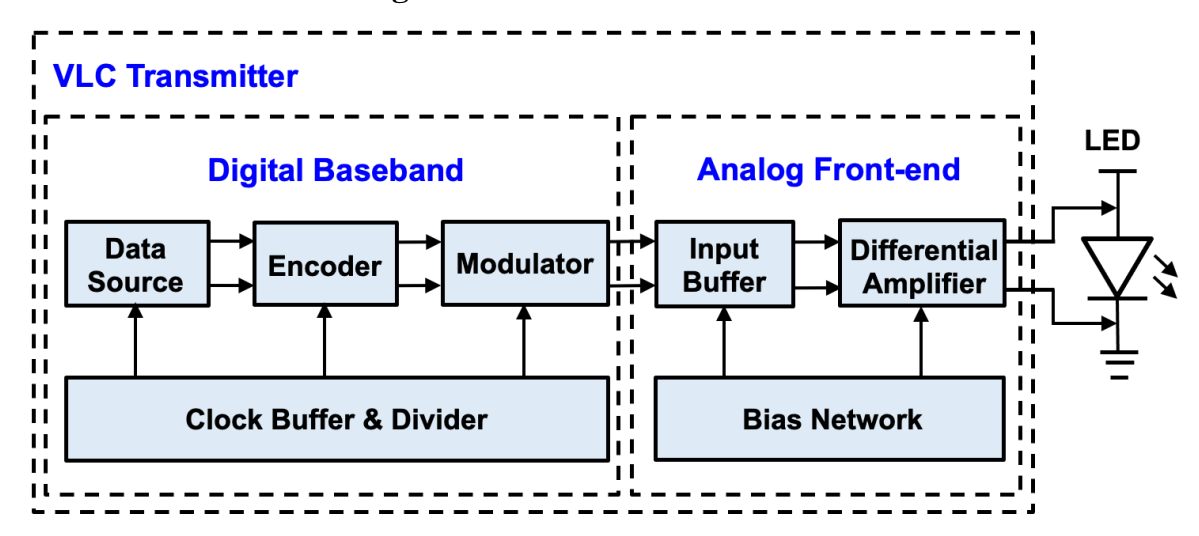


Fig. 4.2. Typical architecture of integrated VLC transmitter.

Due to the similarity between LED and laser diode (LD), the design of integrated VLC transmitter can refer to the typical structure of optical transmitter. The architecture of integrated VLC transmitter in PD-based VLC system is presented in Fig. 4.2. It consists of a digital baseband, an analog front-end (AFE) circuit and a light source. The transmitter adopts differential structure for decreasing the signal noise and suppressing the EMI. In the digital baseband, the data sequence is generated from data source as a differential signal pair. The digital encoder codes the original data sequence with corresponding encoding schemes, then the coded data sequence is sent to the digital modulator for modulation process. The common modulation schemes for VLC technique are OOK modulation, pulse amplitude modulation (PAM) and orthogonal frequency division multiplexing (OFDM) modulation. The high-order modulation schemes can increase communication data rate through increasing bandwidth efficiency. The clock buffer and divider block process the outside clock signal to several clock signals with different frequency which are sent to the corresponding digital blocks. In the AFE, the input buffer locates between the digital baseband and main amplifier for increasing the driving capability of the amplifier. The following differential amplifier is utilized as driver unit in the AFE block, and it normally adopts the current mode logic (CML) structure or other CML-

based structures to convert the input voltage signal into a current output. The bias network provides suitable bias voltage to the analog blocks for managing the transistors to the appropriate working states.

4.2.2 Different Types of Light Sources

In the PD-based VLC system, the light source varies with different application scenarios as well as different design requirements. Moreover, the communication data rate of whole VLC system is related to the light source since light source limits the modulation bandwidth of VLC transmitter. There exist three types of typical light sources which are LEDs, micro-LEDs (μ LEDs) and laser diodes (LDs), and their characteristics are summarized in Table 4.1.

- 1. LEDs. The commercial LED utilized in PD-based transceiver system includes single-color LED and phosphorescent white LED and the typical size of the commercial LED chip is around 1 mm². This kind of LED owns the advantages that they are cost effective and easy of access. However, the modulation bandwidth of commercial LED is quite low, the phosphorescent white LED own modulation bandwidth of serval MHz while the bandwidth of single-color LED is about 10-20 MHz [4.3]. The low bandwidth is caused by large intrinsic capacitor up to 5 nF and parasitic capacitor of trace in LED chip. The phosphorescent coating of phosphor white LED can also decrease the bandwidth of LED due to the slow secondary emission switch of phosphor. Besides, commercial LED suffers from low directivity which decreases the communication distance as the light signal is spread out with high loss in the free space channel.
- 2. μLEDs. The μLED is a new type of LED with smaller size and higher intensity which is designed for improving the quality of display. The diameter of μLED is normally shorter than 50 μm and this compact size dramatically reduced the value of intrinsic capacitance. It contributes to increase the modulation bandwidth and μLED usually has dozens of MHz to hundreds of MHz bandwidth [4.4] which guarantees the application of high-speed VLC. Typically, there are three LED chips in one μLED and they are red, green and blue so that the color and light intensity can be controlled. However, due the limitation of technology, fabricating large size of display screen with μLED is difficult so the μLED is adopted to small screen such as the wearable watch now, which decreases the communication distance.

3. LDs. LD generates the light through stimulated radiation which guarantees the direction, frequency, phase and polarization of the stimulated photons are consistent. Due to this high coherence characteristic, laser owns high directivity and high power efficiency. With the high directivity, the communication distance of VLC using LD is longest among these types of light sources. Moreover, the modulation bandwidth of LD is high enough to support high-speed communication due to the small parasitic capacitors in LD chip. The typical bandwidth of LD is beyond 1 GHz [4.5] which is much larger than LED. But the manufacture process of LD is complex and this improves the cost of LD.

Table 4.1 Comparison of Different Types of Light Sources

Type of Light Sources	LEDs	μLEDs	LDs	
Size of Chip	~ 1 mm ²	$< 2500 \ \mu m^2$	$< 0.1 \text{ mm}^2$	
Modulation Bandwidth	5 - 20 MHz	20 - 500 MHz	> 1 GHZ	
Communication Distance	Middle	Short	Long	
Directivity	Low	Low	High	
Power Efficiency	Low	High	High	
Cost	Low	High	High	

4.2.3 Modulation Scheme

The modulation scheme in the PD-based VLC system is significant and there are various schemes that can be utilized to the VLC technique for increasing the bandwidth efficiency so that to improve the communication data rate.

- 1. OOK modulation. The most basic modulation scheme is OOK modulation, due to its simple implementation, this modulation scheme is widely adopted in both CIS- and PD-based low complexity VLC system. As presented in Fig. 4.3. (a), there are two levels of amplitude in the OOK modulation showing the turn-on and turn-off states of LED respectively. The turn-on state of LED representing bit "1" and turn-off state representing bit "0".
- 2. PAM. To increase the communication data, high-order modulation schemes such as PAM can be applied to the PD-based VLC system [4.6]. PAM utilizes the different amplitude

levels to represent different logical bits. As shown in Fig. 4.3. (b), the lowest level represents the two bits "00", the second-lowest level is "01", the second-highest level is "10" and the highest level is "11". Therefore, each symbol in the PAM-4 represents 2 bits, which realizes utilizing the same bandwidth to double the transmitted data and increase the data rate two times. Since the PAM scheme only modulates signal level, the implementation is relatively simple without time domain to frequency domain conversion. Similarly, for the PAM-8 requires 8 different levels to represent 3 bits, which causes one disadvantage of the PAM scheme that it has a high requirement of signal-to-noise to noise ratio (SNR) so that there are enough levels for transmitting data.

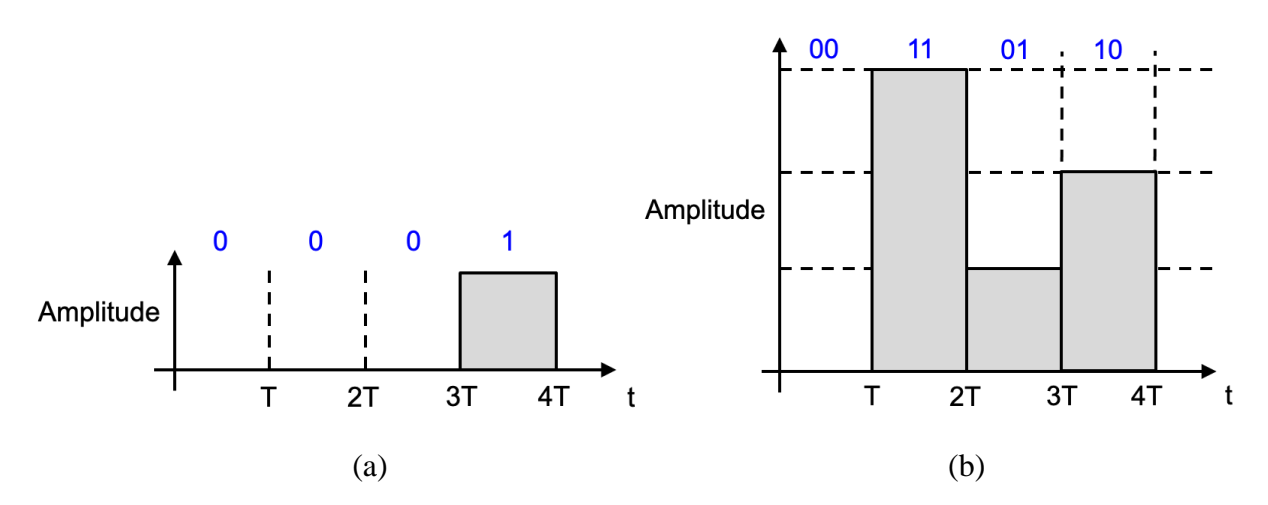


Fig. 4.3. Modulated waveforms of (a) OOK modulation scheme, and (b) PAM-4 scheme.

3. OFDM and Quadrature amplitude modulation (QAM). OFDM is a multiple carrier modulation scheme in the frequency domain to improve the communication data rate as well as solve inter-symbol interference (ISI) issue [4.7]. The OFDM utilizes multiple orthogonal sub-carries with a narrow band to split the input data stream and transmit the data in multiple carriers simultaneously so that the data stream in each sub-carrier is transmitted at low speed. Therefore, the system can work with a higher data rate under the same ISI condition. Besides, the low speed in the subcarrier provides convenience to add guard interlevel for decreasing the ISI. As shown in Fig. 4.4. (a), the sub-carriers are all orthogonal so that there can exist frequency over-lapping in adjacent two sub-carriers for increasing the spectrum efficiency. When applying the OFDM into a PD-based VLC system,

the generated signal contains real and imaginary part but only the real part is required for the output signal. Therefore, a Hermitian symmetry is adopted in the frequency domain to generate the required signal. In each sub-carrier, QAM is a typical modulation scheme used in the OFDM and it utilizes both the phase and amplitude of the sub-carrier signal to represent different bits. As presented in Fig. 4.4. (b), the modulated information of 16-QAM is mapped into the polar coordinates. The distance between the blue point which is one symbol to the original point is the modulated amplitude and the angle between the point to image axis is the value of modulated phase. Therefore, 16-QAM can utilize one symbol to represent 4 bits which dramatically increases the transmitted data rate.

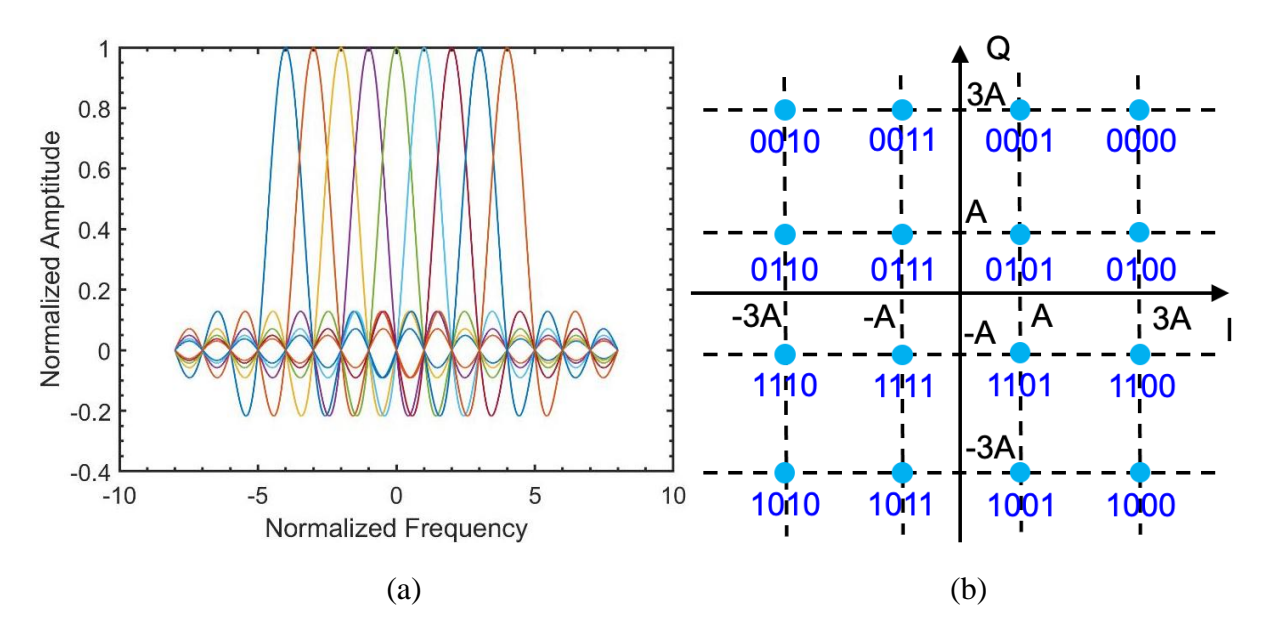


Fig. 4.4. (a) Spectrum diagram of OFDM containing different subcarriers with frequency overlapping; (b) Constellation diagram of 16-QAM.

4.3 Integrated VLC Receiver

4.3.1 Architecture of Typical PD-based VLC Receiver

The typical architecture of the PD-based VLC receiver is presented in Fig. 4.5, and it consists of a PD as detector, an analog front-end and a digital baseband. A PD is designed as the visible light detector to convert the light signal to a photo-electric current. The PD adopted in the VLC system owns high responsivity to the whole visible light spectrum. This photo-electric current

is the input to the AFE, then it is converted to a voltage signal which is also amplified by the TIA circuit. A gain control unit connected to the TIA manages the gain of amplifier according to the variation of communication distance and intensity of received signal. The following equalizer unit extends the limited modulation bandwidth to improve the data rate. A decision circuit determines the output signal by extracting data from the equalized signal according to the clock signal from clock recovery unit. An output buffer locates at the end of the AFE to connect the analog circuits with digital baseband. The demodulating and decoding processes are performed in the digital baseband to recover the original transmitted digital data sequence.

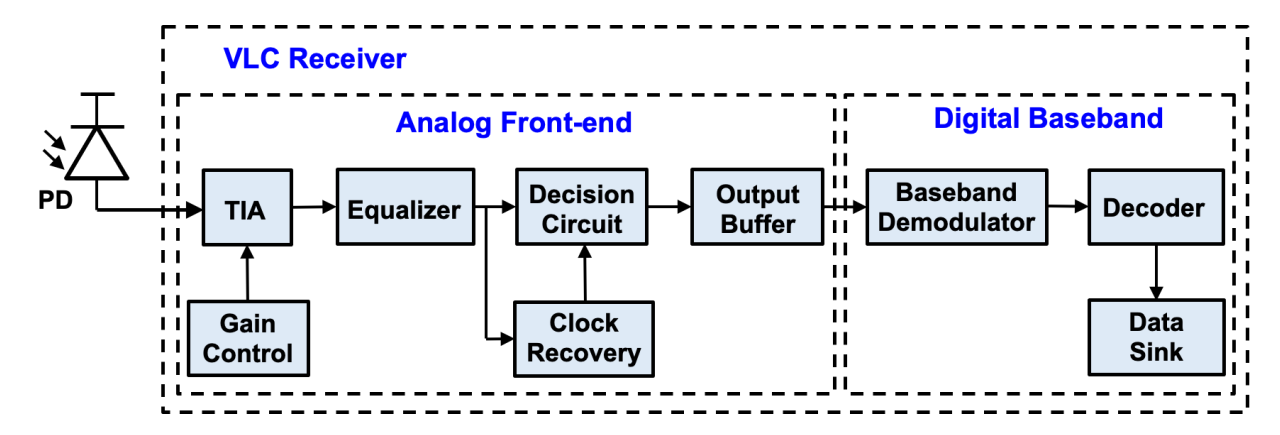


Fig. 4.5. Typical architecture of PD-based VLC receiver.

4.3.2 Different Types of PDs

In the PD-based VLC receiver, the light detector should own high responsivity to the entire visible light spectrum so that it can convert the white light to current while avoiding the noise generated from the waves in other optical spectrums. Typically, there are two types of PDs being utilized as a detector in the VLC system, which are the PIN PD and the avalanche PD (APD). PIN PD is widely adopted in VLC systems for detecting high-speed light signals since it has fast responsivity to the visible light. Moreover, it also owns the advantages of low-cost and low noise while its disadvantage is the large dark current. The APD is more sensitive to weak intensity scenarios and its response speed is higher than PIN PD, so it can also be applied to high-speed VLC systems. Its drawbacks include a higher cost and larger shot noise due to a higher gain of photo-electric current.

4.4 Equalization Schemes

Limitations in signal transmission includes device limitation, channel loss, and channel noises, which restrict the modulation bandwidth and the communication data rate. To overcome these limitations and improve quality od received signals, various equalization schemes can be adapted to the transceiver system.

4.4.1 Passive and Active Equalizers

The analog equalizers, they can be roughly divided into two categories named a passive equalizer and active equalizer [4.8]-[4.9]. The passive equalizer usually only contains passive components such as a resistor, capacitor, and inductor. These passive components constitute a high-pass filter to decrease the low-frequency signals while remaining the high-frequency signals so that the overall bandwidth is extended. The active equalizer consists of active components such as transistors as well as passive components. The zero and pole points of an equalizer can be controlled separately, and multiple stages of an equalizer can be adopted for flexible compensation. Therefore, the active equalizer is more suitable for complex occasions.

4.4.2 Digital Based Equalization

Digital equalization schemes are implemented in the digital baseband with a dedicated algorithm to compensate for the channel loss and solve limited bandwidth. The most common digital equalization schemes are feed-forward equalization (FFE), decision feedback equalization (DFE) [4.10], and Volterra nonlinear equalization (VNE) [4.11]. FFE is a linear equalization scheme that owns the simplest algorithm and can be applied in both transmitter and receiver. Moreover, FFE can be implemented through an analog method using delay units, amplifiers, and adders. DFE is a nonlinear equalization scheme that is widely adopted in the receiver with not amplifying the noise and interference. VNE is also a nonlinear equalization scheme and is more common for compensating the nonlinear effects. Moreover, the neural network (NN) [4.12] supported digital equalization algorithms have attracted research focus for their superior performance in solving the limited bandwidth problem as well as nonlinear effects.

4.4.3 Hybrid Equalization

For real applications in PD-based VLC systems, the various equalization schemes are adopted in hybrid mode. Typically, the passive equalizer is designed in the transmitter with the FFE

algorithm, while the active equalizer such as continuous-time linear equalizer (CTLE) and DFE implemented in the receiver. The hybrid equalization scheme combines the advantages of these schemes while getting rid of the disadvantages so that the performance of the VLC system can be improved maximumly. In [4.13], PAM-4 and FFE are combined to increase the communication data rate to 2 Gbps. In [4.14], 64-QAM is adopted for the higher data rate with an adaptive deep-learning equalizer. CAP modulation scheme with a hybrid post-equalizer is utilized in [4.14] and the data rate can be as high as 8 Gbps. DMT modulation with an adaptive bit- and the power-loading algorithm is adopted in [4.15] to achieve a data rate of 1 Gbps. [4.16] the combination of DCO-OFDM and long-short term memory (LSTM) while [4.17] is the 64-QAM signal transmission with a joint time-frequency neural network to realize a data rate of 2.85 Gbps underwater VLC system. In [4.18], the PAM-4 and PAM-8 schemes are adopted with LSTM equalizer to reach a communication distance of 1.2 m with 1.15 Gbps. An UVLC system with data rate of 1.22 Gbps is implemented in [4.19] with PAM-7 modulation and density-based spatial clustering of applications with noise (DBSCAN) algorithm.

4.5 Applications of PD-based VLC System

The PD-based VLC system can be applied to various scenarios. In the occasions which require high communication security, the VLC technique can be adopted to guarantee safety due to its high anti-intercept capability. Moreover, this VLC system is suitable for EMI sensitive scenarios such as hospitals, airports, and banks. As for the communication channel, it can be water or fiber in addition to free space.

4.5.1 High-speed Point-to-Point VLC

The PD-based VLC system is suitable for the indoor environment since it combines illumination function with wireless communication. Due to the one-way communication characteristic of the VLC technique, it can be a supplemental component of existing RF-based communication systems as the downlink to provide data transmission in the indoor environment, while the RF-based wireless communication system offers the uplink to construct a high-speed two-way communication method with combining the advantages of two types of communication techniques. The LEDs equipped with the VLC function can serve as AP Since

a PD-based VLC system can support high-speed data transmission, it can be utilized as a data access point (AP) for the portable devices to connect with the Internet. The high-speed indoor point-to-point VLC can also be utilized to transmit signals among domestic intelligent appliances to construct an IoT network at home.

4.5.2 Smart Display

μLED is designed for display screens and it can be applied for smart display applications after being equipped with the VLC technique. PD-based VLC system is appropriate for smart display with high-speed communication. The transmitter is a μLED screen that can simultaneously display the video or figures and transmit signals. Due to the requirement of constant DC bias voltage for the screen, the coding method should be RLL encoding to guarantee the duty ratio is a constant value. Since there are red, green, and blue LED chips existing in one μLED, the modulation schemes for smart display can be wavelength division multiplexing (WDM) modulation or color shift keying (CSK) to increase the communication data rate [4.20]-[4.21]. As for the receiver, it will be a dedicated designed PD-based VLC receiver to detect and decode the transmitted signal. One drawback of the smart display is the short communication distance which is caused by the small area of screen due to the limitation of fabrication technology.

4.5.3 Underwater Communication

A PD-based VLC system using the LD as the light source is one solution to underwater communication. Since the RF-based technology suffers from dramatic signal loss in water due to the absorption of water to RF signal, the communication distance is extremely short to meter level. Though the acoustic-based system is used in water occasions to transmit signals and the communication distance is as far as dozens of kilometers, it suffers from a critical disadvantage that the communication latency is quite large. Besides, the data rate of the acoustic-based system is as low as the kbps level. Compared with the two types of underwater communication methods, the PD-based VLC system is more suitable for the water occasion. The blue and green laser light can be applied to the underwater communication as signal carriers due to the low attenuation and high directivity. The communication data rate can reach to Gbps level and the distance varies from dozens of meters to serval hundreds of meters [4.22]-[4.23]. Besides, to

save cost and energy, the normal blue and green visible light generated by LEDs can also be utilized to carry signals. Moreover, the underwater VLC system can be combined with an acoustic system and RF system to form a two-way communication system according to the actual scenarios.

4.6 References

- [4.1] S. Rajbhandari, et al., "High-Speed Integrated Visible Light Communication System: Device Constraints and Design Considerations," in *IEEE Journal on Selected Areas in Communications*, vol. 33, no. 9, pp. 1750-1757, Sept. 2015.
- [4.2] S. Arnon, "Underwater optical wireless communication network," in *Opt. Eng.*, vol. 49, no. 1, Jan. 2010.
- [4.3] H. Li, et al., "High bandwidth visible light communications based on a post-equalization circuit," in *IEEE Photon. Technol. Lett.*, vol. 26, no. 2, pp. 119–122, Jan. 2014.
- [4.4] J. J. D. McKendry, et al., "Visible-light communications using a CMOS-controlled microlight-emitting-diode array," in *Journal of Lightwave Technology*, vol. 30, no. 1, pp. 61-67, Jan. 2012.
- [4.5] C. Lee, et al., "4 Gbps direct modulation of 450 nm GaN laser for highspeed visible light communication," in *Optical Express*, vol. 23, no. 12, pp. 16232–16237, Jun. 2015.
- [4.6] X. Li, et al., "Wireless Visible Light Communications Employing Feed-Forward Pre-Equalization and PAM-4 Modulation," in *Journal of Lightwave Technology*, vol. 34, no. 8, pp. 2049-2055, Apr. 2016.
- [4.7] D. Tsonev, et al., "A 3-Gb/s Single-LED OFDM-Based Wireless VLC Link Using a Gallium Nitride μLED," in *IEEE Photonics Technology Letters*, vol. 26, no. 7, pp. 637-640, Apr. 2014.
- [4.8] H. Zhang, A. Yang, L. Feng and P. Guo, "Gb/s Real-Time Visible Light Communication System Based on White LEDs Using T-Bridge Cascaded Pre-Equalization Circuit," in *IEEE Photonics Journal*, vol. 10, no. 2, pp. 1-7, April 2018.
- [4.9] H. Li, et al., "High bandwidth visible light communications based on a post-equalization circuit," in *IEEE Photonics Technology Letters*, vol. 26, no. 2, pp. 119–122, Jan. 2014.

- [4.10] G. Stepniak, J. Siuzdak and P. Zwierko, "Compensation of a VLC Phosphorescent White LED Nonlinearity by Means of Volterra DFE," in *IEEE Photonics Technology Letters*, vol. 25, no. 16, pp. 1597-1600, Aug. 2013.
- [4.11] N. Stojanovic, et al., "Volterra and Wiener Equalizers for Short-Reach 100G PAM-4 Applications," in *Journal of Lightwave Technology*, vol. 35, no. 21, pp. 4583-4594, Nov. 2017. [4.12] N. Chi, J. Jia, F. Hu, Y. Zhao and P. Zou, "Challenges and prospects of machine learning in visible light communication," in *Journal of Communications and Information Networks*, vol. 5, no. 3, pp. 302-309, Sept. 2020.
- [4.13] H. Chen, et al., "Adaptive deep-learning equalizer based on constellation partitioning scheme with reduced computational complexity in UVLC system," in *Optical Express*, vol. 29, no. 14, pp. 21773-21782, Jun. 2021.
- [4.14] Y. Wang, L. Tao, X. Huang, J. Shi and N. Chi, "8-Gb/s RGBY LED-Based WDM VLC System Employing High-Order CAP Modulation and Hybrid Post Equalizer," in *IEEE Photonics Journal*, vol. 7, no. 6, pp. 1-7, Dec. 2015.
- [4.15] A. M. Khalid, et al., "1-Gb/s Transmission Over a Phosphorescent White LED by Using Rate-Adaptive Discrete Multitone Modulation," in *IEEE Photonics Journal*, vol. 4, no. 5, pp. 1465-1473.
- [4.16] N. A. Amran, M. Dehghani Soltani, M. Yaghoobi and M. Safari, "Deep Learning Based Signal Detection for OFDM VLC Systems," in 2020 IEEE International Conference on Communications Workshops (ICC Workshops), 2020, pp. 1-6.
- [4.17] H. Chen, Y. Zhao, F. Hu and N. Chi, "Nonlinear Resilient Learning Method Based on Joint Time-Frequency Image Analysis in Underwater Visible Light Communication," in *IEEE Photonics Journal*, vol. 12, no. 2, pp. 1-10, April 2020.
- [4.18] Xingyu Lu, et al., "Memory-controlled deep LSTM neural network post-equalizer used in high-speed PAM VLC system," Opt. Express 27, 7822-7833 (2019).
- [4.19] M. Shi, et al., "Enhanced Performance of PAM7 MISO Underwater VLC System Utilizing Machine Learning Algorithm Based on DBSCAN," in *IEEE Photonics Journal*, vol. 11, no. 4, pp. 1-13, Aug. 2019.

- [4.20] H. Chun, et al., "LED Based Wavelength Division Multiplexed 10 Gb/s Visible Light Communications," in *Journal of Lightwave Technology*, vol. 34, no. 13, pp. 3047-3052, Jul. 2016.
- [4.21] E. Monteiro and S. Hranilovic, "Design and Implementation of Color-Shift Keying for Visible Light Communications," in *Journal of Lightwave Technology*, vol. 32, no. 10, pp. 2053-2060, May. 2014.
- [4.22] X. Liu, et al., "34.5 m underwater optical wireless communication with 2.70 Gbps data rate based on a green laser diode with NRZ-OOK modulation," in *Opt. Express*, vol. 25, no. 22, pp. 27937–27947, 2017.
- [4.23] J. Wang, et al., "100 m/500 Mbps underwater optical wireless communication using an NRZ-OOK modulated 520 nm laser diode," in *Opt. Express*, vol. 27, no. 9, pp. 12171–12181, 2019.

CHAPTER 5 Design of PAM-4 VLC Transmitter with Feed Forward Equalization

5.1 Introduction

With the typical structure of the PD-based VLC transceiver system and equalization methods of modulation bandwidth extension introduced in Chapter 4, a PAM-4 VLC transmitter equipped with FFE and passive equalizer is proposed in this chapter. The traditional PD-based VLC system consists of discrete components with separate offline digital baseband faces the disadvantages such as large size, large parasitic components, and high power consumption. The integrated structure can solve these problems and is suitable for practical application and achieving high reliability. However, the VLC transmitter in an integrated PD-based VLC system suffers from low data rate since the modulation bandwidth is severely limited by the LED device [5.1]-[5.2]. To accomplish high-speed VLC applications, high-order modulation schemes like PAM, OFDM, WDM, and various equalization schemes such as passive equalizer and digital equalization are applied in the discrete transceiver system but few of the integrated designs adopt these schemes. Therefore, to realize a high-speed integrated VLC transmitter, this chapter proposes a VLC transmitter with PAM-4 scheme, passive equalizer and FFE.

However, several challenges need to be addressed in the implementation of these bandwidth extension methods. At the system level, this transmitter is a mixed-signal design consisting of a digital baseband and an analog front-end. The digital baseband offers the modulated signal with FFE, which requires a systematic analysis of digital signal generation, modulation, equalization and corresponding implementation processes. The analog front-end should combine the functions of a digital to analog converter (DAC) and LED driver. The resolution of DAC should be properly chosen so that it can convert the digital equalized signal to the analog signal with accurate amplitude. As for the LED driving function, the amplitude of the driving current should be carefully determined within the linear range of LED.

5.2 Analysis of Modulation Bandwidth Extension Schemes

5.2.1 Device Limitation

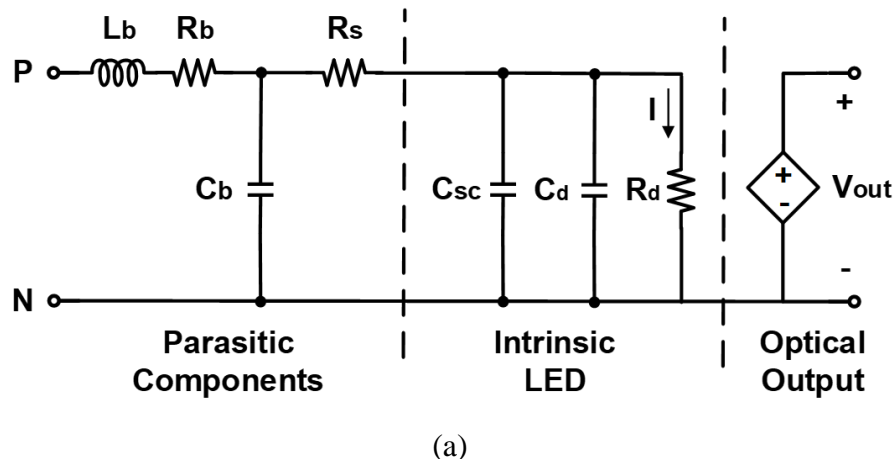
Device limitation is the main reason for decreasing the communication data rate of integrated PD-based VLC systems since the modulation bandwidth of typical LED is as low as 5-20 MHz. To analyze the device limitation caused by LED, constructing an accurate model of LED is essential. As shown in Fig. 5.1. (a), the typical equivalent circuit model of LED consists of parasitic components circuit, intrinsic LED circuit, and optical output circuit [5.3]. The parasitic circuit containing the series bonding inductor L_b, the series bonding resistor R_b, the parallel bonding capacitor C_b, and the series resistor R_s. These components represent the test fixture and bonding wires of the LED device. The intrinsic model of LED consists of the space charge capacitor C_{sc}, the diffusion capacitor C_d and the differential resistor R_d. The final optical output is a current control voltage source whose output is a voltage determined by the current through R_d in the intrinsic model. Therefore, the impedance of this LED model is:

$$Z_{LED} = j\omega L_b + R_b + \frac{1}{j\omega C_b} / \left[R_s + \frac{1}{j\omega (C_{sc} + C_d)} / / R_d \right]$$
 (5.1)

This equivalent model can be treated as a first-order low-pass filter with the transfer function as below:

$$H_{LED}(s) = \frac{V_{out}(s)}{V_{in}(s)} = \frac{R_d}{Z_{LED}} \approx \frac{1}{1 + s(C_{sc} + C_d)R_d}$$
(5.2)

where s is the complex variable and $s = i\omega$. Since the parasitic components are negatable comparing with the components of intrinsic device in the low-frequency domain, this parasitic model mainly affects signal operating in the frequency domain beyond 500 MHz with second order distortion. The component values of this model are summarized in Table 5.1.



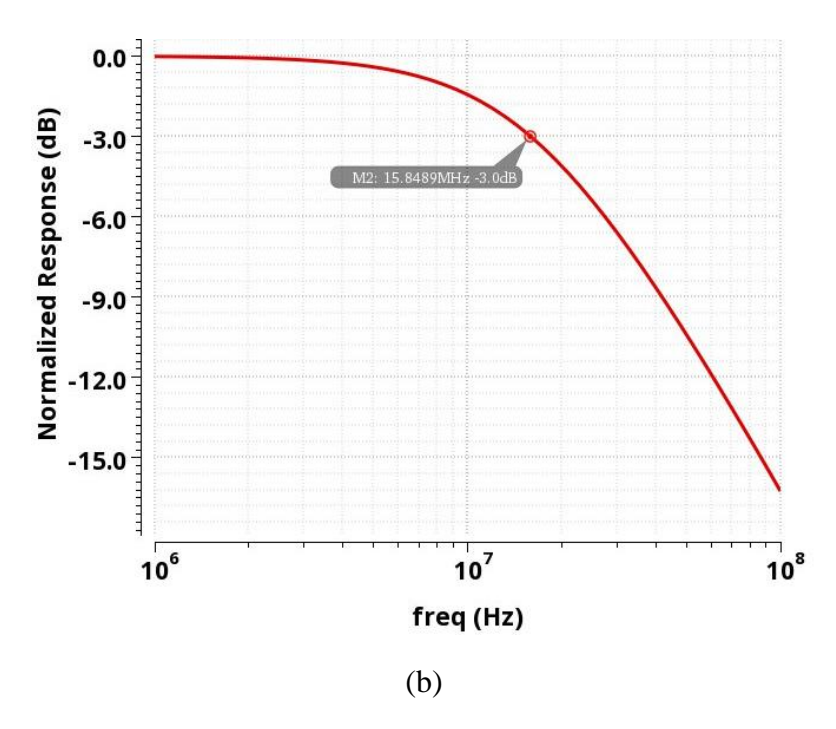


Fig. 5.1. (a) Typical equivalent circuit model of LED; (b) Simulated modulation bandwidth of this LED model.

Table 5.1 Component Values of Equivalent LED Model

Component	L _b	R _b	C_b	R_s	C_{sc}	C_d	R_d
Value	0.2 nH	1.2 Ω	0.5 nF	0.5 Ω	1.5 nF	1 nF	4 Ω

The simulated modulation bandwidth of this equivalent model is presented in Fig. 5.1. (b). It can be noticed that this bandwidth curve is similar to the performance of a first-order low pass filter which is corresponding with the previous analysis. The -3 dB bandwidth of this LED model is 15 MHz which dramatically limits the system modulation bandwidth.

5.2.2 Principle of PAM-4 Scheme

PAM-4 scheme is widely adopted in the high-speed optical wireless communication (OWC) system as the modulation scheme for it can double the bandwidth efficiency. Similarly, it can be adopted into the PD-based VLC system considering the system structure. As shown in Fig. 5.2, the PAM-4 scheme is implemented by using one symbol to represent two bits with four different signal levels. With this modulation scheme, the symbol in one period carries two bits

to double the modulation bandwidth efficiency. The corresponding eye diagram of the signal modulated with PAM-4 is also presented in Fig. 5.2, and it can be noticed that the eye height of the PAM-4 signal is one-third of the eye height of the NRZ signal with the same amplitude. This smaller eye height brings a higher requirement on the SNR of the signal.

As for the implementation of the PAM-4 scheme in the PD-based VLC system, most of the VLC prototypes equipped with a high-order modulation scheme are composed of discrete components [5.4]. On the transmitter side, a high-speed and compact LED driver unit for PAM-4 scheme is neglected. Since PAM-4 signal has a higher requirement on the SNR, increasing the signal amplitude can contribute to the SNR of PAM-4 signal and improve the data rate. However, this increase of amplitude leads to another problem which is the nonlinear effect of LED [5.5] since higher driving current can cause the LED working in the nonlinear region. To solve this problem, the generated driving current should be modulated within the range of the linear range of the LED device, which is one of the design indicators for generating the PAM-4 signals.

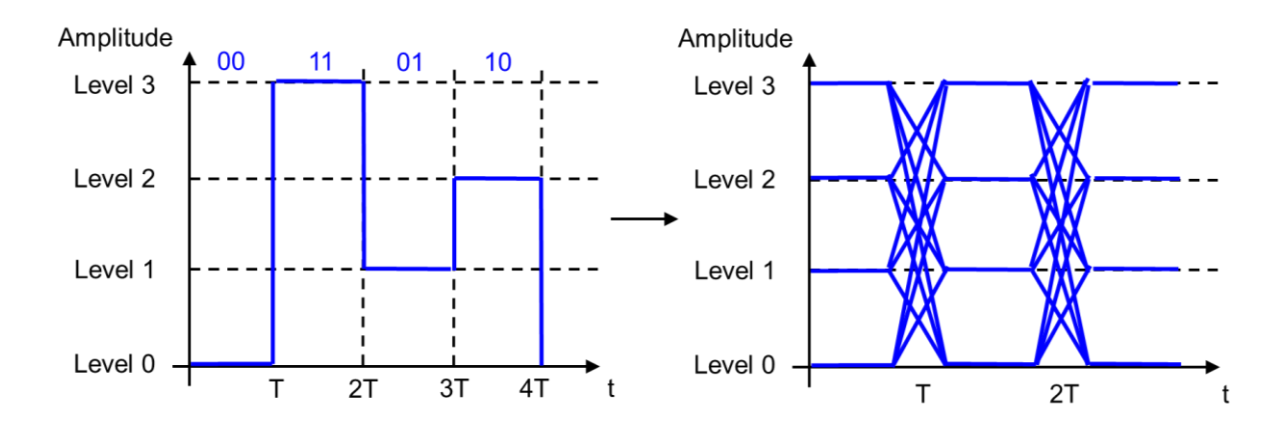


Fig. 5.2. Principle of PAM-4 scheme corresponding eye diagram of PAM-4 signal.

5.2.3 Principle and Implementation of FFE

FFE is an equalization method that is widely adopted in the high-speed optical wireless and wireline communication transceiver systems to improve the system performance. The principle of waveform combination of a 3-tap FFE is illustrated in Fig. 5.3. (a), which is presented by the combination of original waveform and two post-taps generated by delaying the reverse original

signal for 1-UI [5.6]. The blue waveforms are generated signals from transmitter baseband while the red waveforms are the limited transmission signals with tails. The main reason for causing the ISI of signal is the tail spreading to the adjacent symbols, which can be cancelled by the FFE. In the original signal, the tail affects two symbols with tail heights of h1 and h2 separately. The two post-taps from reverse main signal can generate signals with height of h1 and h2 at 3T and 4T when their amplitudes are equal to Ah1/h0 and Ah2/h0 separately. After adding these two pot-taps to the original signal, the undesired tail can be counteracted as shown in Fig. 5.3 (a). The improvement on eye diagram is presented in Fig. 5.3. (b), the blue dotted lines on the left side represent the eye diagram of the originally generated signal and the solid line the left side is the eye diagram of the limited signal, which is attenuated in amplitude and suffers from loss of high-frequency components. After being equipped with FFE, the eye diagram is presented the right side as solid lines. Since the low-frequency components are decreased and the high-frequency components are compensated, the corresponding eye opens more widely. Therefore, the signal transmission quality is improved but sacrifices the eye height which requires the trade-off between SNR and transmission quality.

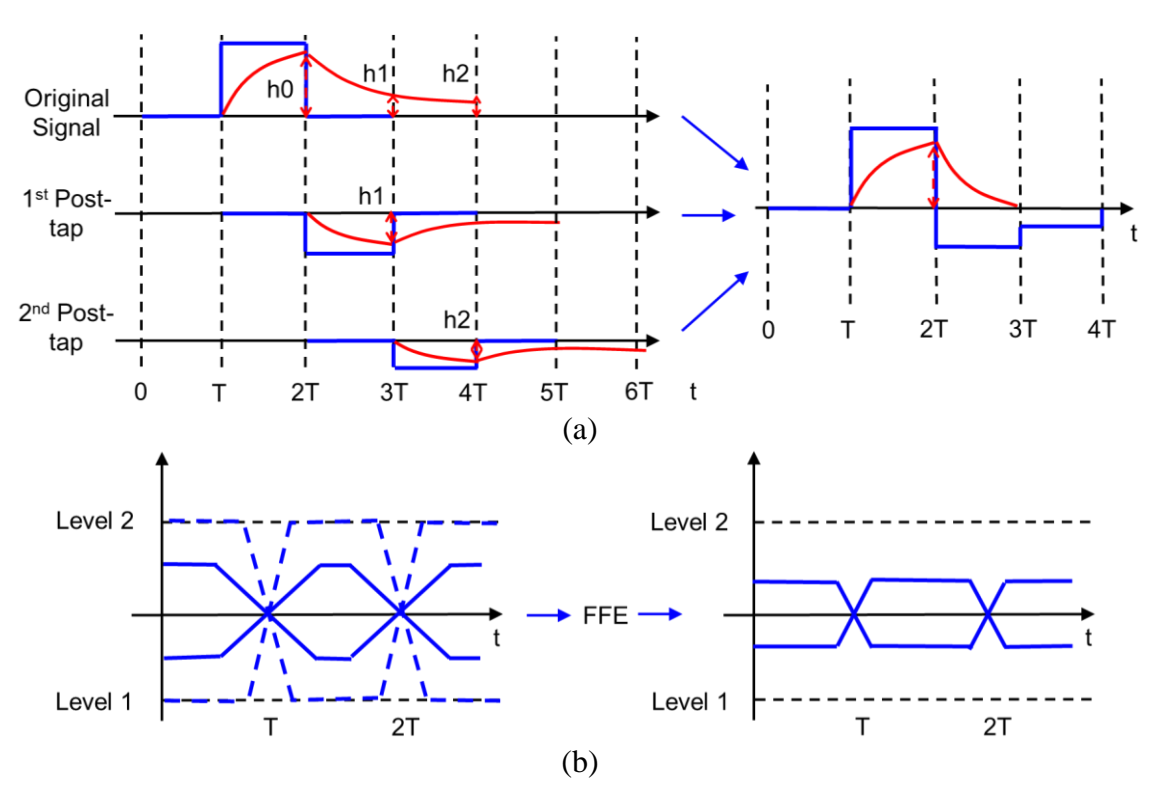


Fig. 5.3. (a) Principle of the waveform combination in FFE; (b) Improvement on the NRZ eye diagram by adopting FFE.

To calculate the value of tap weights, an analysis of signal delay after transmitting through the communication channel is necessary. As shown in Fig. 5.4, the black line is the original signal with a tail caused by channel limitations, the yellow line is the first post-tap signal of FFE while the blue line is the second post-tap. h_1 is the tail height at sample point t_1 which requires to be canceled by FFE. Therefore, the tails of the first post-tap and second post-tap at sample point t_1 will be utilized to cancel the tail of the original signal at t_1 . The tap weights of these two post-taps are related to the canceling tail height and can be calculated with the following equation:

$$h_1 = h_{0.5} \times \omega_1 + h_0 \times \omega_2 \tag{5.3}$$

where ω_1 is the tap weight of the first tap, ω_2 is the tap weight of the second tap and $h_{0.5}$ is the tail height of the original signal at sample time $t_{0.5}$. Similarly, to cancel the tail height of h_2 ,

$$h_2 = h_{1.5} \times \omega_1 + h_1 \times \omega_2 \tag{5.4}$$

With these two equations and the measured values of original tail heights, the tap weights of these two post-taps can be calculated. This method can be extended to determine the tap weights of the FFE method with more taps.

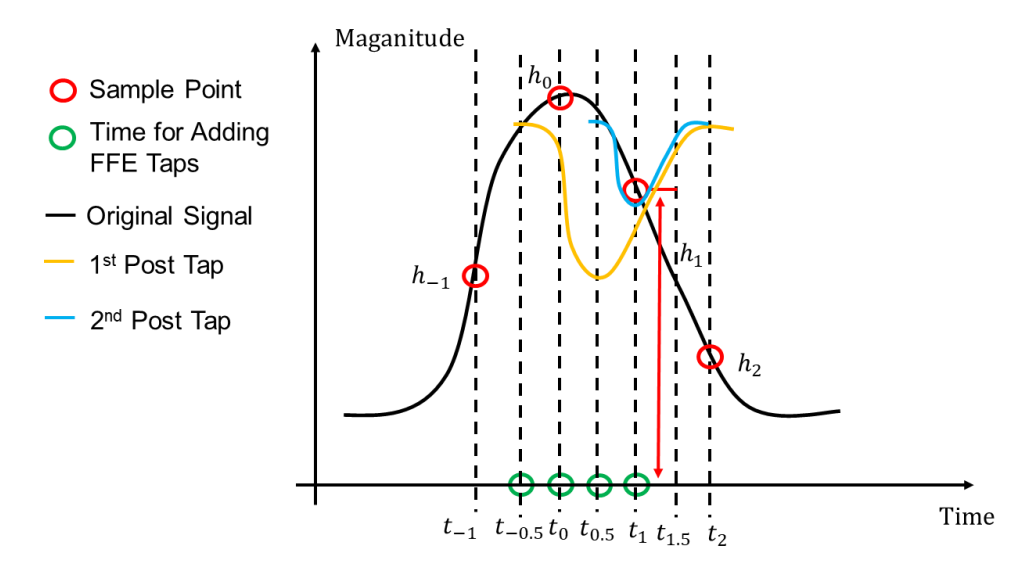


Fig. 5.4. Analysis of calculating the tap weights in FFE.

After obtaining the tap numbers and corresponding tap weights, the final expression of the FFE signal is as below [5.6]:

$$y[n] = \sum_{k=0}^{M} \omega_k x[n-k]$$
 (5.5)

where y[n] is the final output FFE signal, M is the tap number, ω_k is the tap weight and x[n-k] is the delayed tap signal.

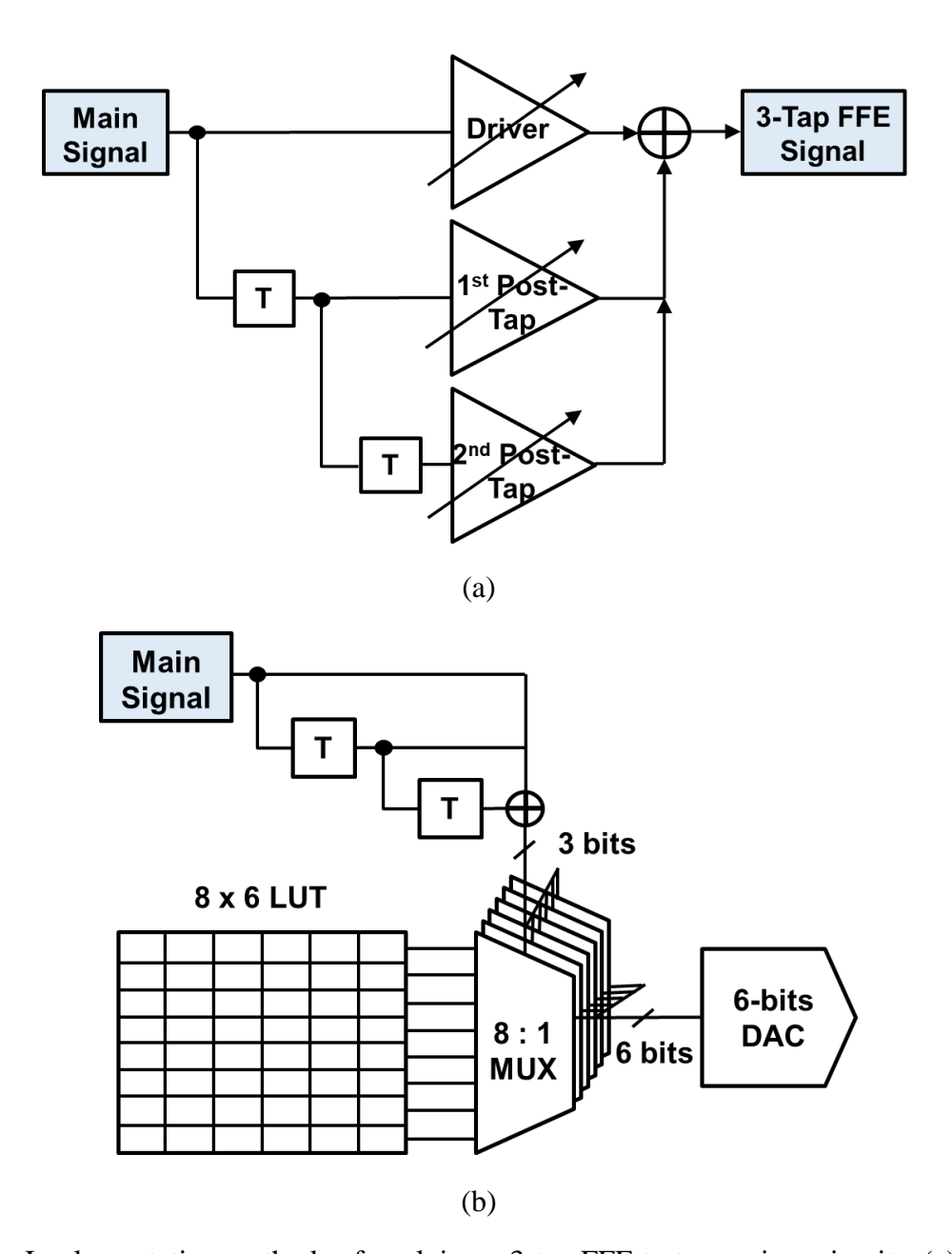


Fig. 5.5. Implementation methods of applying a 3-tap FFE to transceiver circuits. (a) Analog implementation method. (b) Digital implementation method.

The typical implementation methods of applying this 3-tap FFE to system circuits can be analog implementation or digital implementation. As shown in Fig. 5.5 (a), the analog implementation method firstly delays the main signal for once and twice separately to generate the 1st post-tap and 2nd post-tap signals. Then it utilizes amplifiers with adjustable gain to modulate the two

different taps of signal with desired weights. Finally, these two post-taps are summed with the main signal to form the final 3-tap FFE signal. This analog implementation method owns a simple structure, but it is not energy efficient. Besides, the accuracy of tap weights is quite low due to relying on the gain control of analog amplifier. For the digital implementation method presented in Fig. 5.5 (b), it adopts LUT to store weights and uses MUX to select the stored data for more accurate tap weights. The first step is the same as the delay process in analog implementation. Then the 3-bits delayed signals are utilized as selecting signals to control six 8:1 MUXs reading out data from an 8 x 6 LUT, whose size is determined by the control bits and resolution of DAC. Since there are 8 transitions of these three control bits, the corresponding row number of this LUT is 8 while the chosen resolution of DAC is 6-bits so that the column number is 6. Digital implementation owns the advantages of higher accuracy and less power consumption, but it sacrifices area with a more complex structure than the analog implementation method.

5.2.4 Passive Equalizer

The schematic of adopted passive equalizer is presented in Fig. 5.6, and it is a basic high-pass filter utilized as an equalizer for simplifying the structure of discrete circuits. When the signal frequency is low, the capacitive reactance is large since $X_c = 1/(2\pi fC)$ while the inductive reactance is small since $X_L = 2\pi fL$. For the high frequency signal, these two component values change reversely. Thus, the low-frequency signals are bypassed to ground through the inductor while the high-frequency signals are sent to the output of this filter. Therefore, this high-pass filter can decrease the low-frequency gain while increase the high-frequency gain of system frequency response which then contributes to the modulation bandwidth extension. By properly setting the zeros and poles of this high-pass filter, the high-frequency gain loss can be compensated at the target frequency. Moreover, the values of L and C determine the zeros and poles of this filter which can be determined by the following:

$$L = \frac{L_0 \times K}{2\pi \times f_{target}} \tag{5.6}$$

$$C = \frac{C_0}{K \times 2\pi \times f_{target}} \tag{5.7}$$

where L_0 is the unique inductor with the value of 1 H, C_0 is the unique capacitor equal to 1 F, and K is impedance ratio of the designed filter to standard filter which is normally equal to 50 due to the 50Ω impedance matching.

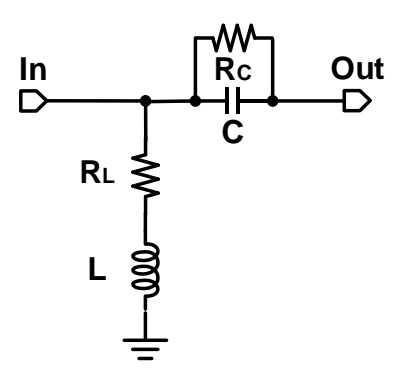


Fig. 5.6. Schematic of the adopted passive equalizer.

5.3 Architecture of Proposed PAM-4 VLC Transmitter with FFE

5.3.1 Schematic of VLC Transmitter System

As presented in Fig. 5.7, the overall architecture of the proposed PAM-4 VLC transmitter consists of digital baseband and analog front-end with both digital and analog equalizations. In detail, this transmitter is comprised of a clock unit, a digital baseband, and a DAC-based LED driver. The clock unit generates proper clock sequences from an external clock source to support the synchronization of different circuits. The pseudo-random bit sequence (PRBS) generator in the digital baseband aims to generate the original signal which is a PRBS sequence compromised of the most significant bit (MSB) and the least significant bit (LSB). Then the digital modulator modulates these two data sequences into a sequence with PAM-4 scheme. The following delay unit generates a 0.5-UI delay time to delay this original PAM-4 signal for creating two different taps which are the main-tap and the delayed 1st post-tap. These two taps compose the compensating signals for forming the digital equalizer. They are utilized to control the states of six 16:1 MUXs by serving as the selecting signals to choose corresponding data from a LUT with size of 16 x 6. The data stored in LUT are the FFE signals with pre-calculated tap weights and are utilized to compensate for the high-frequency loss [5.7]. The analog frontend is a DAC-based LED driver with current mode logic (CML) structure and it converts the digital input signal to analog output driving current signals. A D flip-flop (DFF) synchronizes the input signal of each slice of DAC and guarantees the correct sample time. Then this signal drives the LEDs in current mode to the desired working states. Except for the on-chip digital equalization method, passive analog equalizers are also adopted off-chip to assist with further signal improvement.

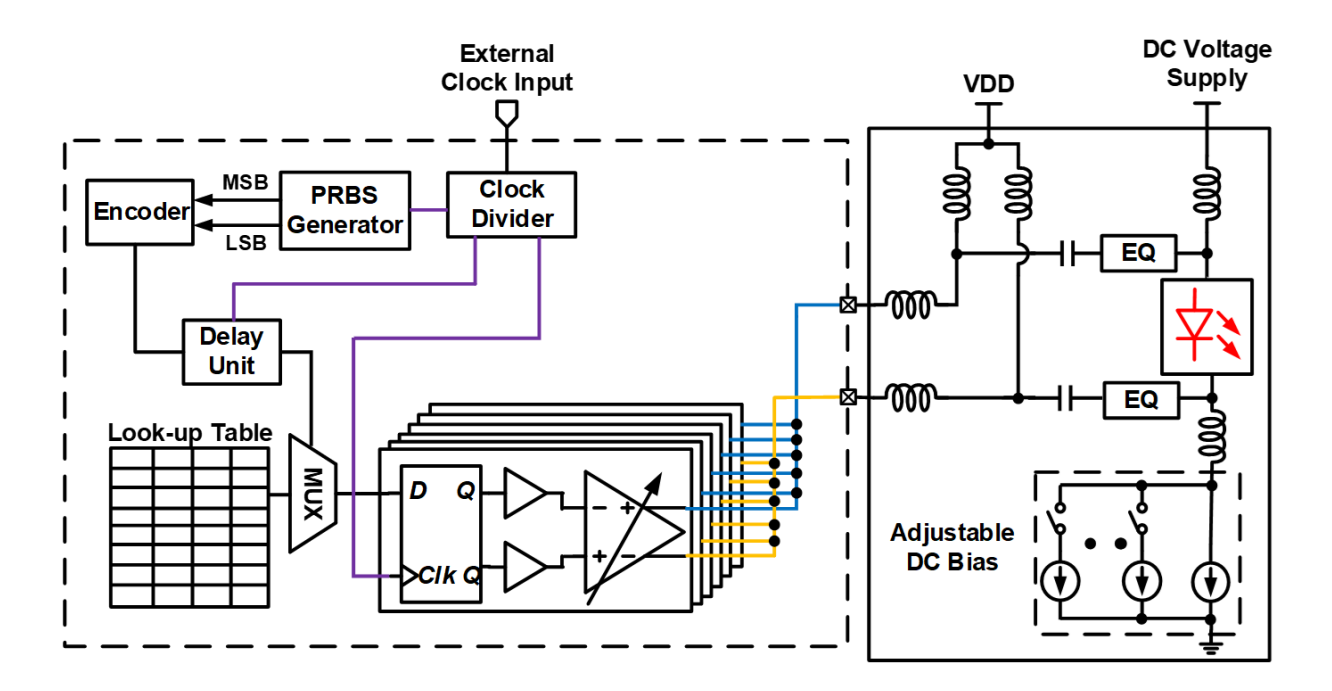


Fig. 5.7. Architecture of proposed PD-based VLC transmitter system.

5.3.2 Current-Steering DAC-based LED Driver

A current-steering DAC-based LED driver is utilized to convert the digital voltage signal from the digital baseband to an analog driving current to drive the LEDs. As presented in Fig. 5.7, there are six slices of circuits in the DAC to realize the function of 6-bits resolution. Each slice consists of one DFF, two input buffer chains, and one differential main driver. The DFF synchronizes the input digital signals of these six slices with the clock signal from the clock divider, and it also samples the input data with a sample period of 0.5-UI. The input buffer chain targets to increase the driving capability and match the impedance between digital baseband circuit and analog main driver.

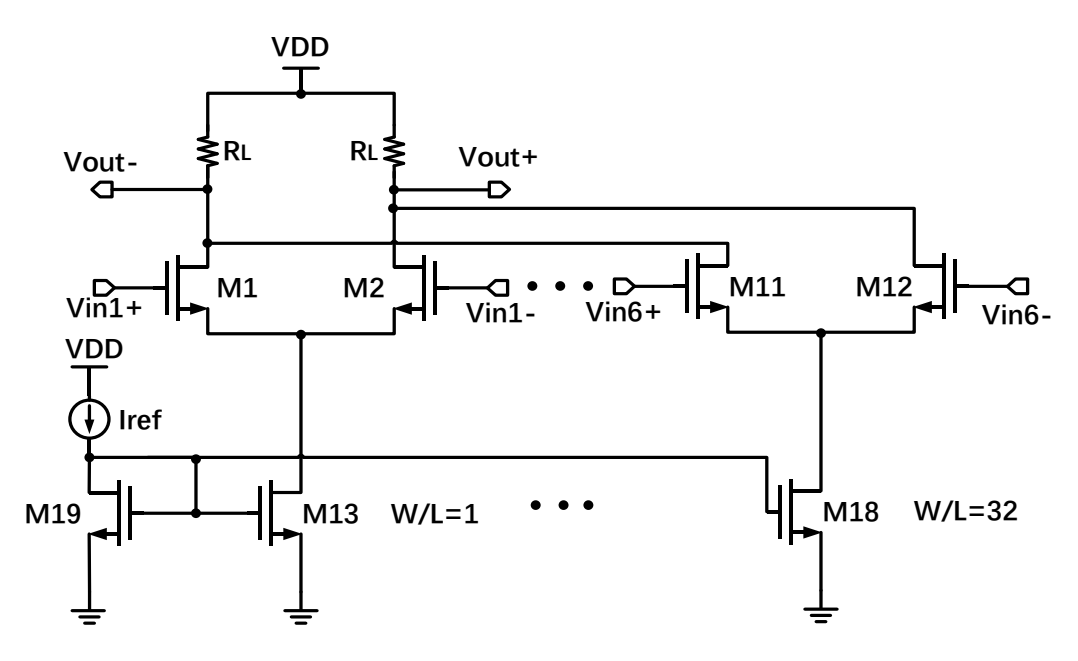


Fig. 5.8. Schematic of current-steering DAC-based driver with CML structure.

As shown in Fig. 5.8, the current-steering DAC-based driver adopts a CML structure due to its simple architecture, low common-mode noise, and high output impedance. The size of transistors in each slice is ratioed from the first slice to the sixth slice with the value of 1:2:4:8:16:32, thus the current ratio of each slice follows this value and forms 6 binary-weighted driving currents. These binary-weighted currents are summed together to generate an output driving current with 6-bits resolution as expressed below:

$$I_{out} = A_5(2^5 I_u) + A_4(2^4 I_u) + A_3(2^3 I_u) + A_2(2^2 I_u) + A_1(2I_u) + A_0 I_u$$
 (5.8)

where I_{out} is the analog output current, A_0 - A_5 are the digital input data and A_0 is the LSB while A_5 is the MSB, I_u is the unit value current which is equal to the tail current in the first slice. With this method, the DAC-based driver can support the LEDs with a high-resolution driving current to realize FFE.

5.3.3 Digital Baseband

The digital baseband in the proposed PAM-4 VLC transmitter is presented in Fig. 5.7, and it consists of a clock divider unit, PRBS generator, a PAM-4 modulator, a delay unit, LUT and MUX. The clock divider unit generates the control clock signals with different frequencies from the external input clock to support the corresponding digital blocks. The PRBS generator and PAM-4 modulator cooperates to generate the original PAM-4 signal. With the support of a

delay unit, the different taps of signal can be created. The calculation has determined the parameters of FFE that it requires two taps in total with tap weights equaling to 1 and 0.5 respectively, and the resolution of DAC is 6-bits. Therefore, the size of LUT is equal to 16×6 due to the transition of two taps of PAM-4 signal is 2^4 and 6 bits of selected results are required for the DAC. It also requires six 16:1 MUXs to select the 6 bits from LUT.

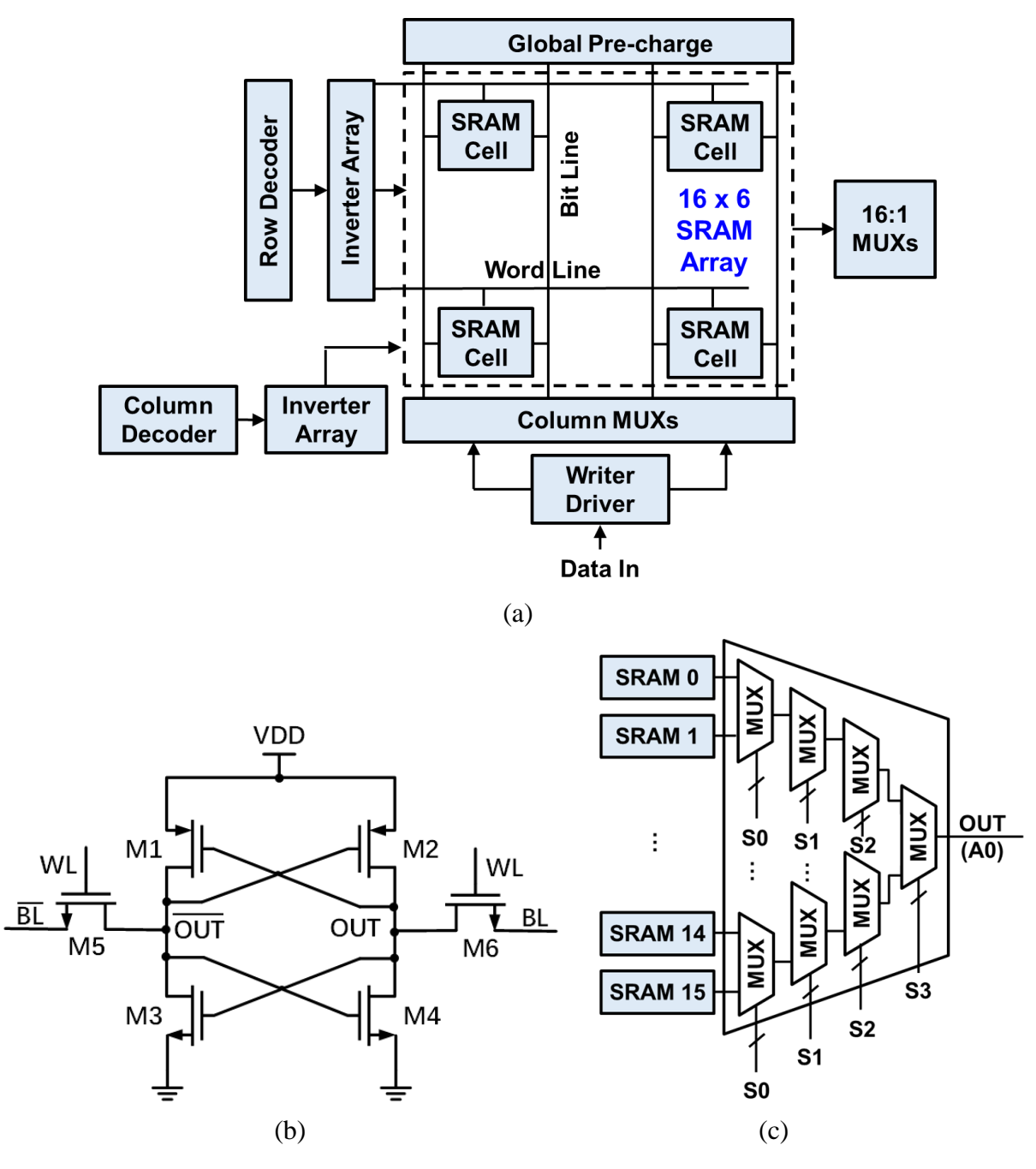


Fig. 5.9. (a) Block diagram of 16 x 6 LUT in the digital baseband; (b) Schematic of 6-trasistor SRAM cell; (c) Structure of 16:1 MUX and connection with LUT.

As shown in Fig. 5.9 (a), the 16 x 6 LUT consists of a 16 x 6 static random-access memory (SRAM) cell array, row and a column decoder, inverter arrays, pre-charge circuit, write driver, column MUX and six 16:1 MUXs. The SRAM cell with the size of 16 x 6 is utilized to store the coefficients of FFE, which are prepared for the selection process to generate the 6-bits parallel data sequences as DAC input signals. As presented in the Fig. 5.9 (b), each cell of SRAM uses the structure of a typical six transistor (6T) SRAM cell [5.8], which is a latch with two access transistors to store one bit of data. The connection of LUT and MUX as well as the structure of 16:1 MUX is presented in the Fig. 5.9 (c). This 16:1 MUX consists of fifteen 2:1 MUXs, and the first column contains eight 2:1 MUXs each of which connects to two SRAM cells. The 4-bits selecting data control the state of this 16:1 MUX and each column is managed by 1-bit to decide which SRAM cell is read out.

	S3	0	0	0	0	0	0	0	0	1	1	1	1	1	1	1	1
FFE	S2	0	0	0	0	1	1	1	1	0	0	0	0	1	1	1	1
Data	S1	0	0	1	1	0	0	1	1	0	0	1	1	0	0	1	1
	S0	0	1	0	1	0	1	0	1	0	1	0	1	0	1	0	1
	A5	0	0	0	0	0	0	0	0	1	1	1	1	1	1	1	1
	A4	1	1	1	1	0	0	0	0	0	0	0	0	1	1	1	1
DAC	А3	0	0	0	0	0	0	0	0	1	1	1	1	1	1	1	1
Input Data	A2	0	0	1	1	0	0	1	1	0	0	1	1	0	0	1	1
	A1	1	0	0	1	1	0	0	1	1	0	0	1	1	0	0	1
	A0	0	0	1	1	0	0	1	1	0	0	1	1	0	0	1	1

Fig. 5.10. Mapping rule of LUT for selecting DAC input data according to FFE data.

During the writing process, the row and column decoders are designed for searching the corresponding address of each SRAM cell with the control of the addressing signal. A write driver is required for amplifying the input writing data so that to pulldown the bit line voltage to the ground. In the following column, MUX selects the read or write a line for each column of SRAM cells. The global pre-charge unit is utilized to pullup the bit line equal to the drain voltage and prepare for the writing process. During the reading process for the LUT, the six

16:1 MUXs are directly connected to each column of SRAM cells. With the selecting signal generated from the delay unit, the corresponding stored data is selected for reading out through the MUXs. The mapping rules of selecting corresponding DAC input with FFE data in shown in Fig. 5.10, which is utilized for implementing the 2-tap FFE with PAM-4 modulation.

5.4 Simulation Results and Discussion

To verify the feasibility and assess the improvement of the proposed equalization schemes including the 2-tap FFE and passive equalizer to high-speed VLC data transmission, the transmitted results with 1.2 Gbps PAM-4 data as input are simulated. The whole transmitter system is designed in Cadence with TSMC 45 nm technology. A LED model with 15 MHz modulation bandwidth is utilized as the light source and limits the modulation bandwidth in this transmitter, which adopts the same equivalent compact model as illustrated in section 5.2.1.

5.4.1 Verification of Digital Baseband

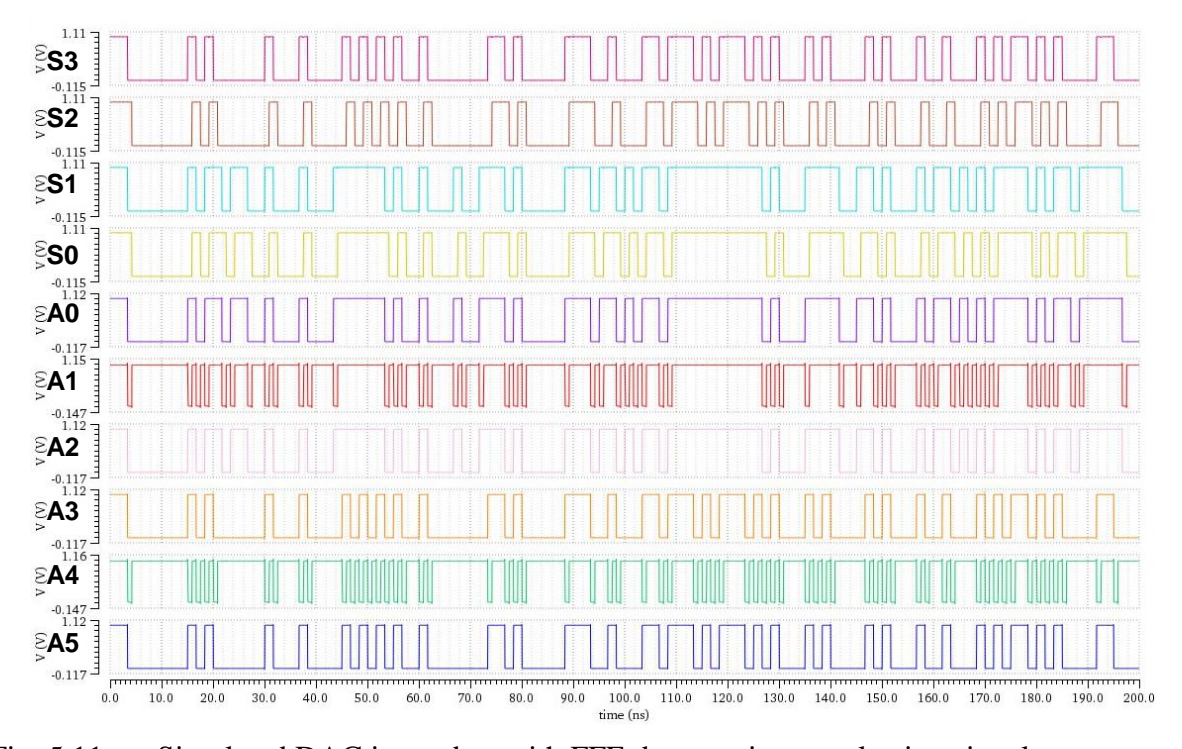


Fig. 5.11. Simulated DAC input data with FFE data serving as selecting signal.

The simulation results of using the generated 2-tap FFE signal as selecting signal to choose the data stored in LUT is presented in Fig. 5.11. S0-S3 are the 4-bits selecting data and A0-A5 are the read out data from LUT. It can be noticed that with the change of 4-bits selecting signals,

the 16:1 MUX selects corresponding 6 bits data from the 16 x 6 LUT and sends them to the input of 6-bits DAC-based LED driver for generating the PAM-4 driving current with 2-taps FFE. This selection process follows the mapping rules illustrated in Fig. 5.10.

5.4.2 Verification of 6-bits DAC-based LED Driver

The simulated input and output waveforms of this 6-bits DAC-based LED driver are presented in Fig. 5.12. In Fig. 5.12 (a), the 6-bits digital input data of DAC are presented as A0 to A5 which are corresponding with the selected output in Fig. 5.11. The output driving currents of this DAC-based driver are shown in Fig. 5.12 (b). It can be noticed that with the change of input data, the output driving currents are changed consistently, and the amplitude of driving currents follows the ratio of 1:2:4:8:16:32. The sum of these six driving currents is labeled as I_total and also presented in Fig. 5.12 (b) which is the finial driving current of LED.

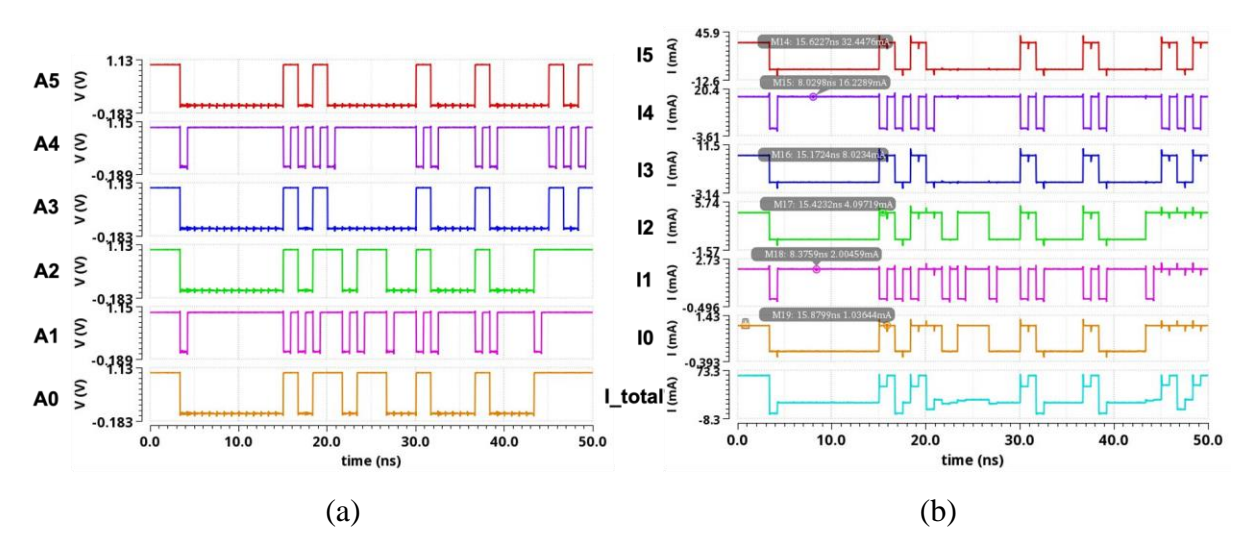


Fig. 5.12. Simulated waveforms of 6-bits DAC-based LED driver. (a) DAC input data. (b) DAC output driving currents.

5.4.3 Verification of Equalization Schemes

The improvement in modulation bandwidth is the most direct method to verify the bandwidth extension feasibility of proposed hybrid equalization schemes. However, since the FFE is implemented in digital baseband, the baseband simulation can only prove the function of passive equalizer. As presented in Fig. 5.13, the red line is the original –3 dB modulation bandwidth of this transmitter limited by LED with a value of around 15 MHz. After equipping

the passive equalizers, the -3 dB bandwidth of the transmitter has been extended to around 100 MHz which is presented by the blue line. With the sacrifice of low-frequency gain and proper compensation of high-frequency, the modulation bandwidth can be improved.

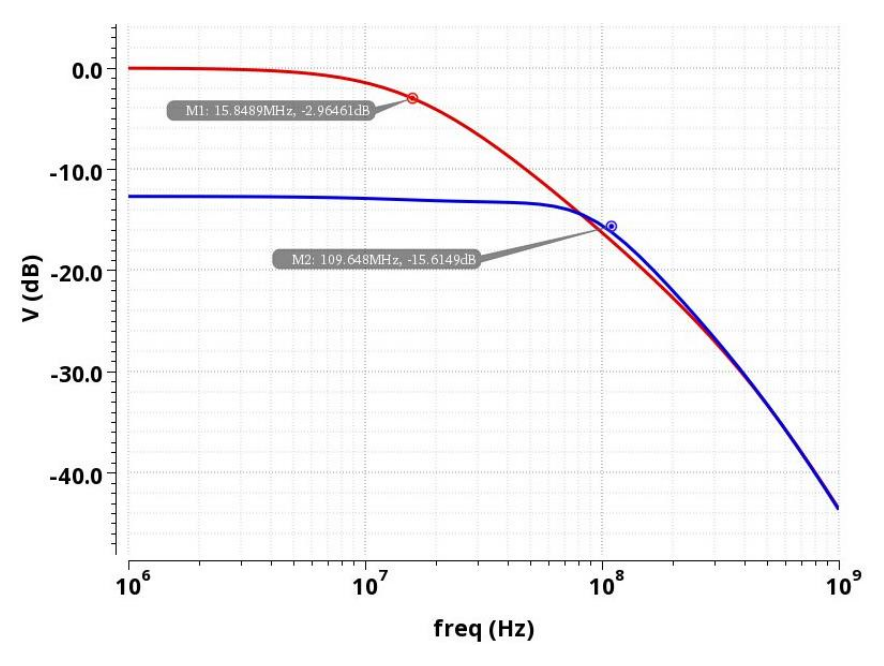


Fig. 5.13. Simulated modulation bandwidth of transmitter.

The eye diagrams of output signal under 1.2 Gbps data transmission with and without equalization are simulated and compared to verify the feasibility of proposed equalization schemes. The FFE tap number and weights are calculated in section 5.2.2 and one main-tap with one post-tap are applied to compensate the loss from transmission limitation. The delay time of each tap is 0.5-UI, and the main driving current is 60 mA. The quality of the eye diagram under PRBS-9 1.2 Gbps PAM-4 data transmission has been improved obviously as shown in Fig. 5.14 (a) and (b). With the proposed cooperation scheme of 2-tap FFE and passive equalizer, a 15 MHz LED model can support 1.2 Gbps PAM-4 data in schematic level simulation. The eye width of the top, middle and bottom eyes are measured and summarized in Table 5.2. The eye width of all three eyes is around 0.9 ns with a ratio of 54% to 1-UI, while the eye heights of each eye are 6.741 mV, 7.061 mV, and 7.885 mV. Another important factor to evaluate the PAM-4 eye diagram quality is the level separation mismatch ratio (R_{LM}), which can be used to represent the linearity of the transmitter. According to the IEEE 802.3 standard [5.9], the is important for measuring the quality of the PAM-4 eye diagram. R_{LM} can be calculated through:

$$V_{mid} = \frac{V_0 + V_3}{2} \tag{5.9}$$

$$ES1 = \frac{V_1 - V_{mid}}{V_0 - V_{mid}} \tag{5.10}$$

$$ES2 = \frac{V_2 - V_{mid}}{V_3 - V_{mid}} \tag{5.11}$$

$$R_{LM} = \min((3 \times ES1), (3 \times ES2), (2 - 3 \times ES1), (2 - 3 \times ES2))$$
 (5.12)

where the V_0 , V_1 , V_2 and V_3 are the first, second, third and fourth eye level in PAM-4 eye diagram correspondingly, V_{mid} is the middle level of total eye height, ES1 is the percentage of bottom eye to the middle eye level and ES2 is the percentage of top eye to the middle eye level. The calculated R_{LM} of this eye diagram under 1.2 Gbps PAM-4 data transmission is 97.6%, which has met the requirements that the R_{LM} should be higher than 90%. Therefore, the performance of proposed transmitter in linearity is acceptable.

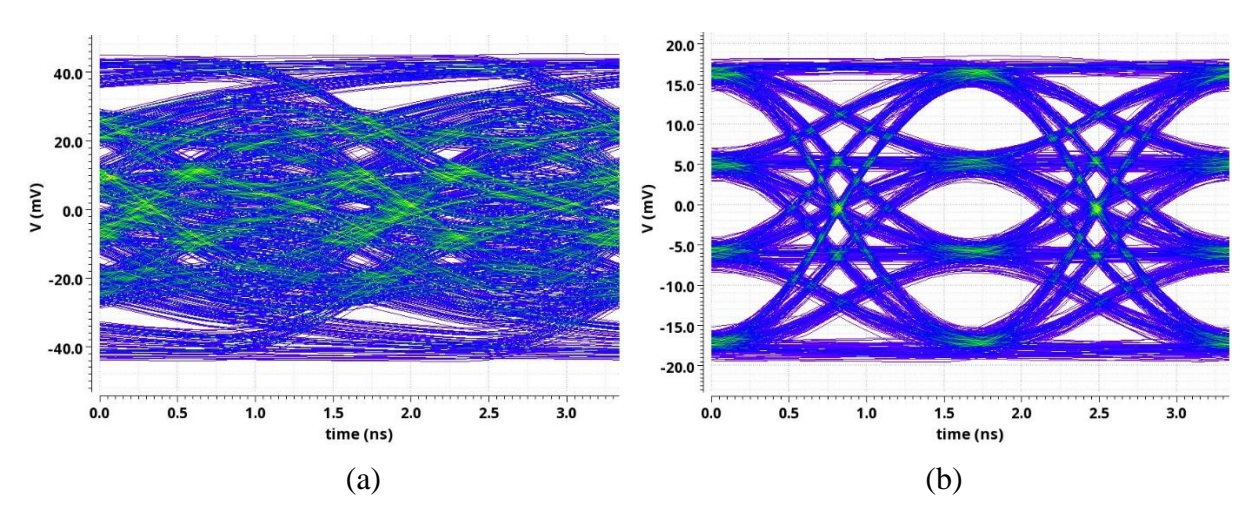


Fig. 5.14. Transient eye diagram simulation results of proposed PAM-4 VLC transmitter under 1.2 Gbps PAM-4 data transmission: (a) without equalization; (b) with both FFE and passive equalizers.

Table 5.2 Analysis of Eye Diagram

Eye Parameters	Eye Height 0/1	Eye Height 1/2	Eye Height 2/3	Eye Width 0/1	Eye Width 1/2	Eye Width 2/3	R_{LM}
Measured Results	6.741 mV	7.061 mV	7.885 mV	0.843 ns	0.897 ns	0.907 ns	97.6 %

5.4.4 Results Discussion

The proposed VLC transmitter can support PAM-4 scheme and is equipped with hybrid equalization methods including digital-based FFE and passive equalizer. The performances of this transmitter are summarized in Table 5.3 below. Both the digital baseband and analog frontend are designed with the 45 nm CMOS technology. The output swing of the LED driver is $1.8~V_{pp}$ with the differential CML structure. Equipped with the combination of FFE and passive equalizer, this PAM-4 VLC transmitter can achieve a 1.2~Gbps data transmission with a total power consumption of 10~W.

Table 5.3 Performance Summary of Proposed PAM-4 VLC Transmitter

Performance	CMOS	Output	PAM-4	Transmit	Power	Equalization
	Technology	Swing	Data Rate	Power	Consume	Scheme
Value	45 nm	1.8 V _{pp}	1.2 Gbps	10 W	152.7 mW	FFE + Passive EQ

5.5 References

[5.1] P. H. Pathak, X. Feng, P. Hu and P. Mohapatra, "Visible Light Communication, Networking, and Sensing: A Survey, Potential and Challenges," in *IEEE Communications Surveys & Tutorials*, vol. 17, no. 4, pp. 2047-2077, Fourthquarter 2015.

[5.2] K. Lee, H. Park and J. R. Barry, "Indoor Channel Characteristics for Visible Light Communications," in *IEEE Communications Letters*, vol. 15, no. 2, pp. 217-219, February 2011. [5.3] X. Li, Z. Ghassemlooy, S. Zvanovec, M. Zhang and A. Burton, "Equivalent Circuit Model of High Power LEDs for VLC Systems," in *2019 2nd West Asian Colloquium on Optical Wireless Communications (WACOWC)*, 2019, pp. 90-95.

[5.3] M. -A. Khalighi, S. Long, S. Bourennane and Z. Ghassemlooy, "PAM- and CAP-Based Transmission Schemes for Visible-Light Communications," in *IEEE Access*, vol. 5, pp. 27002-27013, 2017.

- [5.4] H. Elgala, R. Mesleh and H. Haas, "An LED Model for Intensity-Modulated Optical Communication Systems," in *IEEE Photonics Technology Letters*, vol. 22, no. 11, pp. 835-837, June, 2010.
- [5.5] S. Dimitrov, S. Sinanovic and H. Haas, "Signal Shaping and Modulation for Optical Wireless Communication," in *Journal of Lightwave Technology*, vol. 30, no. 9, pp. 1319-1328, May, 2012.
- [5.6] A. Roshan-Zamir, O. Elhadidy, H. Yang and S. Palermo, "A Reconfigurable 16/32 Gb/s Dual-Mode NRZ/PAM4 SerDes in 65-nm CMOS," in *IEEE Journal of Solid-State Circuits*, vol. 52, no. 9, pp. 2430-2447, Sept. 2017.
- [5.7] B. Zhai, D. Blaauw, D. Sylvester and S. Hanson, "A Sub-200mV 6T SRAM in 0.13μm CMOS," in 2007 IEEE International Solid-State Circuits Conference. Digest of Technical Papers, 2007, pp. 332-606.
- [5.8] "IEEE Standard for Ethernet," in *IEEE Std 802.3-2015 (Revision of IEEE Std 802.3-2012)*, vol., no., pp.1-4017, Mar. 2016.

CHAPTER 6 Design of PAM-8 VLC Transceiver System Employing Neural Network-based FFE and Post-Equalization

6.1 Modeling of Proposed PD-based VLC System

In a communication system, the data rate of transmitted signals is limited by the physical restrictions of the transmitter, channel, and receiver. The limitations in this proposed PD-based VLC system are mainly caused by intrinsic characteristics of optical devices, channel loss, and various noises which will lead to the inter-symbol-interference (ISI) and distortion of the original signals. Since accurate model can provide systematical analysis about how the physical restrictions from VLC link related to the interferences on the signal, building realistic models of the optical devices and communication channel are necessary for better elimination on these limitations. In the proposed PD-based VLC system, the model of VLC link consists of μ -LED model, LOS channel model or underwater channel model, and PD model.

6.1.1 μ-LED Model

The LED device utilized to generate light signals in the proposed PD-based VLC system is a red-green-blue (RGB) μ -LED with a pixel size of 200 μ m x 100 μ m and whole package dimensions of 0.79 mm x 0.79 mm. As shown in Fig. 6.1, the fixed components in this compact equivalent circuit model are comprised of the PCB test fixture model and bonding wire model. The variable part, it includes the intrinsic device model and a Verilog-A code model [6.1]-[6.2]. L₁, R₁, C₁, L₂, R₂ and R₃ are the passive components representing the PCB fixture model, while L_B, R_B and C_B consist of the model of bonding wires. The intrinsic device model of LED consists of a contact resistor R_S, an active region capacitor C_J and a junction resistor R_J, which are all current dependent. The code model represents opto-electric conversion in an LED device in which the output optical power and the current through R_J follow the relationship of the first-order low-pass filter function. Similar to the LED model illustrated in Chapter 5, this μ -LED model can be treated as a first-order low-pass filter for analysis due to the dominance of intrinsic model. The value of these resistors, capacitors, and inductors in the compact model is extracted from the measured S-parameters of a fabricated μ -LED with the fitting process in ADS.

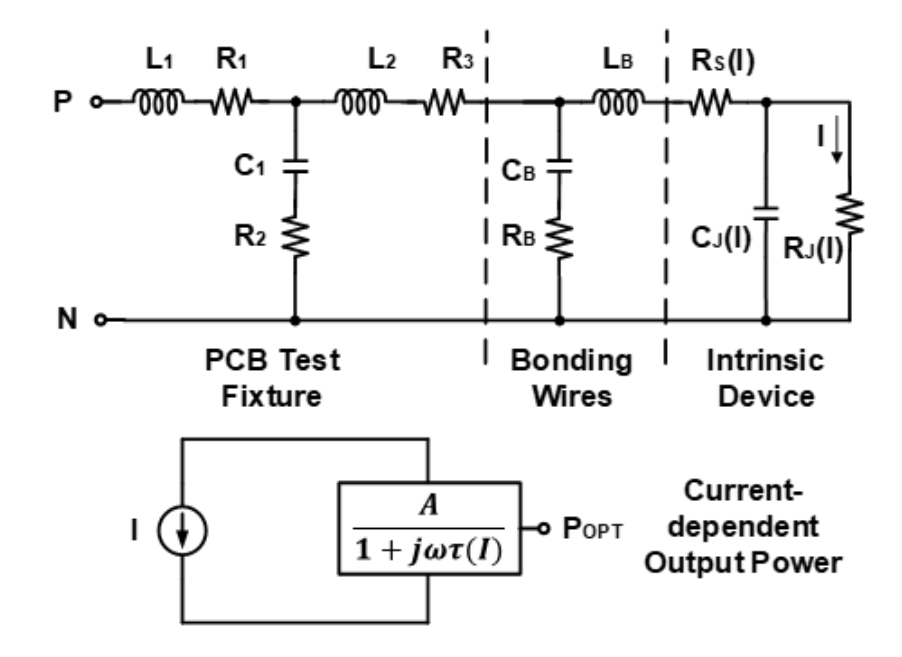


Fig. 6.1. Compact equivalent circuit model of μ-LED.

The simulated results of bandwidth with this proposed compact equivalent model of μ -LED under different bias currents are corresponding with the measured bandwidth curves. These results are presented in Fig. 6.2, and it can be noticed that the -3 dB bandwidth of this μ -LED is 50 MHz when the bias current is 70 mA. This limited bandwidth will be the main obstruction that the -3 dB bandwidth of this μ -LED is 50 MHz when the bias current is 70 mA. This limited bandwidth will be the main obstruction to increasing the communication data rate.

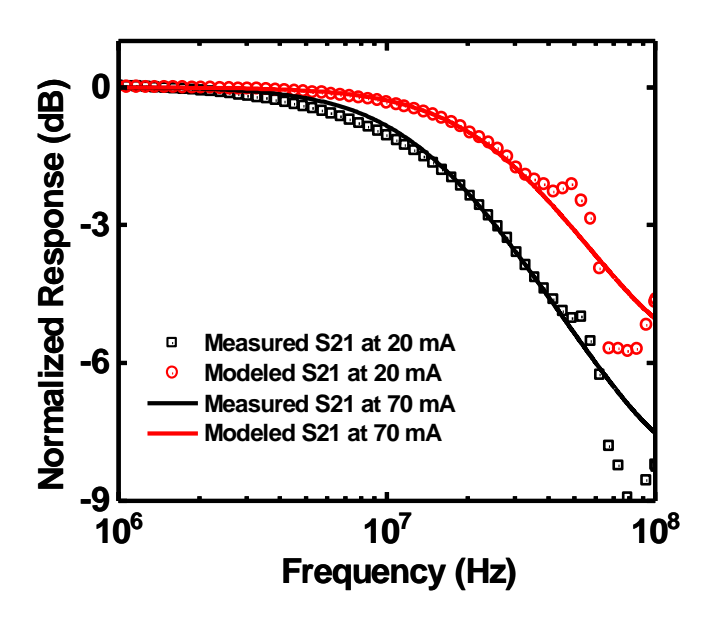


Fig. 6.2. Simulated and measured bandwidth curves of μ-LED.

6.1.2 PD Model

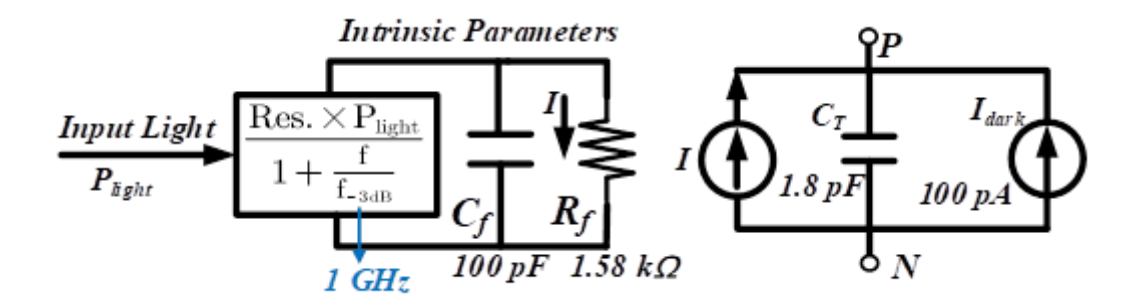


Fig. 6.3. Equivalent circuit model of PD.

The equivalent circuit model of PD is presented in Fig. 6.3 and it consists of intrinsic bandwidth limitation model and diode dark current noise model. The intrinsic model is comprised of Verilog code model representing carrier lifetime and photoelectric response, and intrinsic parasitic capacitor C_f with parasitic resistor R_f for the -3 dB bandwidth of PD. For the dark current noise model, C_T is the terminal capacitance which includes capacitances of PD, pad and bonding wire. To determine the values of these components for accurate PD model, physical manufacturing principles and photoelectric conversion are adopted to build the Verilog model, while test results and data from data sheet are used for parameter fitting.

6.1.3 LOS Channel Model and Underwater Channel Model

In the PD-based VLC communication system, the most common channel is free space, and the loss of this channel has a previous effect on waveform transmission. For visible light transmission, due to the rectilinear propagation characteristic, this free space channel can be treated as a LOS channel in which the main restations are signal loss and background noise. The gain of the LOS channel can be expressed as below [6.3]:

$$PL_{LOS} = 10 \log_{10} \left(\frac{A_{PD}(m+1)}{2\pi D^2} cos^{(m)}(\alpha) cos(\beta) G_{ct} G_{cr} \right)$$
 (6.1)

where A_{PD} is the PD area, D is the distance between the light source and PD, α and β are the emission and receive angles with $cos(\varphi) = cos(\psi) = h/D$ in which h is equal to D when the PD aligns to LED, and m is the Lambert emission order following the expression with half-power angle $\theta_{1/2}$ as [6.3]:

$$m = \frac{-\log 2}{\log[\cos(\theta_{1/2})]} \tag{6.2}$$

 G_{ct} is the gain of lens at transmitter side that utilizes to increase intensity by narrowing the half-power angle [6.4]:

$$G_{ct} = \frac{m_1 + 1}{m_0 + 1} \cos^{m_1 - m_0}(\theta)$$
 (6.3)

where m_0 and m_1 can be calculated through equation (6.2) with corresponding half-power angles before and after narrowing, and θ is the radiation angle which can be considered as 0 at the center of the transmitted light beam. G_{cr} is the gain of non-imaging concentrator gain which is applied before PD at receiver side and it can be calculated with [6.4]:

$$G_{cr} = \frac{n^2}{\sin^2(\psi)} \tag{6.4}$$

where n is the refraction coefficient of non-imaging concentrator and it is around 1.5 for typical glass, ψ is the field-of-view angle of PD.

Another typical communication channel for PD-based VLC system is water which leads to a popular research direction for VLC application. Due to the superior characteristics of visible light that it attenuates much less than RF signals, visible light has become a prospective signal carrier in underwater circumstance. For the underwater VLC, path loss consists of attenuation loss and geometrical loss which should be taken into consideration for the diffused light sources such as LEDs [6.4]. The geometrical loss for LEDs can be represented by the LOS channel loss since it is caused by spreading during transmission. The attenuation loss is determined by [6.5]:

$$PL_{AT} = 10 \log_{10}(e^{-c(\lambda)D})$$
 (6.5)

which is the Beer-Lambert law [6.5] and D is the distance between light source and PD. $c(\lambda)$ is the extinction coefficient which is the summation of water absorption coefficient $a(\lambda)$ and water scattering coefficient $b(\lambda)$. For the underwater VLC system, a glass tank is normally utilized to store water and it also attenuate signal when visible light transmits through it. Therefore, an extra attenuation coefficient $a_T(\lambda)$ should be added into $c(\lambda)$ [6.7]:

$$c(\lambda) = a(\lambda) + b(\lambda) + a_T(\lambda) \tag{6.6}$$

The final overall channel loss of underwater channel is expressed as:

$$PL_{Water} = PL_{AT} + PL_{LOS} (6.7)$$

With the path loss equations of both free space channel and underwater channel, the path loss varies with distance of these two types of channels can be simulated and the corresponding curve is presented in Fig. 6.4. For the channel length equal to 3 m, path loss of free space channel is 57.4 dB while underwater channel is 62.5 dB. The parameters of VLC link model that applied to simulation are summarized in Table 6.1.

Table 6.1 Simulation Parameters for the VLC Link Model

VLC Link	Parameters	Typical Value		
	Total Power	20 W		
Transmitter (μ-LED Model)	Half-power Angle	50°		
(1-	-3 dB Bandwidth	~ 50 MHz		
	PD Area	0.12 mm^2		
	Photosensitivity	0.51 A/W		
Receiver	Dark Current	100 pA		
(PD Model S5973-01)	Terminal Capacitance	1.6 pF		
	Field-of-view Angle	30°		
	-3 dB Bandwidth	1 GHz		
	Link Range	0.1 m – 5 m		
Free Space Channel	Emission Angle α	0°		
	Receive Angle β	0°		
	Link Range	0.1 m – 5 m		
	Water Type	Clear sea water		
Underwater Channel	Absorption Coefficient a(λ) [6.6]	0.114 m ⁻¹		
	Scattering Coefficient $b(\lambda)$ [6.6]	0.037 m ⁻¹		
	Tank Attenuation Coefficient $a_T(\lambda)$ [6.7]	0.265 m ⁻¹		

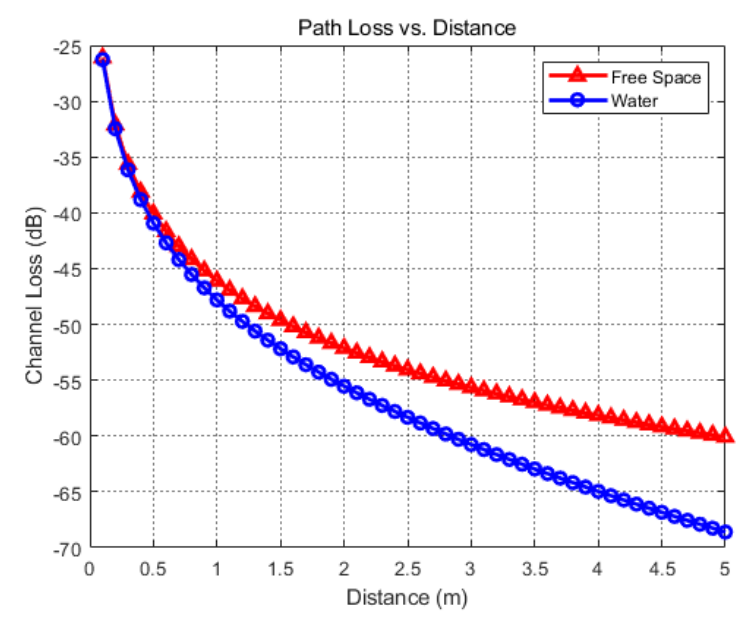


Fig. 6.4. Simulated path loss versus distance in free space channel and water channel.

6.1.4 Bandwidth Limitation and Nonlinearity

With the equivalent model of μ -LED mentioned in the last section, analyzing the bandwidth limitation and nonlinearity effect of LED on signal transmission through mathematical calculation is possible. The whole transmission process of the input signal in this PD-based VLC system can be expressed through the transformation of equations.

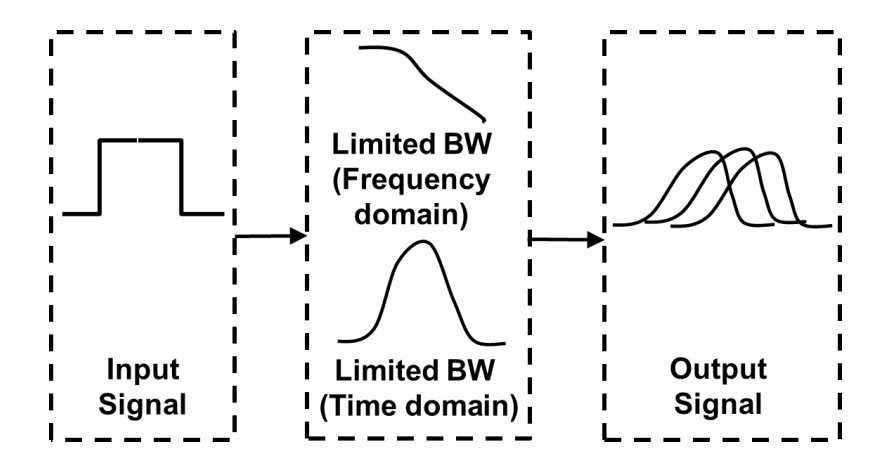


Fig. 6.5. Effects of limited bandwidth of LED at transmitted signal.

The input signal in time domain can be expressed as follows [6.8]:

$$s(t) = \sum_{n=0}^{\infty} I_n x_t(t - nT)$$

$$(6.8)$$

where I_n represents the signal amplitude and $x_t(t)$ is the transmitted waveform at the baseband. The bandwidth limitation due to the LED device can be treated as a first-order low-pass filter as analyzed previously. Considering the analysis on impulse response, the expression of this low pass filter in the s-domain as below:

$$c(s) = \frac{A}{1 + \frac{s}{\omega_0}} \tag{6.9}$$

where A is the amplitude of signal and ω_0 is the characteristic frequency of this low-pass filter. After applying the inverse Laplace transform to equation (6.9), the limited bandwidth expression in the time domain is shown as the equation below:

$$c(t) = \omega_0 A \times e^{-\omega_0 t} \times u(t) \tag{6.10}$$

where u(t) is the unit step function and $e^{-\omega_0 t}$ is the time-dependent item complying of exponential attenuation. Therefore, c(t), which is the effect of limited bandwidth on signal transmission, causes undesired tails leading to the ISI effect in the time domain by adding the time-dependent exponential attenuation to input signals. In the frequency domain, it can be treated as decrease on the high-frequency components in transmitted signal. This effect of bandwidth limitation on the original input signal is shown in Fig. 6.5, and it can be noticed that the generated tails spread into adjacent symbols and overlap with each other. Therefore, when the final output signal is sampled at times $t = kT + \tau_0$, k = 0,1,..., the sampled output signal can be expressed as [6.8]:

$$r(kT + \tau_0) = \sum_{n=0}^{\infty} I_n x_r (kT - nT + \tau_0) + v(kT + \tau_0)$$
 (6.11)

where $x_r(t)$ is the received signal, v(t) is the noise item in the received signal and τ_0 is the transmission delay. This equation can be equivalently expressed as:

$$r_k = I_k x_0 + \sum_{n \neq k}^{\infty} I_n x_{k-n} + v_k$$
 (6.12)

where $I_k x_0$ is the desired symbol sampled at k-th sampling point, the term $\sum_{n\neq 0,k}^{\infty} (I_n x_{k-n})$ represents the ISI caused by the original signal tails and v_k is the noise at k-th sampling point.

To evaluate the intrinsic nonlinearity of LED device, the I-V relationship of LED at forward bias needs to be calculated and it is [6.9]:

$$I_{LED} = (I_n + I_p) \left(e^{\frac{qV}{KT}} - 1 \right) \tag{6.13}$$

where $(I_n + I_p)$ is the electrons and holes current, and $e^{\frac{qV}{KT}}$ is a temperature-dependent item that has an exponential relationship with the bias voltage. It can be noticed that the driving current through LED is nonlinear with bias voltage of LED which causes amplitude asymmetry with DC bias point.

6.2 Link Budget Analysis

Link budget analysis is critical for communication system analysis since it can predict the performance of whole system and determine the feasibility of system implementation with design specifications. In link budget analysis, the relationship among transmitted power, path loss of communication channel, channel length, and receiver input sensitivity will be calculated. Then the SNR margin in receiver can be determined with the received signal strength.

The transmitted optical power of VLC light source and be attained through taking integral of spectrum response in the range of effective wavelength [6.10]:

$$P_t = \int_{\lambda_L}^{\lambda_H} S_t(\lambda) d\lambda \tag{6.14}$$

where $S_t(\lambda)$ is the spectrum response, λ_H is the maximum effective wavelength of light source and λ_L is the minimum wavelength. However, spectrum response is not directly provided, and it can be obtained by the product of normalized spectrum response $S'_t(\lambda)$ which is provided by data sheet and scaling factor c:

$$S_t(\lambda) = cS_t'(\lambda) \tag{6.15}$$

The normalized spectrum response of adopted LED is shown in Fig. 6.6. (a), and the scaling factor c will be calculated with the expression of luminous flux ϕ_V :

$$\phi_V = 683 \int_{380nm}^{780nm} S_t(\lambda) V(\lambda) d\lambda$$
 (6.16)

where $S_t(\lambda)$ can be substituted by equation (6.15), thus c will be expressed as:

$$c = \frac{\phi_V}{683 \int_{\lambda_L}^{\lambda_H} S_t'(\lambda) V(\lambda) d\lambda}$$
 (6.17)

 $V(\lambda)$ is the spectral luminous efficiency function which reflect the responsivity of human eyes to different light wavelengths, and it can be represented by the following equation through Gaussian curve approximation [6.11]:

$$V(\lambda) = 1.019e^{-285.4(\lambda - 0.559)^2}$$
(6.18)

After obtaining the value of scaling factor c, the spectrum response $S_t(\lambda)$ can be derived so that the transmit power can be determined by equation (6.14).

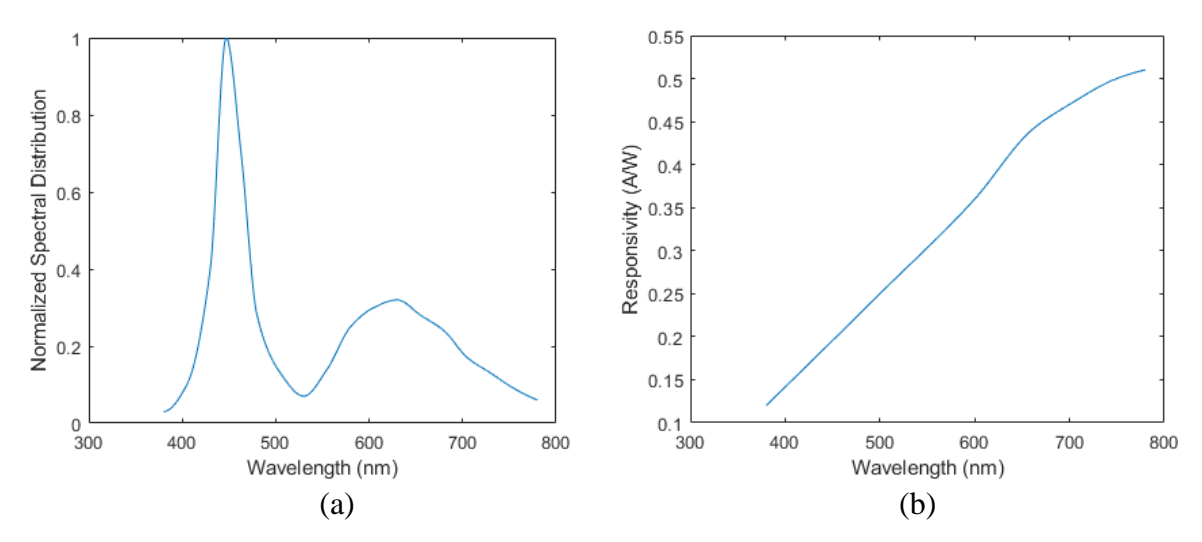


Fig. 6.6. (a) Normalized spectrum response distribution of LED; (b) Responsivity curve of PD.

With the obtained transmit power and path loss which has been analyzed in last section, the received optical power can be calculated:

$$P_r = P_t \cdot PL \tag{6.19}$$

This received optical power will be converted to photoelectronic current through PD, which can be represented by the integration of spectrum response after path loss times PD responsivity over effective wavelengths is obtained to represent the photocurrent:

$$I_{PD} = 0.5PL \int_{\lambda_L}^{\lambda_H} S_t(\lambda) R_{PD}(\lambda) d\lambda$$
 (6.20)

With the received PD photocurrent as input signal of receiver, SNR of receiver can be determined by the ratio of photocurrent and input referred noise:

$$SNR = I_{PD}^2 / I_{IRN}^2 (6.21)$$

To calculate the minimum required SNR, the relationship of SNR with BER and modulation scheme is analyzed as below [6.12]:

$$BER_{M-PAM} = 0.5erfc\left(\frac{\sqrt{SNR \cdot \log_2 M}}{2\sqrt{2}(M-1)}\right)$$
(6.22)

The calculated results of OOK, PAM-4 and PAM-8 modulation schemes are presented in Fig. 6.7. With a target BER of 3.8x10⁻³ and specific PAM-8 modulation scheme, the minimum required SNR to support signal transmission is 26.5 dB.

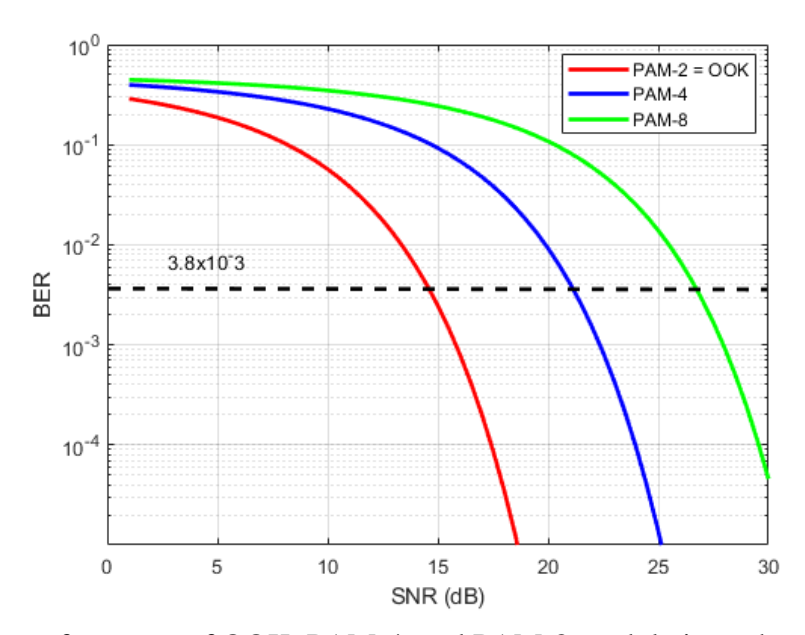


Fig. 6.7. BER performance of OOK, PAM-4, and PAM-8 modulation schemes versus SNR.

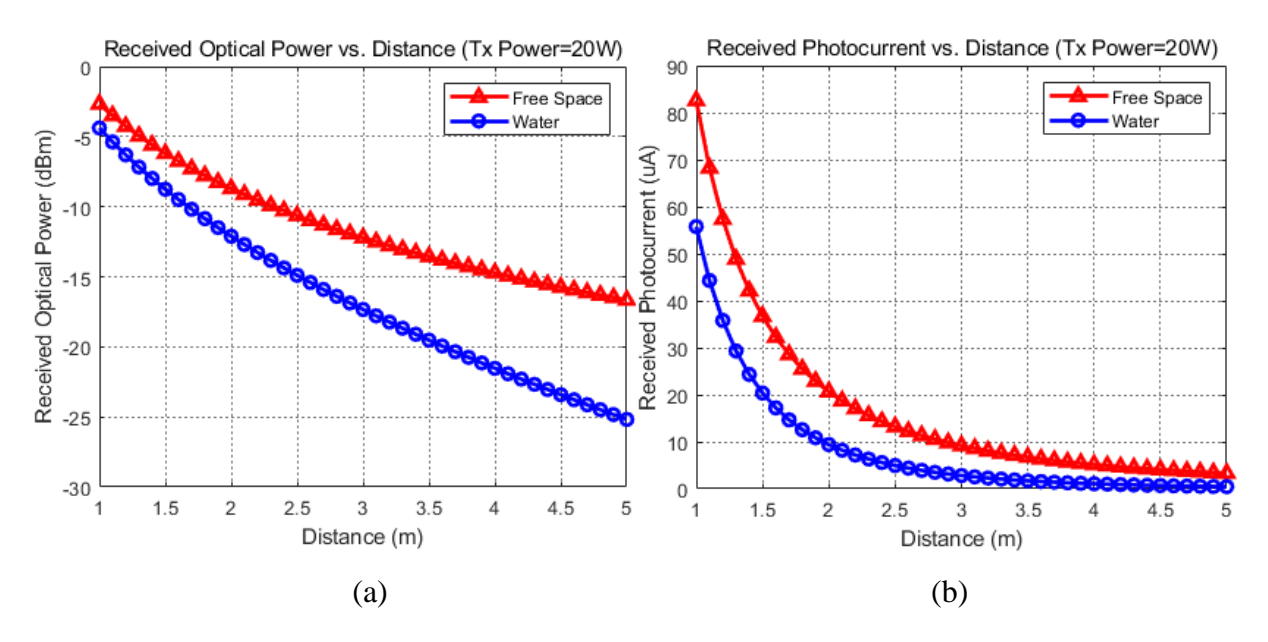


Fig. 6.8. Simulated 20 W transmitted power through free space and water channel: (a) Received optical power by PD versus communication distance; (b) Received photocurrent of PD versus communication distance.

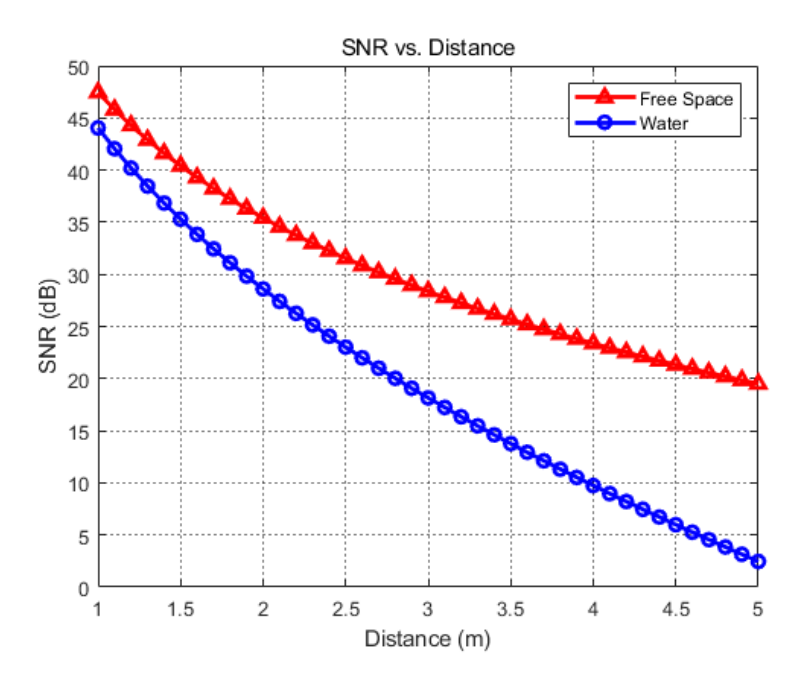


Fig. 6.9. Analysis of receiver SNR versus distance in both free space and water channels.

Table 6.2 VLC Link Budget Calculation

Parameters	Free Space Channel	Water Channel		
Transmitted Power	43 dBm	43 dBm		
Path Length	3 m	1.2 m		
Modulation Format	PAM-8	PAM-8		
Path Loss	55.2 dB	49.8 dB		
Receiver Sensitivity	-18.5 dBm	-18.5 dBm		
Received Power	-12.2 dBm	-6.8 dBm		
Receive Loss	5.1 dB	5.1 dB		
Link Margin	1.2 dB	1.3 dB		

6.3 Analysis of Equalization Methods

As mentioned in the last section, the main restriction at a transmission data rate in the integrated PD-based VLC system is caused by the limited bandwidth. To extend the limited bandwidth of the PD-based VLC system, a single equalization method is not enough so different equalization methods are combined to corporately contribute to the data transmission with the best performance. At the VLC transmitter side, both passive equalizer and NN-based FFE

algorithms are adopted, while the RBFNN-enabled equalization algorithm is utilized in the baseband of the VLC receiver.

6.3.1 Passive Equalizer

Except from FFE method, the passive equalizer is also adopted in the proposed VLC transmitter for extending the limited bandwidth. The passive equalizer utilizes the same structure as introduced in Chapter 5, which consists of passive components to construct the inductor and capacitor (LC) high-pass filter circuit. This passive equalizer can reduce the low-frequency components and boost the high-frequency components so that the limited modulation bandwidth can be compensated.

6.3.2 FFE

FFE is an equalization technology that is commonly adopted in high-speed optical communication transmitter systems since it is easy to facilitate through digital or analog ways and owns superior performance at eliminating ISI [6.13]. The conventional implementation of FFE is properly delaying for 1 or 0.5 UI and inverting the original signal to generate previoustap and post-tap signals, then combining the original signal which is also called a main-tap signal with these pre-and post-tap signals to form the final signal with FFE. The expression of the FFE signal is as below:

$$y(n) = \sum_{k=0}^{L} w_k x(n+k)$$
 (6.23)

where w_k is the weight of each tap in FFE and x(n+k) is the signal for each tap. FFE contributes to removing the ISI and extending the limited bandwidth since the combined waveforms will reshape the rising and falling edges of the main-tap signal and attenuate the low-frequency components in the signal thus both decreasing low-frequency gain and increasing high-frequency gain of signal frequency response.

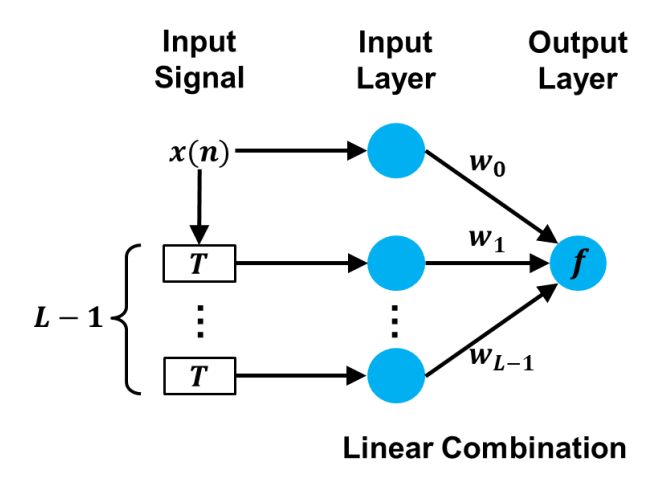


Fig. 6.10. Structure of NN-based FFE.

The traditional method of realizing FFE is either generating modulated signals with FFE in a digital LUT or combining the different taps together through analog circuits. However, these two methods face with problem of low weights precision due to the resolution of DAC or the analog circuit mismatch in fabrication. Therefore, a NN-based FFE implementation method is proposed in this work and adopted in the baseband of the transmitter. As shown in Fig. 6.10, this NN-based FFE consists of two layers of neurons. The input signals with calculated delay time are sent to the input layer towards the corresponding neurons. To train this network, the generated FFE signal is utilized as a train signal, and adjusting the weights in this network to the same as the weights of each FFE tap. After the training process, the number of neurons in the input layer with corresponding weights is fixed. There is only one neuron in the output layer to linearly combine the previous data from the input layer and provide the signal modulated with FFE which is the same as the expression in equation (6.23). With this trained network, the test signal can be modulated into an FFE equalization signal. In the proposed PD-based VLC transceiver system, a 3-tap FFE with 1/3 UI delay is adopted, and the tap weights are calculated through method mentioned Chapter 5 with the value related to data rate.

6.3.3 DNN and RBF-NN

Both DNN and RBF-NN are adopted in this PD-based VLC transceiver system as the post-equalization for comparing the performance of these two types of neural network. The structure of 3-layer DNN is presented in Fig. 6.11 and it contains one input layer, three hidden layers and one output layer. The input signal of this DNN is $X = [x_1, ..., x_n]$, which is generated from

the received signal with delay. In the hidden layer, the input signals X are multiplied with weight W_m then summed together with bias weight b_m for the following process by activation function f. The output of m-hidden neuron is $f(X \cdot W_m + b_m)$ and the final output of DNN can be expressed as:

$$y(n) = f(f(f(X \cdot W_m^1 + b_m^1) \cdot W_m^2 + b_m^2) \cdot W_m^3 + b_m^3) \cdot W_m$$
 (6.24)

where W_m^1 , W_m^2 , W_m^3 are the neuron weights of 1st, 2nd and 3rd hidden layer, and W_m is the weights of output layer. The typical activation function in DNN is sigmoid function and the training target is the original transmitted signal. After training process, the weights in this 3-layer DNN are determined and this trained DNN can be utilized as the post-equalizer to compensate the new received signals.

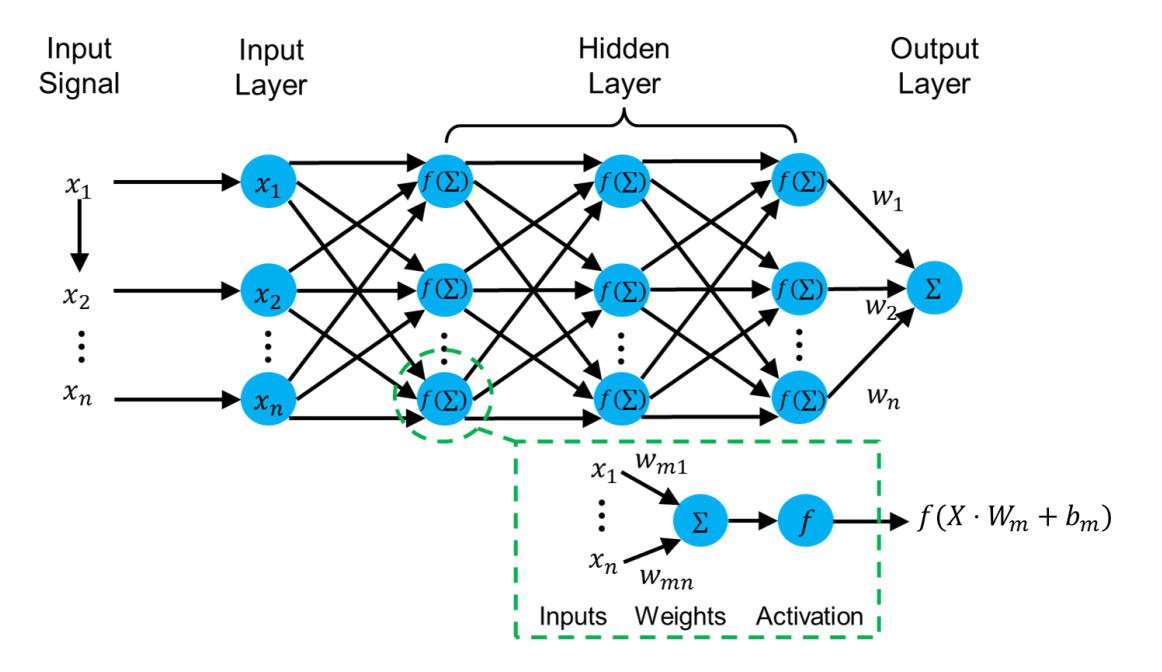


Fig. 6.11. Structure of DNN.

Radial basis function utilizes the distance between input and fixed center point to determine the value of output, and the common expression of this function is:

$$\phi(x) = \phi(\|x - c\|) \tag{6.25}$$

where the function $\phi(\cdot)$ is the radial function, the distance is called Euclidean distance and c is the radial kernel center. With this definition, the RBF-NN is the neural network that utilizes RBF as the activation function [6.14]. The conventional RBF-NN only consists of three neuron layers: input layer, hidden layer, and output layer as shown in Fig. 6.12. The input layer sends

input data to the hidden layer where the activation function is the radial basis function. In this hidden layer, there is only one layer of neurons and the Euclidean distance between input data and the kernel center will be calculated and utilized to determine the output of the hidden layer. There are various choices for the activation function such as the Gaussian kernel function, multiquadric function, and inverse quadric function. The output layer will linearly combine the output from the hidden layer and provide the final output of RBF-NN. The weights of this linear layer are also changed during the training process.

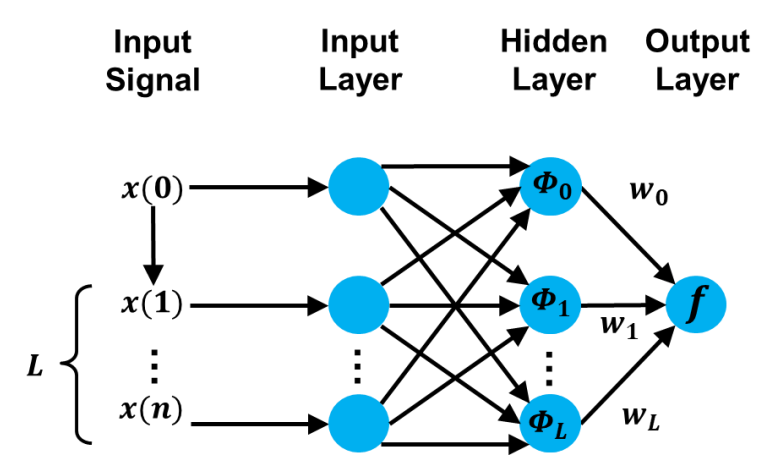


Fig. 6.12. Structure of RBF-NN.

As presented in Fig. 6.12, the RBF-NN adopted in the proposed VLC system consists of three layers. The input signals are received from TIA after down-sampling and synchronization, then the sampled data will be delayed forming a matrix with a scale equal to the window length of (L+1). This input matrix is the input of the radial basis function, and the Gaussian kernel function is adopted as the activation function in the hidden layer considering that the limited bandwidth effect at the transmitted signal in the time domain is similar to the Gaussian function as analyzed in the previous section. The output layer is a linear combination of output from the hidden layer. The training process of this RBF-NN is utilizing the original PRBS-9 signal as the training target, then adjusting the parameters of the activation function in the hidden layer and the weights of the output layer. The final output of RBF-NN is [6.14]:

$$y(n) = f(\sum_{i=0}^{L} w_i \phi_i(x_i) + b)$$
 (6.26)

where b is the extra bias item and $\phi(x)$ is the Gaussian kernel function with expression as below:

$$\phi(x) = e^{-\frac{\|x - x'\|^2}{2\sigma^2}} \tag{6.27}$$

RBF-NN owns serval advantages comparing with traditional DNN for its unique structure and training process with radial basis function as activation function as summarized in the Table 6.3. The first advantage is that the activation function of RBF-NN is more suitable to approximate bandwidth limitation and nonlinear effects. Due to the flexible choice of various activation functions, RBF-NN is capable to compensate the channel models with nonlinear characteristics especially when using the Gaussian kernel function as its radial basis function to approximate the limitations. The second advantage is that RBF-NN is a local approximation neural network, which means that it only requires to change part of the weights of neurons during the training process instead of changing all the weights for each irritation due to the impact of one neuron on the other one is related to the Euclidean distance between them. The traditional neural networks like DNN and CNN utilize the latter method for the training process so that it consumes much more resources and takes longer time to finish the training process. The third advantage is that RBF-NN owns simpler neural network structure since it only contains three layers comparing with other NNs with several hidden layers. This simple structure also contributes to decrease the training time.

Table 6.3 Comparison of RBF-NN and DNN

Type of NN	Activation Function	Approximation Approach	Neuron Layers	
RBF-NN	Gaussian Kennel Function	Local Approximation	3	
DNN Sigmoid Function		Universal Approximation	> 3	

6.4 Architecture of PD-based VLC Transceiver Circuits

The architecture of the proposed PD-based VLC transceiver system is presented in Fig. 6.13, it includes digital baseband which is implemented in MATLAB, and analog front-end which is simulated in Cadence. The digital baseband at the transmitter side aims to generate a transmitted signal, encode and modulate this signal by equipping the NN-based FFE. While the baseband at the receiver side will decode and demodulate the received signal with RBF-NN based equalizer. Besides, the analog front-end circuit in Cadence is comprised of a driver, passive equalizer, LED model, LOS channel, PD model, and TIA. To verify the design of the proposed system, the co-simulation between MATLAB and Cadence is utilized.

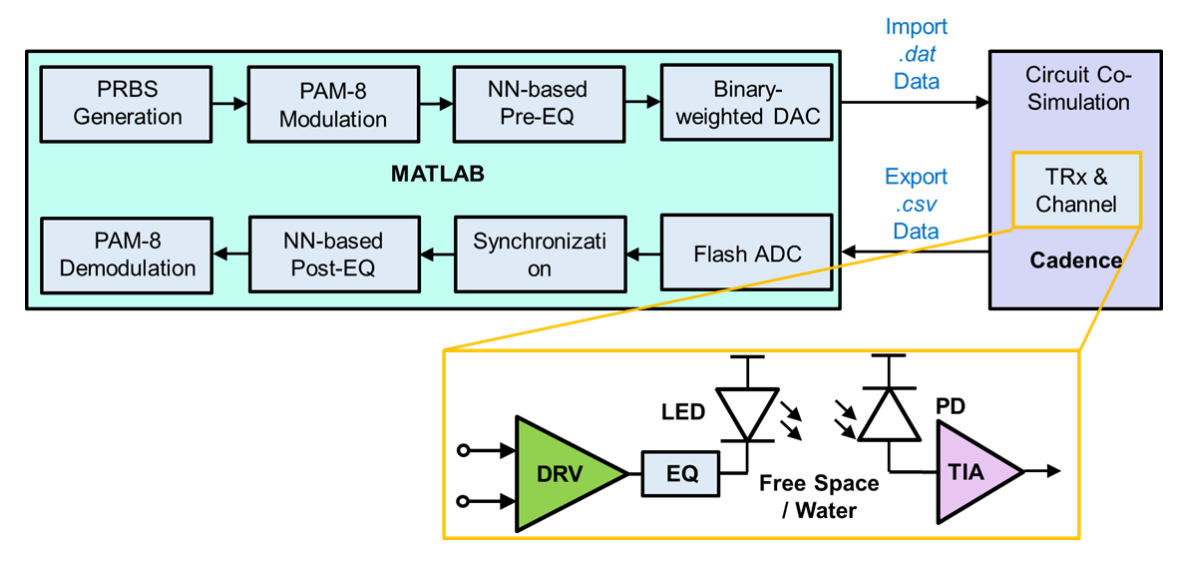


Fig. 6.13. Architecture of proposed PD-based VLC system.

6.4.1 Transmitter in PD-based VLC System

The digital baseband in the proposed PD-based VLC transmitter consists of a pseudo-random binary sequence (PRBS) waveform generator, PAM-8 signal modulator, NN-based preequalizer using the FFE algorithm, and a DAC generates the analog PAM-8 signal with FFE. A PRBS-11 signal is generated and encoded, then it is sent to the modulator for the PAM-8 signal. An NN-based equalizer following the modulator adds an FFE algorithm to this PAM-8 signal to compensate for the limited modulation bandwidth caused by LED. After this equalizer, the PAM-8 FFE signal is up-sampled and transmitted to the analog front-end circuit in the form of .dat format data.

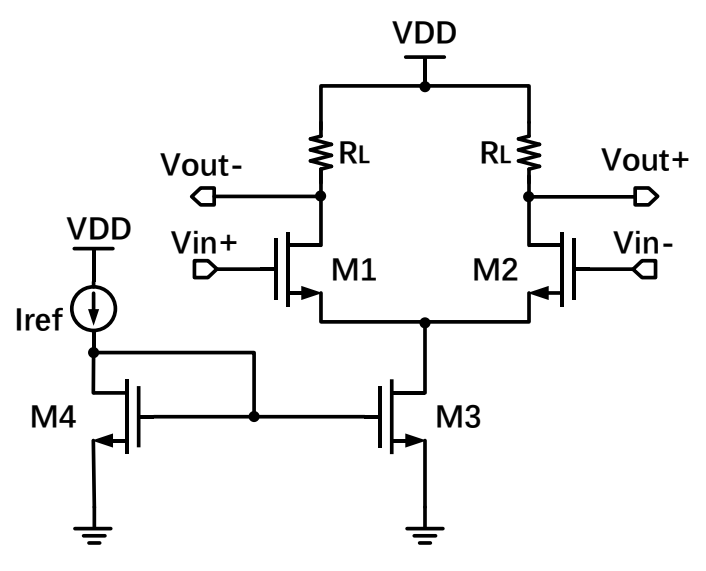


Fig. 6.14. Schematic of CML LED driver.

The analog front-end circuit of the proposed PD-based VLC transmitter is implemented in Candence. The LED driver is the core circuit for transmitter design and the structure of this driver is shown in Fig. 6.14. It adopts a CML structure due to its simple architecture, low common-mode noise, and high output impedance, which consists of a differential pair M1 and M2 working in the saturation region and a current source M3 offering tail current [6.15]. The input voltage signals are sent to the gate of differential pair and differential outputs are elicited out from drain nodes with a gain of $g_m(R_L//r_o)$, in which g_m is the transconductance while r_o is the output resistance of M1 or M2. A current mirror contains M3 and M4 is utilized to provide tail current with a value of $I_{ref}(W_3L_3/W_4L_4)$, in which W_3L_3/W_4L_4 is the transistor size ratio of M3 and M4. The passive equalizers are placed after the LED driver to extend communication bandwidth and the principle of this equalizer has been elaborated in the previous section. The model of LED used in this simulation system is based on the compact equivalent model of μ -LED introduced in section 6.2 with a limited bandwidth of 50 MHz. This μ-LED model is also implemented in Cadence with fixed RLC components and Verilog-A code-based current-dependent model. For the free space and underwater channels, their models are illustrated in section 6.2 and the channel loss at alignment occasion of LED and PD is adopted for total loss.

6.4.2 Receiver in PD-based VLC System

On the receiver side, the optical signal is received by PD and converted into the photo-electronic current, then this current is transformed into voltage and amplified by the TIA. Following the analog front-end, an ADC samples the voltage signal and saves it as .csv format data. In the MATLAB offline baseband, this received signal is synchronized first, then a neural network based post-equalizer compensates for this signal followed by PAM-8 demodulation.

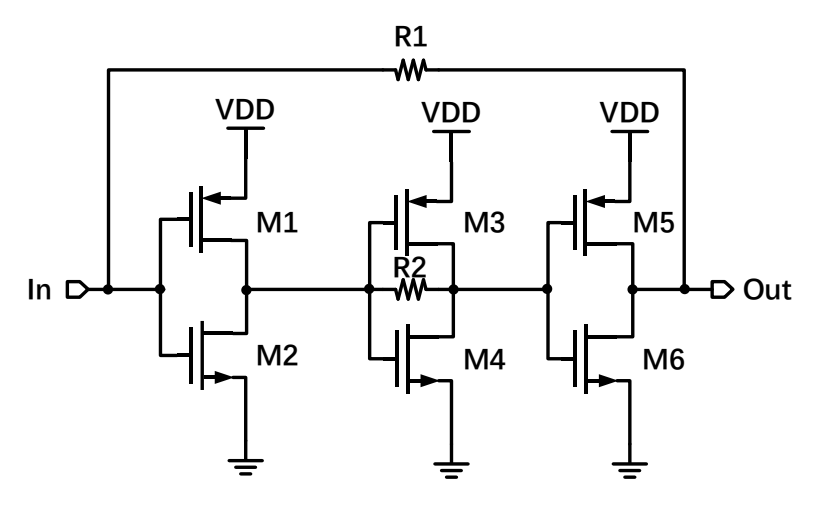


Fig. 6.15. Schematic of TIA circuit.

For the analog front-end circuit in the receiver, TIA is the core circuit, and it realizes the amplification of current to voltage signals. The circuit of TIA is presented in Fig. 6.15, and it is designed with a three-stage inverter structure. The design requirements of this TIA are low-noise and high gain since noise is one of the main influencing factors at the receiving end while a higher gain of TIA provides an advantage for subsequent signal processing [6.16]. The noise of TIA consists of thermal noise of TIA and equivalent input thermal noise of the MOSFET and they are inversely proportional to the transimpedance of TIA. For the gain of TIA, it is determined by the value of the feedback resistor when the stability of the core amplifier is ensured. Therefore, the realization of a high-sensitivity receiver requires a large feedback resistor and a first-stage amplifier with a large transimpedance of TIA. Moreover, the three-stage structure of TIA provides a stable high gain due to the alleviation of bandwidth limitation brought by the low noise requirement.

6.5 Simulation Results and Discussion

To evaluate the performance of the proposed PD-based VLC system which combines NN-based equalizers with a traditional passive equalizer in PAM-8 modulations, a co-simulation platform of MATLAB and Cadence is adopted. This platform is based on the VLC system structure presented in Fig. 6.13, and it combines the digital baseband in MATLAB with the analog frontend circuit in Cadence. This evaluation process incorporates the advantages of these two software design tools, which contribute to acquiring a credible simulation result. The models of devices and communication channels that utilized to the simulation of these two works are built based on the measured data in Cadence. Besides, the main limitations from devices and channels are analyzed and verified to guarantee that these models are accurate and close to the measured results of devices and channels. The analog front-end design in Cadence has considered the parasitic components and noise to guarantee its accuracy. The off-line equalization scheme adopted to process the received signals is designed in MATLAB, which is the same as other experimental works. In this simulation, the PRBS-9 signal is utilized as the signal source and the training target of both the RBF-NN and DNN. The assessment of the proposed VLC system consists of transceiver system performance evaluation, data transmission evaluation and training performance evaluation to study the system performance, quality of data transmitted through this system and the capability of the RBF-NN. Besides, to prove the superiority of RBF-NN, a comparison with DNN as post-equalization is also performed.

6.5.1 Pre-equalization Performance Evaluation

Before simulating the performance of pre-equalization, the adopted binary-weighted DAC and flash ADC models are evaluated first to determine appropriate resolution. The correlation coefficient is utilized for this determination of DAC resolution as below [6.17]:

$$r(X,Y) = \frac{Cov(X,Y)}{\sqrt{Var[X]Var[Y]}}$$
(6.28)

where X is the input digital data set to DAC and Y is the output analog data set of DAC. The calculated coefficient versus DAC resolution is shown in Fig. 6.16 (a) and it can be noticed that the coefficient reaches to maximum value of 0.94 after 7-bits. Mean average error (MAE) is utilized for this determination of ADC as below:

$$MAE = \frac{1}{n} \sum_{i=1}^{n} \left| \frac{X - Y}{X} \right|$$
 (6.29)

where X is the input analog data set to ADC and Y is the sampled output data set of ADC. According to simulation results presented in Fig. 6.16 (b), ADC with 6-bits resolution can sample the signal with 7% error so that 6-bits is used for ADC design.

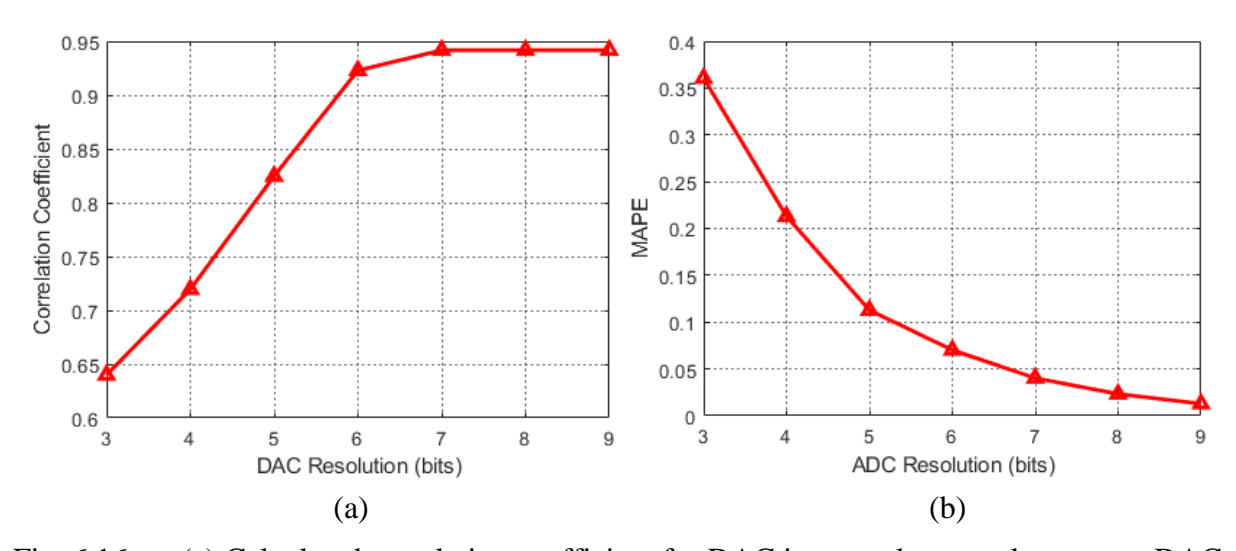


Fig. 6.16. (a) Calculated correlation coefficient for DAC input and output data versus DAC resolution; (b) Calculated error rate for ADC input and sampled data versus ADC resolution.

As for the sampling rate of ADC, it is chosen as 4 times of transmitted symbol rate to sample the analog output signal with higher accuracy. However, due to the high data rate of proposed VLC system, the sampling rate of ADC can achieve to GSps level which is difficult to implement through one ADC. In the real applications, the signal is converted from serial signal to parallel and processed by several ADCs with sampling rate of MSps simultaneously. This architecture is widely adopted into A/D based high-speed SerDes design to decrease the design requirement for ADC.

After determining the specifications of binary-weighted DAC and flash ADC models, the bandwidth of AFE in transmitter is analyzed to evaluate the performance of passive equalizer. As presented in Fig. 6. 17, the -3 dB bandwidth of transmitter including limitation from LED is 52.42 MHz, and it can be extended to 313.39 MHz after adopting the passive equalizers with the sacrifice of low-frequency components loss.

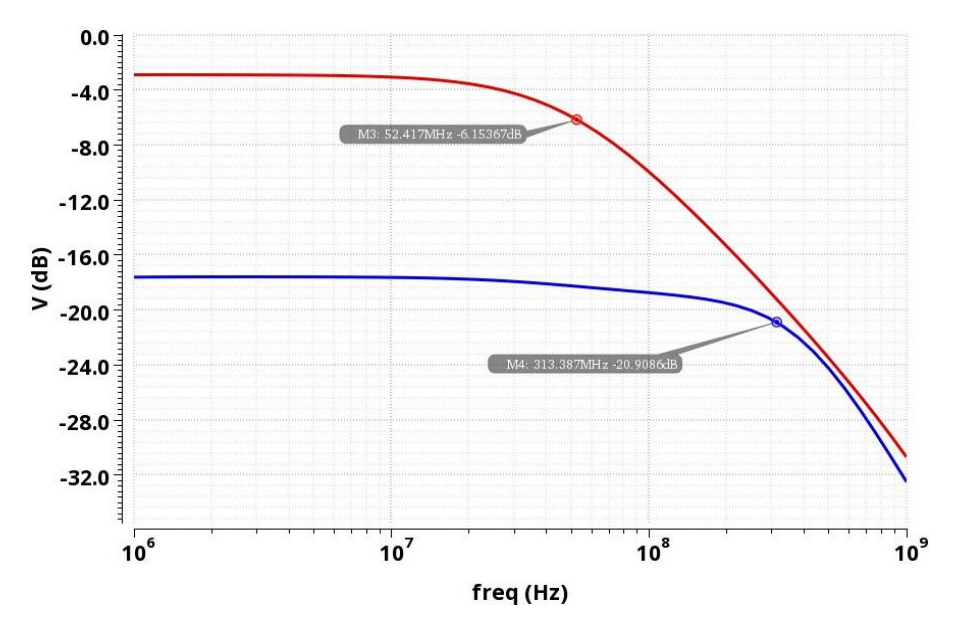


Fig. 6.17. -3 dB bandwidth extension of transmitter through using passive equalizer.

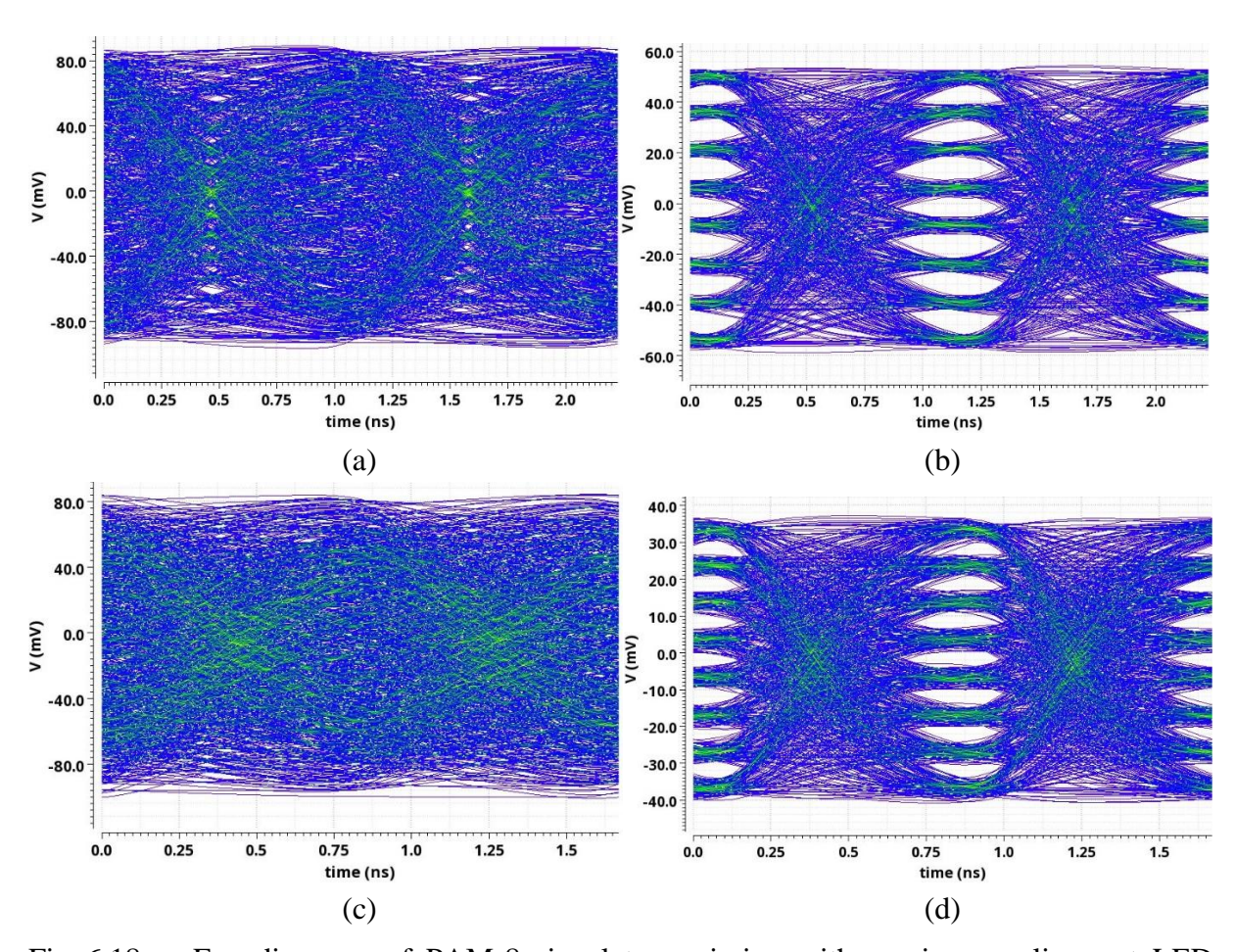


Fig. 6.18. Eye diagrams of PAM-8 signal transmission with passive equalizers at LED output: (a) 2.7 Gbps data rate without FFE; (b) 2.7 Gbps data rate with FFE; (c) 3.6 Gbps data rate without FFE; (d) 3.6 Gbps data rate with FFE.

After verified the feasibility of passive equalizers and obtained the -3 dB bandwidth of VLC transmitter, the corresponding eye diagrams of 2.7 Gbps and 3.6 Gbps PAM-8 signal transmission without and with NN-based FFE are detected at output of LED to verify the feasibility of FFE. The 1st pre-tap weight and 1st post-tap weight for 2.7 Gbps data transmission are 0.05 and 0.35 while the values for 3.6 Gbps are 0.07 and 0.5. As presented in Fig. 6.18, the eyes of 2.7 Gbps data with FFE is open, which owns better quality than 3.6 Gbps data. The top and bottom eyes of 3.6 Gbps data are almost closed and suffer from nonlinearity which remains to be solved by the following RBF-NN supported post-equalization.

6.5.2 Post-equalization Performance Evaluation

To evaluate the post-equalization performance, the bandwidth of AFE at receiver side is analyzed first. The -3 dB bandwidth of AFE in receiver including PD model and the corresponding total gain are simulated as shown in Fig. 6. 19. It can be noticed that the total bandwidth is 906.8 MHz with a TIA gain of 73.9 dB.

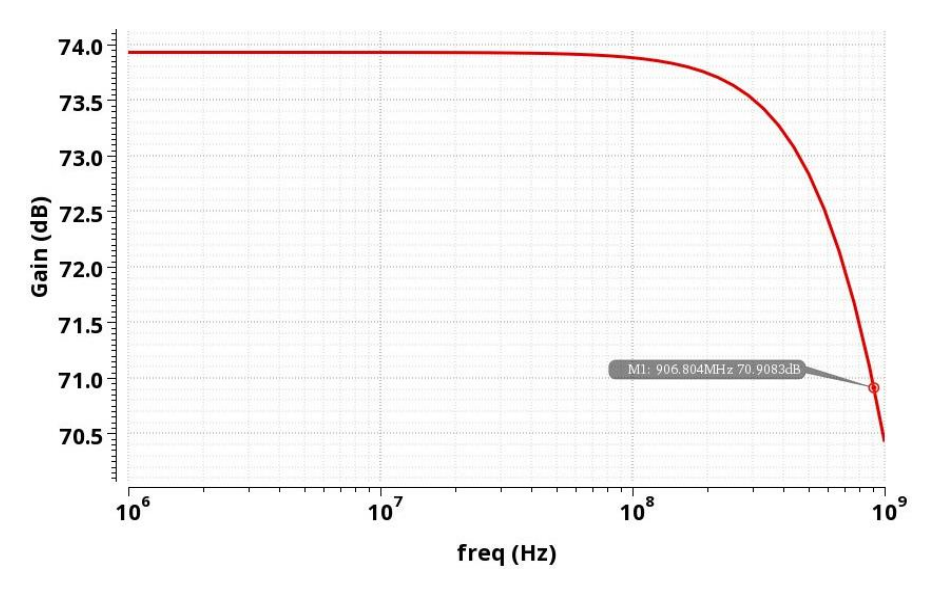


Fig. 6.19. -3 dB bandwidth and gain of receiver AFE including PD.

BER is one of the most important evaluation criteria of data transmission quality, and the relationship of BER with communication data rate is studied to find out the maximum data rate that this PD-based VLC system can support with the BER criteria of 3.8 x 10⁻³. The data transmission quality of using RBF-NN as the equalizer at the receiver side with using DNN as

the equalizer is compared with 3 m free space channel. The simulation results are presented in Fig. 6.20. (a), and it can be noticed that the highest data rate of using RBF-NN as the equalizer with 3 m free space channel is 3.6 Gbps while the highest data rate can be achieved with a DNN equalizer is 3.3 Gbps. By utilizing the RBF-NN as the equalization scheme, the communication data rate can be improved by 20% when compared with the DNN case since the more suitable activation function is adopted in RBF-NN. Besides, the highest data rate that this system can support with different types of channels is also studied. As shown in Fig. 6.20. (b), the achievable highest data rate for 1.2 m water channel is 4.2 Gbps which is higher than 3 m free space channel due to the less channel loss.

The simulated received eye diagrams using the post-equalized data of PAM-8 signal with the RBF-NN equalization scheme at two different data rates and two types of channels are also presented in Fig. 6.21. The eye diagrams with the communication data rate equal to 2.7 Gbps in free space and 3.3 Gbps in water represent the case of BER equal to zero, which is also called error free. The 3.6 Gbps and 4.2 Gbps eye diagrams are under the BER criteria of 3.8 x 10⁻³.

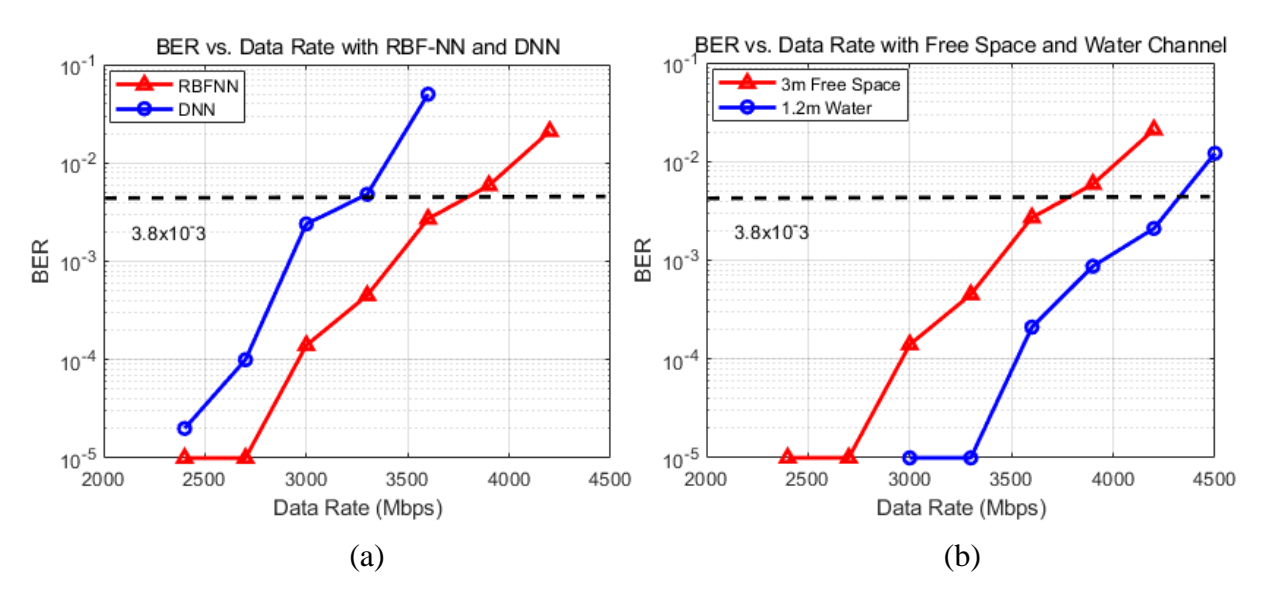


Fig. 6.20. Simulated results of BER vs. data rate: (a) using RBF-NN or DNN as equalizer with 3 m free space channel; (b) through 3 m free space or 1.2 m water channel with RBF-NN.

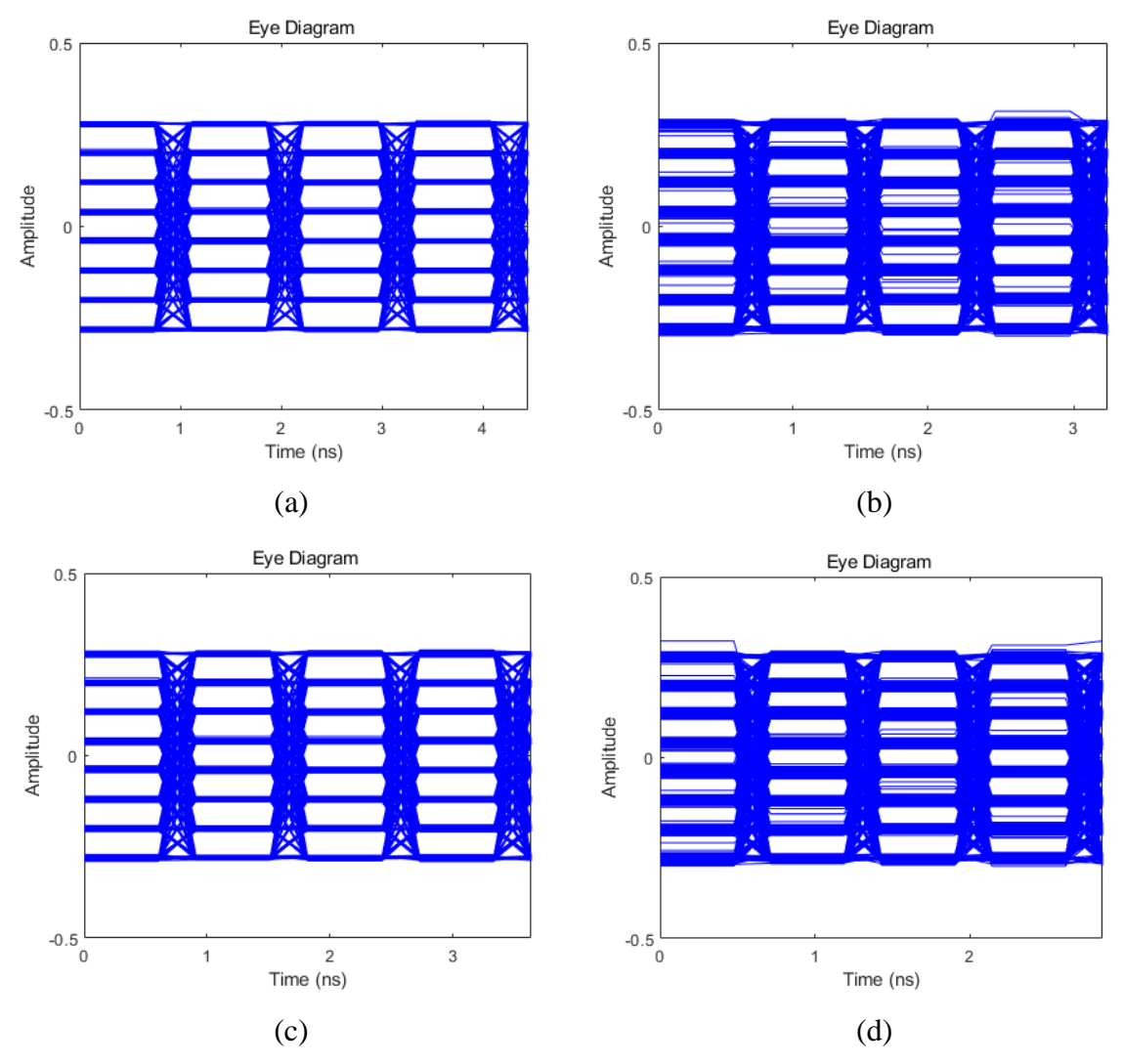


Fig. 6.21. Simulated eye diagrams of PAM-8 signal with RBF-NN as post-equalizer: (a) Communication data rate of 2.7 Gbps with 3 m free space channel; (b) Communication data rate of 3.6 Gbps with 3 m free space channel; (c) Communication data rate of 3.3 Gbps with 1.2 m water channel; (d) Communication data rate of 4.2 Gbps with 1.2 m water channel.

6.5.3 Training Performance Evaluation

For the RBF-NN adopted in the proposed PD-based VLC transceiver system, evaluating its training performance is essential to prove its feasibility and superiority compared with traditional DNN. Besides, the training time of RBF-NN is critical to implement it through hardware design for the real-time signal processing. Since the communication channel of VLC system is time-variant, the neural network utilized as equalizer should be trained repeatedly with time variation. Long training time causes extra delay time for signal transmission and even

leads to the failure of compensating signal loss and distortions. Therefore, decreasing the training time is important for building a real-time signal processing baseband.

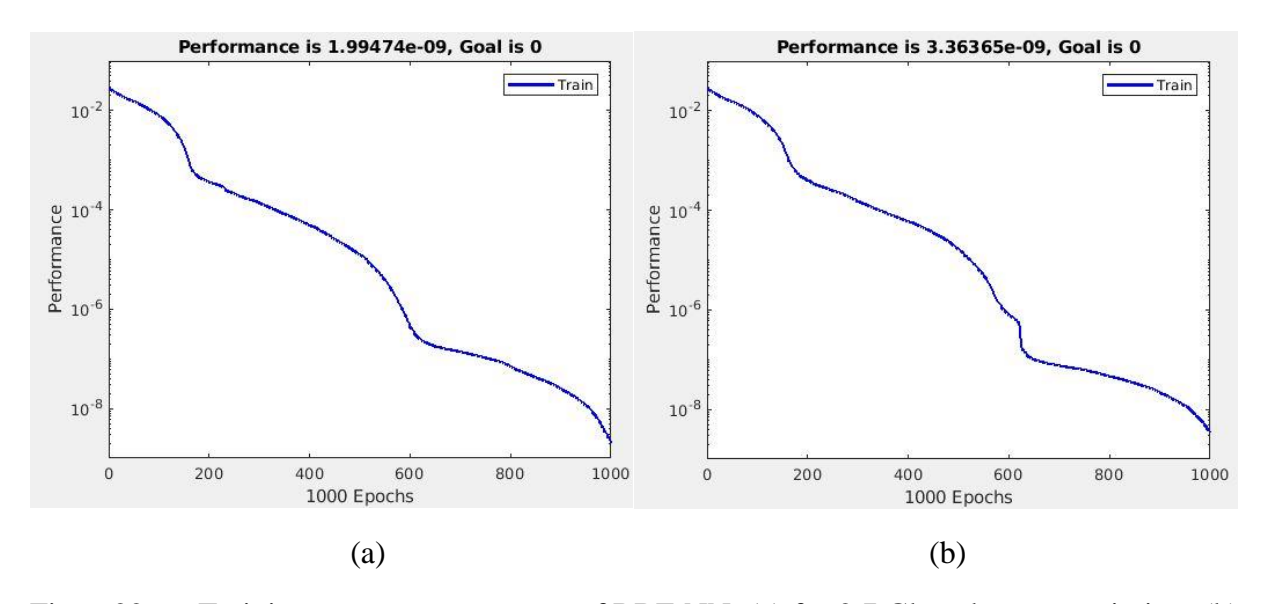


Fig. 6.22. Training convergence curves of RBF-NN: (a) for 2.7 Gbps data transmission; (b) for 3.6 Gbps data transmission.

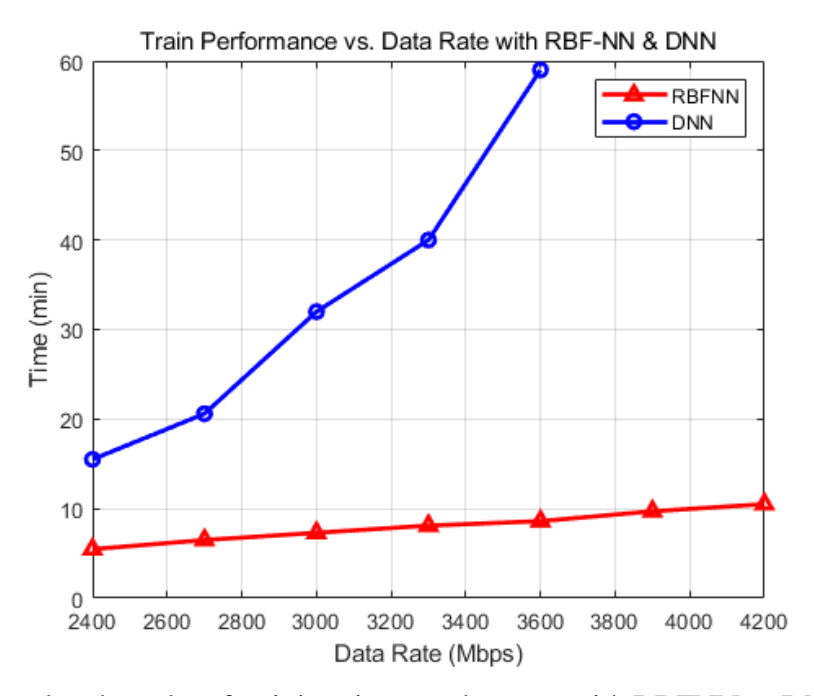


Fig. 6.23. Simulated results of training time vs. data rate with RBFNN or DNN as equalizer.

The convergence curves of training the RBF-NN with 2.7 Gbps and 3.6 Gbps data sets are presented in Fig. 6.22. It can be noticed that the trained model fixes well with expectation and

owns error less than 10⁻⁸ after 1000 epochs, which proves the feasibility of choosing RBF-NN as post-equalizer. The training time of different types of NNs is various since the complexity of their structures and training methods determine the time cost. Taking into consideration the implementation of NNs to systems-on-chip as a real-time equalization method, the training time should be as short as possible. The training time of both the RBF-NN and the traditional DNN at different communication data rates are simulated, and the simulated results are presented in Fig. 6.23. It is obvious that with an increased data rate, the training time for the NN will also increase. This proportional relationship reflects the fact that the training resources are dramatically consumed when the transmitted signal deviates hugely from the original. Moreover, compared with the traditional DNN, the RBF-NN consumes much less training time due to its superior characteristic of local approximation. With the same data rate achieved, the training time of the equalization scheme utilizing RBF-NN can be reduced by 86.7%. Since the RBF-NN is a local approximate network, only parts of the weights of all neurons need to be trained during each iteration, which can speed up the training process of RBF-NN. The DNN requires a much longer training time since it is a global approximation network, which means that the weights of all neurons should be adjusted during each iteration. Therefore, utilizing RBF-NN contributes to saving the computing resources.

6.5.4 Comparison with Other VLC Systems with Neural Network

To evaluate the performance of proposed PD-based PAM-8 transceiver system with NN-based pre- and post-equalization schemes, the system architecture, training performances, and data transmission of the proposed VLC system are compared with those of previous works, as well as summarized the characteristics of these works in Table 6.4. It can be noticed that our proposed VLC transceiver system can achieve the highest data rate with the longest channel length due to the hybrid equalization schemes adopted in both transmitter and receiver as well as highest modulation bandwidth. Besides, the analog front-end of our proposed VLC transceiver system is implemented with integrated circuits, which further improves the performance of the system.

Table 6.4 Comparison of Neural Network Enabled VLC Systems

Specifications of VLC System		[6.18]	[6.19]	[6.20]	[6.21]	[6.22]	This Work
System Architecture	Channel Type	Water	Free Space	Water	Free Space	Water	Free Space / Water
	Channel Length	1.2 m	3 m	1.2 m	1.2 m	1.2 m	3 m / 1.2 m
	PD Bandwidth	250 MHz	/	250 MHz	200 MHz	250 MHz	1 GHz
	Pre-EQ	Passive EQ	/	Passive EQ	Passive EQ	Passive EQ	Passive EQ + FFE
	Post-EQ	NN-based EQ	NN-based EQ	NN-based EQ	NN-based EQ	NN-based EQ	NN-based EQ
	Analog Front- end Type	Discrete Components	Discrete Components	Discrete Components	Discrete Components	Discrete Components	Integrated Circuits
	Implementation	Experiment	Matlab Simulation	Experiment	Experiment	Experiment	Matlab Simulation
Specifications of NNs	Type of NNs	CV-NN	LSTM	TFDN	LSTM	GKDNN	RBF-NN
	Irritations	/	/	/	400	2000	1200
Data Transmission	Data Rate	2.85 Gbps	/	2.85 Gbps	1.15 Gbps	1.5 Gbps	3.6 Gbps / 4.2 Gbps
	Modulation Scheme	64-QAM	DCO-OFDM	64-QAM	PAM-7 / PAM-8	PAM-8	PAM-8

6.6 References

- [6.1] X. Li, Z. Ghassemlooy, S. Zvanovec and L. Alves, "An equivalent circuit model of a commercial LED with an ESD protection component for VLC", in *IEEE Photonics Technology Letters*, vol. 33, no. 15, pp. 777-779, Jul. 2021.
- [6.2] W. Cheung, P. Edwards and G. French, "Determination of LED equivalent circuits using network analyzer measurements", in *1998 COMMAD*, 1998, pp. 232-235.
- [6.3] B. Hussain, X. Li, F. Che, C. P. Yue, and L. Wu, "Visible light communication system design and link budget analysis," in *Journal of Lightwave Technology*, vol. 33, no. 24, pp. 5201–5209, Dec. 2015.

- [6.4] C. Wang, H. -Y. Yu and Y. -J. Zhu, "A Long Distance Underwater Visible Light Communication System With Single Photon Avalanche Diode," in *IEEE Photonics Journal*, vol. 8, no. 5, pp. 1-11, Oct. 2016.
- [6.5] C. D. Mobley, et al., "Comparison of numerical models for computing underwater light fields," in *Appl. Opt.*, vol. 32, no. 36, pp. 7484-7504, 1993.
- [6.6] Z. Zeng, S. Fu, H. Zhang, Y. Dong and J. Cheng, "A survey of underwater optical wireless communications", in *IEEE Commun. Surv. Tut.*, vol. 19, no. 1, pp. 204-238, 2017.
- [6.7] H. Chen, et al., "Toward Long-Distance Underwater Wireless Optical Communication Based on A High-Sensitivity Single Photon Avalanche Diode," in *IEEE Photonics Journal*, vol. 12, no. 3, pp. 1-10, Jun. 2020.
- [6.8] J. G. Proakis, *Digital Communication Fifth Edition*, Boston, McGraw-Hill Higher Education, pp.602, (2008).
- [6.9] A. A. Bergh and P. J. Dean, "Light-emitting diodes," in *Proceedings of the IEEE*, vol. 60, no. 2, pp. 156-223, Feb. 1972.
- [6.10] R. Roberts and Z. Xu, "Update on VLC link budget work," IEEE VLC Standard 802.15.7, Sep. 2009.
- [6.11] J. M. Palmer, Radiometry and Photometry FAQ. (2003). [Online]. Available: http://fp.optics.arizona.edu/Palmer/rpfaq/rpfaq.htm.
- [6.12] T. Y. Elganimi, "Studying the BER performance, power- and bandwidth- efficiency for FSO communication systems under various modulation schemes," in *2013 IEEE Jordan Conference on Applied Electrical Engineering and Computing Technologies (AEECT)*, 2013, pp. 1-6.
- [6.13] S. Dimitrov, S. Sinanovic and H. Haas, "Signal shaping and modulation for optical wireless communication," in *Journal of Lightwave Technology*, vol. 30, no. 9, pp. 1319-1328, May1, 2012.
- [6.14] S. T. Ahmad and K. P. Kumar, "Radial basis function neural network nonlinear equalizer for 16-QAM coherent optical OFDM," in *IEEE Photonics Technology Letters*, vol. 28, no. 22, pp. 2507-2510, 15 Nov.15, 2016.
- [6.15] Razavi B. Design of Integrated Circuits for Optical Communications[M]. John Wiley & Sons, 2012.

- [6.16] R. Y. Chen and Z. Yang, "CMOS Transimpedance Amplifier for Visible Light Communications," in *IEEE Transactions on Very Large Scale Integration (VLSI) Systems*, vol. 23, no. 11, pp. 2738-2742, Nov. 2015.
- [6.17] Abdi H. The Kendall rank correlation coefficient[J]. Encyclopedia of measurement and statistics, 2007, 2: 508-510.
- [6.18] Hui Chen, Wenqing Niu, Yiheng Zhao, Junwen Zhang, Nan Chi, and Ziwei Li, "Adaptive deep-learning equalizer based on constellation partitioning scheme with reduced computational complexity in UVLC system," in *Opt. Express*, vol. 29, 21773-21782 (2021).
- [6.19] N. A. Amran, M. Dehghani Soltani, M. Yaghoobi and M. Safari, "Deep learning based signal detection for OFDM VLC systems," in 2020 IEEE International Conference on Communications Workshops (ICC Workshops), 2020, pp. 1-6.
- [6.20] H. Chen, Y. Zhao, F. Hu and N. Chi, "Nonlinear resilient learning method based on joint time-frequency image analysis in underwater visible light communication," in *IEEE Photonics Journal*, vol. 12, no. 2, pp. 1-10, Apr. 2020.
- [6.21] Xingyu Lu, et al., "Memory-controlled deep LSTM neural network post-equalizer used in high-speed PAM VLC system," in *Opt. Express*, vol. 27, 7822-7833 (2019).
- [6.22] Chi, Nan, et al., "Gaussian kernel-aided deep neural network equalizer utilized in underwater PAM8 visible light communication system," in *Opt. Express*, vol. 26, 26700-26712 (2018).

CHAPTER 7 Conclusion, Future Work, and Publications

7.1 Conclusion

VLC technique has gradually attracted more and more research interests for its wide spectrum bandwidth, no EMI, combability with existing infrastructures, and high communication security. It can be adapted to light sources for simultaneously providing illumination function and data transmission function. The VLC system can be divided into two categories according to the receiver type, and they are the PD-based VLC system and the CIS-based VLC system. In this thesis, a detailed introduction to CIS-based and PD-based VLC systems is presented, then three examples of these two types of VLC systems are illustrated. Firstly, a CIS-based VLC-enabled smart home control system with VLP function is proposed and implemented with a prototype. Secondly, a PAM-4 VLC transmitter equipped with FFE and a passive equalizer for a PD-based VLC system is presented and simulated with corresponding results. Thirdly, a PAM-8 PD-based VLC transceiver system equipped with NN-based pre-equalization, passive equalizer, and RBF-NN-enabled post-equalization is proposed, implemented and evaluated through a co-simulation platform with both free space and water channel models.

(1) A CIS-based VLC-enabled smart home control system with a 3D indoor positioning algorithm supported by directional angle data of a smartphone is presented. This system consists of a VLC lightbulb as a beacon, a smartphone with a control app as a receiver, and a cloud server storing data. A driver-less AC-powered VLC lightbulb is designed as a VLC beacon to offer plug-n-play capability without an extra terminal device for users' convenience. This lightbulb is practical in a real-life environment with a communication distance of 3.4 m and sufficient illuminance. The smartphone control app and back-end cloud server are designed to sort out the information of smart devices by their positions for guaranteeing the availability to users, increasing system scalability, and simplifying the management of multiple devices. A novel control method utilizing the CIS-based VLC technique with the support of a cloud server and smartphone app to divide the control region by the position of the VLC lightbulb is proposed so that users can accurately manage

devices in one room without information disclosure. A directional angle-assisted 3D indoor VLP algorithm is proposed to calculate the world coordinates of the user. This algorithm is adopted in orientation-based and location-based control applications such as directional control, specific point management, and navigation for robots to increase the accuracy, security, and diversity of the system. The proposed CIS-based VLC-enabled smart home control system is implemented and evaluated to verify its feasibility with experimental results of 3.4 m communication distance for VLC and centimeter-level accuracy for 3D indoor positioning with an average PER less than 7%, which proves the accurate control and localization function of this system. In summary, this CIS-based VLC-enabled smart home control system is a user-friendly control system that provides high control accuracy and guarantees system security.

- (2) A PAM-4 VLC transmitter which is equipped with FFE and analog passive equalizer is proposed and simulated with schematic design. This transmitter is designed for the PD-based VLC system, and it employs a 2-tap FFE including one main-tap, one post-tap as well as a passive equalizer to extend the limited modulation bandwidth. The method of determining tap numbers and tap weights is also introduced in detail. This FFE algorithm is implemented in digital baseband which consists of a 16 x 6 LUT storing the coefficients of FFE taps and six 16:1 MUXs to select corresponding data from the LUT. The passive equalizer utilizes the same structure as the high-pass LC filter to reduce low-frequency components and increase high-frequency components. A DAC-based LED driver is also designed at the schematic level to convert the digital data from MUXs to analog driving current so that to transmit the PAM-4 signal through visible light. With the proposed hybrid equalization methods, this PAM-4 VLC transmitter can achieve the highest transmission data rate of 1.2 Gbps.
- (3) A PAM-8 VLC transceiver system designed for PD-based VLC system, which is comprised of digital basebands, analog front-end circuits, LED model, PD model, and LOS channel model is proposed and implemented through co-simulation. The limitations in the proposed PD-based VLC systems caused by the intrinsic characteristics of LED devices and LOS

channels have been systemically studied, which are the modulation bandwidth limitation and the channel loss. Based on ISI and signal loss analysis, a PD-based VLC transceiver system that combines NN-based FFE, a passive equalizer, and an RBF-NN-enabled equalizer to extend the limited communication bandwidth has been proposed. The whole PD-based VLC system is implemented in a co-simulation platform of MATLAB and Cadence. MATLAB is utilized to build the digital basebands, DAC and ADC in both the transmitter and receiver and design the analog front-end circuits with LED and PD device models in Cadence. Besides, both free space and water channel models are established and utilized for simulation to prove that the prosed system can work for different channel models. The data transmission performance of using free space model and water channel model are also analyzed and compared. To verify the feasibility and evaluate the performance of this VLC system, simulations on the data rate of the signal transmission with BER through the RBF-NN and a DNN are conducted, and the training time with an increased data rate is also studied. The simulation results indicate that the RBF-NN-enabled PD-based VLC transceiver system can achieve a data rate of 3.6 Gbps while taking less than 10 min of training time.

7.2 Future Work

For the CIS-based VLC system design, it is suitable for indoor occasions and IoT applications for its simple system structure, compatibility with both existing lighting infrastructures and mobile devices, and supplementary function to an RF-based communication system. In particular, the indoor VLP system is one of the main applications for the CIS-based VLC system which has attracted wide research interest. Even though the typical VLP accuracy can reach to centimeter-level accuracy, increasing the positioning accuracy especially for locating the moving objects is critical for the VLP system. Meanwhile, improving the positioning algorithm is also important, which includes positioning the mobile devices through less than three light sources, solving the blocked light source problem on the indoor occasion, and multiple sensors fusion method. Another attractive research direction for CIS-based VLC systems is IoT application. Since VLC technique can be utilized as a supplementary to the existing RF-based

communication system such as Wi-Fi Zig-Bee and Bluetooth, the CIS-based VLC system is suitable for constructing an IoT network and providing applications such as smart lighting, smart control, and smart display. These IoT-related applications can make a huge difference in people's daily life and are worth exploring. Moreover, the CIS-based VLC system can be adapted to some outdoor scenarios like vehicle communication, which is one developing direction for smart transportation to improve traffic security.

For the PD-based VLC system design, a highly integrated system is critical since it contributes to reducing the parasitic components, decreasing system scale, and improving energy efficiency. However, the research on integrated PD-based VLC system is still in a fledgling stage and many critical techniques remain to be studied. An integrated PD-based VLC system typically consists of digital baseband, analog front-end, LED as light source, and PD as a light signal detector. In the digital baseband, various digital pre- and post-equalization schemes such as FFE, DFE, NNbased equalization, and advanced modulation schemes such as PAM, OFDM, CAP, and WDM are important for extending the limited modulation bandwidth. Implementing these schemes in the integrated digital baseband through the real-time method is the future direction since most of the digital basebands for PD-based VLC systems are designed in MATLAB with an offline process. For the hardware implementation requirement, field programmable gate array (FPGA) is the best choice for realizing the function of an RBF-NN. FPGA owns customized hardware, and it can handle multiple applications simultaneously. It has the characteristics of programmable, high performance, low energy consumption, high stability, parallelism and security. With a dedicated AI core, FPGA can support the required calculation of neural network. In the analog front-end, the energy-efficient LED driver, high impedance gain and low noise receiver amplifier, and multiple-stage equalizer are essential research directions for improving system performance. For the light source, high modulation bandwidth white LED is one significant research focus for VLC device development due to its severe limitation effect on the communication data rate. Besides, an on-chip PD with high sensitivity to visible light is another research focus for VLC device development to reduce limitations from the receiver side. Therefore, from digital design through analog circuit design to VLC device development, there are quite a lot of research topics pending for subsequent work.

7.3 Publications

- [1] **Bo Xu**, Tianxin Min, and C. Patrick Yue, "Design of PAM-8 VLC Transceiver System Employing Neural Network-based FFE and Post-Equalization", *IEEE Photonics Journal*, 2022 (Under Review);
- [2] **Bo Xu**, Babar Hussain, Yiru Wang, Hoichuen Cheng, Tianxin Min, and C. Patrick Yue, "Visible Light Communication Enabled Smart Home Control System with 3D Indoor Localization," *IEEE Transactions on Consumer Electronics*, 2022 (Under revision);
- [3] **Bo Xu**, Babar Hussain, Xinyi Liu, Tianxin Min, Hoichuen Cheng, and C. Patrick Yue, "Smart-Home Control System Using VLC-Enabled High-Power LED Lightbulb," in *2021 IEEE 10th Global Conference on Consumer Electronics (GCCE)*, pp. 744-745, Oct. 2021;
- [4] **Bo Xu**, Li Wang, Jian Kang, Cong Qiu and C. Patrick Yue, "An RGB-LED Driver with Feed-Forward Equalization Used for PAM-4 Visible Light Communication," in *5th International Conference on Machine Learning and Intelligent Communications (MLICOM)*, pp. 228-234, Sep. 2020;
- [5] **Bo Xu**, Zhaojun Liu, and C. Patrick Yue, "An AC-Powered Smart LED Bulb for 3D Indoor Localization Using VLC," in *2019 IEEE 8th Global Conference on Consumer Electronics* (*GCCE*), pp. 236-237, Oct. 2019;
- [6] Tianxin Min, Jian Kang, **Bo Xu**, Weimin Shi and C. Patrick Yue, "Design and Verification of a 334-Mb/s DCO-OFDM Li-Fi Transceiver Using Intergrated System Evaluation Engine," in 2021 IEEE 14th International Conference on ASIC (ASICON), Oct. 2021;
- [7] Fuzhan Chen, Chongyun Zhang, Tianxin Min, **Bo Xu**, Quan Pan, C. Patrick Yue, "Design and Co-Simulation od QPSK and NRZ/PAM-4/PAM-8 VCSEL-Based Optical Links Utiliz-ing

an Intergrated System Evaluation Engine," in 2021 IEEE 14th International Conference on ASIC (ASICON), Oct. 2021;

[8] Weimin Shi, Fuzhan Chen, Xinyi Liu, Chongyun Zhang, Zilu Liu, Tianxin Min, **Bo Xu**, Li Wang, Jian Kang and C. Patrick Yue, "An Integrated Sys-tem Evaluation Engine for Cross-Domain Simulation and Design Optimization of High-Speed 5G Millimeter-Wave Wireless SoCs," in 2021 IEEE 14th International Conference on ASIC(ASICON), Oct. 2021;

[9] Yiru Wang, **Bo Xu**, Jian Kang, Cong Qiu and C. Patrick Yue, "Performance Analysis and Evaluation of Outdoor Visible Light Communication Reception," in *5th International Conference on Machine Learning and Intelligent Communications (MLICOM)*, Sep. 2020;

[10] Li Wang, Caroline Tjoe, **Bo Xu** and C. Patrick Yue, "A Dual-Resonance Matching Circuit for Magnetic Resonance Wireless Power Transfer Systems," in *2019 IEEE 8th Global Conference on Consumer Electronics (GCCE)*, pp. 94-95, Oct. 2019;

[11] Can Wang, **Bo Xu**, Xianbo Li, Li Wang and C. Patrick Yue, "Compact Modeling of Laser Diode for Visible Laser Communication (VLLC) Systems," in 2018 Conference on Lasers and Electro-Optics Pacific Rim (CLEO-PR), pp. 1-2, Jul. 2018.